The influence of conditional *Ski* knockdown in primary cardiac myofibroblasts: fibrosis markers, *Taz* mRNA abundance and alternative *Ski* exon splicing.

by
Rebeca C. Fehr

A thesis submitted to the Faculty of Graduate Studies of
The University of Manitoba
in partial fulfillment of the requirements for the degree of

MASTER OF SCIENCE

Department of Physiology & Pathophysiology
Rady Faculty of Health Sciences
University of Manitoba

Abstract

Background: SKI is a protein that functions as a transcriptional cofactor and is expressed in cardiac muscle. It is encoded by 7 exons in mouse and its primary function is that of a negative regulator for TGF-β_1 signaling. While TGFβ_1 stimulates cardiac scar formation and fibrosis, SKI is known to negatively regulate TGFβ_1 and deactivate cardiac myofibroblasts, the main cells responsible for cardiac fibrosis. Our lab has recently shown that SKI may influence the Hippo signaling pathway however *Ski* downregulation has not been studied in heart. Hypotheses: In vitro *Ski* knockdown in primary cardiac myofibroblasts modifies gene transcription of Hippo pathway component proteins and marker genes for cardiac fibrosis. Further, SKI may exist in two different exon splice variants in mouse heart. Methods: In all experiments, P0 primary cardiac myofibroblasts from Ski-floxed (transgenic) and wild-type (non-transgenic) mice were cultured. After optimization, these cells were infected with adenoviral-GFP as control or adenoviral-Cre (Ad-Cre) to specifically excise *Ski* exons 2 and 3; and harvested 72h hours after infection. Samples were prepared for qPCR, cytotoxicity (live-dead) assay, and DNA sequencing. Results: Two different transcriptional variants (Tv) of mouse *Ski* were confirmed in Ski-floxed and control cells, with and without exon 2. The presence of Ad-Cre did not influence cell death in treated control or Ski-floxed cells. Excision of exons 2 and 3 (as well as significant knockdown of exons 1, and 4 - 7) was confirmed in Ad-Cre-treated Ski-floxed cells in the presence of Cre, and exon frameshift was noted following this excision. Ad-Cre was shown to influence mRNA expression of both control and Ski-floxed treated cells – Cre treated myofibroblasts were compared to GFP infected controls. We observed that *Taz* mRNA expression is significantly elevated in basal conditions with Ad-Cre treated *Ski* knockdown P0

myofibroblasts vs Ad-GFP treated controls. On the other hand, the mRNA expression of fibrillar *collagens I α 1, collagen III α 1, Eda- fibronectin, Limd1, Lats2, α-Sma and Pdgfr-α* genes were not altered in Ski-floxed Ad-Cre treated cells vs controls. Conclusion: *In vitro Ski* downregulation in P0 myofibroblasts (in the absence of any other stimulus and in serum-starved conditions) does not directly influence fibrillar collagen gene transcription. This notwithstanding the steady state mRNA abundance of the Hippo effector protein *Taz* is significantly upregulated by *Ski* knockdown vs Ad-GFP treated controls. The discovery of novel differentially spliced *Ski* transcripts may impact future investigation of SKI function in heart. We suggest that *Ski* knockdown will provide a useful model to investigate the role of *Ski* in activation of various cytokines, including $TGF\beta_1$.

Acknowledgments

First of all, I would like to thank The Lord God Almighty for this opportunity, knowledge and strength to complete this project. I could not have done it without Jesus' blessings and guidance. I must also thank my advisor Dr. Ian Dixon for his support during my master's program, for all the conversations and encouragement to work with excellence in my project, as well as inspiring me to deepen my knowledge in molecular cardiology and helping me grow as a person and as a scientist. Thanks to my advisory committee members, Dr. Christine Doucette and Dr. Etienne Leygue who have always given me valuable advice to complete my project and expand my knowledge in basic science. Also, thank you to Dr. Naranjan Dhalla, who not only was part of my advisory committee, but also my first mentor at St. Boniface Research Centre in 2016 during my summer internship and who inspired me to give my best in science and encouraged me to keep pursuing my medical career. I could not forget to thank our lab members. Sunil Rattan, thank you for all your scientific and technological knowledge which helped me tremendously. Also, for all fun and deep talks about life, food, and series. Thank you for your friendship. Dr. Mark Hnatowich, thank you for all guidance, troubleshooting advice, for instigating me to learn more and discover new methods and abilities. Also, thank you for your friendship, and priceless support and advice in the midst of adversity. I learn to admire scientific thought process and investigation through your extensive knowledge and integrity. I must also thank Dr. Natalie Landry, who introduced me to experimental methodology; your expertise and excellence guided me throughout my masters. I will always be grateful for all advice, fun talks, and for being part of my bridal shower and attending my wedding. Many thanks to all the summer students who helped me complete endless qPCR, cell culture and western blots: Ken Xing, Jooyeon Seung, Claire Meier and Dora Modrcin. Thank you to my fellow master's student Besher and his wife Omaymah Abualanaz for bringing new insights and helping me improve my teaching skills, and also family fun moments and new food discoveries.

A great thank you to ICS extended family, to Cameron Eekhoudt, Sonu Varghese, and Matthew Guberman for all the fun and relaxing moments in the "Cheese Club". Thank you to Matthew Love, Sikta Chattopadhyaya, Akshi Malik, Niketa Sareen, Abhay Srivastava and Raghu Nagalingam for long conversations, advice in my project and friendship. The journey became lighter and rich because of you. I would like to thank Dr. Jeff Wigle, Dr. Grant Pierce and Dr. Michael Czubryt for their support, collaboration, and advice during my academic journey. I must

also thank Dr. Barbara Nickel, Robert Fandrich, Shirley Mager, Kairee Ryplanski and Mae Villamor for always being ready to help and advise.

I am also grateful for University of Manitoba and the Physiology and Pathophysiology Department head, Dr. Peter Cattini, and staff: Judith Olfert, Gail McIndless, Sharon McCartney and Vanessa Perinot for your patience and orientation with paperwork. Also, thank you to the funding agencies: Canadian Institutes of Health Research, Research Manitoba, and the Heart & Stroke Foundation.

In addition, I would like to thank my dear Brazilian friends, Lica, Samira, and Anne; and friends from Waverley Church who gave me tremendous support, prayer, and advice in the most difficult moments. To my family, who I miss immensely, my eternal "Muito Obrigada" for all sacrifice and support in my academic journey, for the countless calls, talks, advice, and great encouragement in pursuing my dreams. And lastly, but certainly not least, to my husband, Karlyn, my biggest fan, and supporter. Thank you for building life together, for being my safe place, comforter, and best friend in this journey. You amaze me with your enthusiasm, empathy, and wisdom, I could not have made it without you.

Not to us, O Lord, not to us, but to your name give glory, for the sake of your steadfast love and your faithfulness.

Psalm 115:1

Dedication

To my beloved husband, Karlyn Fehr,
and in memory of my grandfather Oswaldo Loiola de Camargo

Table of Contents

List of figures

List of Tables

List of Abbreviations

4TH	4-Hydroxytamoxifen
Acta2	Alpha-actin-2
Ad-Cre	Adenovirus Cre Recombinase
Ad-GFP	Adenovirus Green Fluorescent Protein
AHA	American Heart Association
ALDH2	Aldehyde Dehydrogenase 2
ALK-5	Activin Receptor-like Kinase 5
AngII	Angiotensin II
ANOVA	Analysis of Variance
α-SMA	alpha-smooth muscle actin
BMP	Bone Morphogenic Protein
CCAC	Canadian Council on Animal Care
cDNA	complementary DNA
CF	Cardiac Fibroblast
CMV	Cytomegalovirus
CO2	Carbon Dioxide
Cre	Cyclization Recombination Enzyme
CRISPR-Cas9	Clustered Regularly Interspaced Short Palindromic Repeats - CRISPR-associated protein 9
CTGF	Connective Tissue Growth Factor
DAB	Diaminobenzidine
DAMPs	Damage-Associated Molecular Patterns
DDR2	Discoidin Domain Receptor 2
DMEM/F10	Dulbecco's Modified Eagle Medium Nutrient Mixture F-10
DMEM/F12	Dulbecco's Modified Eagle Medium Nutrient Mixture F-12
DMSO	Dimethyl Sulfoxide
DNA	Deoxyribonucleic Acid
dNTP	Deoxyribonucleoside Triphosphate
dsDNA	Double-Stranded DNA
ECM	Extracellular Matrix
ED-A Fn	Extra Domain A - Fibronectin
EDTA	Ethylenediaminetetraacetic Acid
ELISA	Enzyme-Linked Immunosorbent Assay
ER	Estrogen Receptor
ERK1/2	Extracellular Signal-Regulated Kinases 1/2
ESC	European Society of Cardiology
Eth-1	Ethereum-1
FBS	Fetal Bovine Serum
FITC	Fluorescein Isothiocyanate
FN-1	Fibronectin-1
FRT	Flippase Recognition Target
GDF	Growth Differentiation Factors
gDNA	Genomic DNA

GENCODE39	Generalized Coding 39
HDAC	Histone Deacetylase
HEK293A	Human Embryonic Kidney 293A
HEPES	4-(2-hydroxethyl)-1-piperazineethanesulfonic Acid
HF	Heart Failure
HPRT1	Hypoxanthine-Guanine Phosphoribosyl Transferase 1
IFN-γ	Interferon-gamma
IL-10	Interleukin-10
IL-18	Interleukin-18
IL-1β	Interleukin-1 beta
IL-4	Interleukin-4
IL-6	Interleukin-6
IPF	Idiopathic Pulmonary Fibrosis
ITS-A	Insulin-Transferrin-Selenium-Sodium Pyruvate
JNK1/2	c-Jun N-terminal Kinases
KCl	Potassium Chloride
LacZ	Beta-Galactosidase
LAP	Latency-Associated Peptide
LATS2	Large Tumor Suppressor Kinase 2
LIMD1	LIM Domain Containing 1
LoxP	Locus of X-over P1
LTBP-1	Latent TGF-b Binding Protein
LV	Left Ventricle
LVEDP	Left Ventricular End-Diastolic Volume
LVEDV	Left Ventricular End-Diastolic Pressure
MAPK/p38	p38 Mitogen-Activated Protein Kinases
MAPKs	Mitogen-Activated Protein Kinases
Meox2	Mesenchyme Homeobox 2
MerCreMer	Tamoxifen Inducible Cre Recombinase
MgCl	Magnesium Chloride
MH1/2	MAD Homology 1
MI	Myocardial Infarction
miR-155	micro-RNA-155
miR-29	micro-RNA-29
MMP-1	Matrix Metalloproteinase-1
MMP-14	Matrix Metalloproteinase-14
MMP-8	Matrix Metalloproteinase-8
MOB1	Mps One Binder kinase
MOI	Multiplicity of Infection
mRNA	Messenger Ribonucleic Acid
MST1/2	Macrophage Stimulating 1 and 2
NaCl	Sodium Chloride
NaH2PO4	Monosodium Phosphate
NCOR	Nuclear Receptor Corepressor

Neo	Neomycin
NF-κb	Nuclear Factor Kappa beta
PBS	Phosphate-Buffered Saline
PCR	Polymerase Chain Rection
PDGFRα	Platelet-Derived Growth Factor
PDGF	Platelet-Derived Growth Factor Receptor-alpha
PI3K/AKT	Phosphatidylinositol 3-Kinase/Protein Kinase B
PIROUETTE	Pirfenidone in Heart Failure with Preserved Ejection Fraction
PPRA-γ	Peroxisome Proliferator- Activated Receptor Gamma
qPCR	Quantitative Polymerase Chain Rection
RAAS	Renin-Angiotensin-Aldosterone System
RAS/MAPK	Rat Sarcoma Virus / Mitogen-Activated Protein Kinases
Rho GTPase	Ras Homologous/Guanosine Triphosphate Hydrolyse Enzyme
RhoA/Rho Kinase	Ras Homology Family Member A/ Ras Homology Kinase
RISC	RNA-induced Silencing Complex
RNAi	RNA Interference
ROS	Reactive Oxygen Species
RT-qPCR	Real-Time Quantitative Polymerase Chain Rection
SAND-like domain	Sp100, AIRE-1, NucP41/75, DEAF-1 - like domain
SAV	Salvador-Like Homolog
SBE	Smad-Binding Elements
SDS	Sodium Dodecyl Sulfate
SGLT2	Sodium-Glucose Cotransporter-2
shRNA	Short Hairpin RNA
siRNA	Small Interfering RNA
Ski	Sloan-Kettering Institute (gene)
SKI	Sloan-Kettering Institute (protein)
Ski tv1	Ski full-length
Ski tv2	Ski without exon 2
SMAD	Small Body Size Mother Against Dpp
S-MEM	Minimum Essential Medium Modified for Suspension Cultures
SnoN	Ski-Related Novel Protein N
TAE	Tris-acetate-EDTA
TAZ	Transcriptional co-Activator with PDZ-binding motif (i.e., WWTR1)
TC	Tetracycline
TCAG	The Centre for Applied Genomics
TCF-21	Transcription Factor 21
TEA domain	Transcriptional Enhanced Associate Domain
TGF-β	Transforming Growth Factor-beta
TIMPs	Tissue Inhibitor of Metalloproteinases
TNF-α	Tumor Necrosis Factor Alpha
Tris-HCl	Tris-aminomethane Hydrochloride
TV	Transcriptional Variant
VEGF	Vascular Endothelial Growth Factor

WNT3	WNT Family Member 3
WT-1	Wilms Tumor 1
WWTR1	(TAZ) WW Domain-Containing Transcription Regulator Protein 1
YAP	Yes Associated Protein
YWHAZ	Tyrosine 3-monooxygenase/Tryptophan 5-monooxygenase Activation Proteins Zeta
ZEB2	Zinc Finger E-Box Binding Homeobox 2

List of Appendices

Chapter 1: Literature Review

1.1 Heart Failure

In 1888, Dr. Charles Smart Roy and John George Adami published the first report about heart failure (HF) pathophysiology. The historical definition includes overstrain, overload and overwork to define a heart condition in which there is a failure to meet the requirements of the body for the systemic demand for blood[1]. Not surprisingly, these terms (overstrain, overload and overwork) are still accurate when referring to HF. Comprehensive definitions of heart failure are related to clinical aspects found in HF patients. The American Heart Association definition aligns well with Dr. Roy and Adami's report and establishes that HF is a complex clinical syndrome in which structural and/or functional cardiac abnormalities culminate in incapability to sustain systemic metabolic demands[2-4]. Thus, the pumping function of the heart is insufficient to supply blood flow to adequately meet basal homeostasis, and ultimately, this imbalance leads to cardinal symptoms such as fatigue, edema, and dyspnea [5, 6].

Although these descriptions are accurate from a clinical perspective, a definitive description of heart failure from a molecular approach is unavailable. Microscopically, the structure of the heart is mainly comprised of cardiomyocytes, macrophages, endothelial cells, Purkinje cells, pericytes and fibroblasts, with most of the volume of the myocardium occupied by the cardiomyocytes [7-9]. Cardiomyocytes are surrounded by extracellular matrix (ECM), mostly constituted by fibroblasts responsible for maintaining the molecular architecture of the myocardium[10, 11]. In the healthy heart the normal activity of the cardiac fibroblast is to regulate the relatively slow and continuous collagen turnover – this contributes to the preservation of normal cardiac compliance and Young's modulus of strain of 5 kPa to 8kPa[12, 13]. However, after

cardiac injury (such as myocardial infarction (MI)) fibroblasts are activated to myofibroblasts, wherein they become less motile, contractile and increase their production of ECM proteins including fibrillar collagens, all within the context of wound healing [14, 15]. Acute wound healing of the damaged myocardium follows and complements the rapid immune system response, and the deposition of ECM in acute wound healing may prevent ventricle wall rupture[16, 17].

Following the chronic activation of fibroblasts to myofibroblasts in the heart following the evolution of myocardial infarction and development of the infarct scar, the infarct scar itself matures into a permanently fibrosed tissue. However, unlike dermal wound healing, the chronic cardiac wound healing may not be limited to the regions marked by myocyte death following MI and indeed may undergo abnormal deposition of ECM in surrounding noninfarcted or viable regions of the heart[9, 18], leading to pathological cardiac fibrosis. As the fibrotic tissue in the heart does not possess the same strain characteristics (e.g., Young's modulus) as is normal ECM, the heart's capacity to contract and to relax normally is lost with attendant loss of filling capacity and contractility may be evident[19, 20].

According to the European Society of Cardiology (ESC) and the American Heart Association (AHA), HF is now considered an epidemic disease and with enormous societal and fiscal burdens, being diagnosed in 1.5% of Canadians[2, 21, 22]. The prevalence counts for almost 1% of the world population, representing more than 60 million people[23-25]. To date, there are no specific therapies available that are efficacious for the amelioration of the progression of cardiac fibrosis, which is now recognized as one of the main underlaying cause of HF[26, 27].

1.2 Cardiac Fibrosis

The hallmark of cardiac fibrosis is fibrosed cardiac ECM at tissues remote to the infarct scar itself, which follows the onset of myocardial infarction MI. According to the origin of the cardiac injury, the fibrotic process is divided in three different subtypes: interstitial, perivascular and replacement fibrosis.[9, 28, 29]

The first two subtypes (interstitial and perivascular) are characterized by scar formation not consequent of cardiomyocyte death[28, 30]. In the etiology of essential hypertension, the left ventricle must overcome relatively high afterload prior to ejection of blood from the left ventricle to the systemic circulation through the aorta.[31, 32] Usually this event is marked by delayed opening of the aortic valve and early onset of their closure, with a narrowing of the width of the pressure volume loop, in comparison to the normal patient control. As the heart functions to overcome elevated mean arterial pressure, the myocardium hypertrophies to sustain homeostatic levels[32, 33]. Enlargement of myocardial myocytes (cardiac hypertrophy) is attended by concomitant activation of cardiac fibroblasts activation through neurohormal, cytokine-mediated and mechanical stimulation and subsequent cardiac fibrosis [34-38]. A similar mechanism is found in valvulopathies including aortic regurgitation which is a *de facto* case of volume overload and is marked by an elevation in the left ventricular end-diastolic pressure (LVEDP) and well as left ventricular end-diastolic volume (LVEDV) [39]. These changes are closely and causally tied to elevated LV preload, elevated left ventricular wall strain, elevated biomechanical input to fibroblasts, activation of fibroblasts to myofibroblasts and consequently fibrosis [32, 39].

The third variety of fibrosis e.g., replacement fibrosis, is the most common and studied category. In contrast to interstitial and perivascular fibrosis mechanisms, replacement fibrosis is associated with post-ischemic injuries, and is defined in association of macro-pathophysiological

aspects of acute cardiac injury responses[40, 41]. After prolonged ischemia, cardiomyocytes undergo cell death, mainly by necrosis, characterizing myocardial infarction[40, 42].

Hypoxia or hypoxia/reperfusion is well known to damage cardiomyocytes by triggering apoptotic and necrotic events[9, 42, 43], and also leads to disruption of the extracellular matrix (the cardiac interstitium). As cells are injured, reactive oxygen species (ROS), pro-inflammatory cytokines, chemokines, and mechanical signals are released, contributing to elevated endothelial permeability and intense recruitment of immune cells[35, 42]. This initial response is essential to prevent ventricular wall rupture and it corresponds to the inflammatory phase, where leukocytes and M1-like pro-inflammatory macrophages remove debris and damaged cells[44]. At this stage, danger-associated molecular patterns (DAMPs) are secreted ultimately activating mitogen-activated protein kinases (MAPKs) and nuclear factor κβ (NF-κβ) pathways and finally releasing interleukin-1β (IL-1β), IL-6, IL-18, and tumor necrosis factor-α (TNF-α), the main cytokines of the inflammatory phase[45, 46].

The transition of this first phase to a proliferative phase occurs when the inflammatory cells start to die through apoptosis and necrosis, releasing signals to recruit M2-like anti-inflammatory macrophages, lymphocytes, and fibroblasts[10, 19]. The signals during this stage oppose the inflammatory activity of the previous phase by secretion of IL-10, IL-4, vascular endothelial growth factor (VEGF) and the activation of transforming growth factor-β_1 (TGF-β_1) pathway[29]. Throughout the healing process and in normal physiological conditions, cardiomyocytes present with limited proliferative capacity, and thereby the proliferative phase of cardiac wound healing is largely limited to and marked by fibroblast activation to cardiac myofibroblasts and restoration of the cardiac architecture via secretion of a substrate rich in mostly fibrin and fibronectin (Fn)[10, 37]. This cellular activation is promoted by TGF-β_1 signalling which is stimulated by several

stimuli, such as ROS, matrix-metalloproteinase-14 (MMP-14), mechanical stress and angiotensin-II (AngII)[14, 47]. A cascade of protein associations results in translation of pro-fibrotic factors and activation of myofibroblasts which promotes elevate collagen secretion. This new matrix is a provisionary and somewhat fragile substrate that allow cells to migrate and synthesize a more mature matrix. [48, 49]

The maturation phase of cardiac wound healing is the final step of the healing process, and it is characterized by increased production of collagen I and III at differential rates, with collagen III more prominent at the beginning of this stage and collagen I more intensively at a later step[50, 51]. During this stage, part of the myofibroblast population undergo apoptosis.[52] However, a large portion enters a senescent and chronically activated state[8], where the cells maintain a constant but low production of collagen, expanding the fibrotic tissue to viable areas surrounding the injury epicentre. Due to this scar expansion, the capacity of the heart to contract is reduced, impairing the cardiac function even more[19, 53]. With the purpose of counterbalancing uncontrolled healing (e.g., pathological deposition of ECM) there are several mechanisms capable of supressing fibrosis. Sloan-Kettering Institute (SKI) protein is a transcriptional factor that serves as a negative regulator of TGF-β1/Smad signalling and thus regulates cardiac fibrosis by reducing the impact of TGF-β_1-inducing myofibroblast inactivation and reducing the scar tissue[54, 55].

1.3 Cardiac Fibroblasts and activated Myofibroblasts

Cardiac fibroblasts (CF) are abundant and active mesenchymal cells present in the cardiac interstitium[56, 57]. These cells differ from cardiomyocytes and other cells by the absence of basement membrane. They are essential during cardiac embryogenesis in organogenesis, by

promoting myocyte multiplication [56]. In the postnatal period, cardiac fibroblast numbers proliferate growth in parallel with increased cardiac contractility, which counterbalances the sudden increase in hemodynamic afterload experienced by the ventricles following birth[58]. After this period, the number of cardiac fibroblasts does not vary extensively, unless there is an injury, hypertension, or hypertrophy[59, 60].

There is considerable debate as to the origins of cardiac fibroblasts. Several groups claim that CFs develop from the endocardium and epicardial sources, while others also consider neural crest as a source for CFs[52, 58]. Despite their origin, exclusive biomarkers to distinguish CF from other cells are not available. Several markers have been studied and are still in analysis such as transforming co-factor 21 (TCF-21), vimentin, platelet-derived growth factor receptor alpha (PDGFR-α), as well as Discoidin Domain Receptor Tyrosine Kinase 2 (DDR2)[52, 61]. The main challenge with these markers is the low sensitivity and medium specificity. TCF21 seems to be more specific to fibroblasts, but not all fibroblasts present this marker while non-fibroblast cells may also exhibit this marker[62, 63]. It is likely that the breadth of fibroblast phenotypes is such that they may be accurately treated as a related group of mesenchymally derived cells.

The characterization of CFs is usually attempted by the cataloging of several specific markers as parameters. This work has led to a novel discussion as to the wide variety of fibroblast sub-types in the heart [8, 52, 61]. Morphologically, CFs are spindle-shaped with an elongated cytoplasm, one or two nucleoli and a central-circular nucleus. Their primary responsibility is the slow turnover and maintenance of the cardiac extracellular matrix. This process involves matrix-metalloproteinases that degrade collagen and stimulate CF synthesis of collagen[57, 59].

Following cardiac injury, CFs are activated to myofibroblasts, and develop an enhanced cytoplasmic space, a complex endoplasmic reticulum, and Golgi apparatus and stress fibres. These characteristics confer the ability to contract and synthesize large amounts of collagen[49, 64, 65]. Myofibroblasts also lack a definitive biomarker, but the problem is addressed by analyzing several markers. Alpha smooth muscle actin (α-SMA) is incorporated in the stress fibres and was one of the first to be described[15, 35, 66, 67]. Other markers are common to CFs and myofibroblasts, such as vimentin and PDGFR-α[9, 45, 68]. The most promising biomarker to date is secreted periostin, a matricellular protein secreted mostly by myofibroblasts but also by other mesenchymal cells, such as vascular smooth muscle cells [69, 70].

Myofibroblasts are the main cells to contribute to cardiac wound healing during scar formation and are activated in the proliferation phase and remain highly active during this stage[14, 16]. However, in the maturation phase, some cardiac myofibroblasts undergo apoptosis, while some persist in the surrounding viable areas, being recently named matrifibrocytes featuring bone and cartilage characteristic [27, 71-74]. The literature reveals some controversy in this respect, as some may contend that cardiac myofibroblasts become senescent after evading apoptosis due to survival signals produced by fibrosed ECM.[8 51, 75, 76].

Pathological cardiac fibrosis is a complex process involving numerous pathways and molecules responsible for CF activation in myofibroblasts. A major pathway involves the TGF-β superfamily, in which TGF-β_1 is the most studied isoform followed by TGF-β_2 and TGF-β_3[77]. The first two isoforms showed early upregulation post-coronary reperfusion murine studies, while TGF-β_3 has a delayed and prolonged elevation[78, 79]. The canonical TGF-β_1 signaling pathway, especially through Smad3 stimulation is closely related to CF[80, 81]. However, in vitro studies showed that TGF-β_3 is found to stimulate Smad7 (a repressor of the canonical pathway),

promoting fibroblast phenotype[82, 83]. Several other non-canonical pathways involved with TGF-β_1 also contribute to myofibroblast activation, such as MAPL/p38, JNK1/2, ERK1/2, Rho GTPase, PI3K/AKT and Hippo[73, 82, 84, 85]. Most of these pathways depend on the biomechanical stressors of ECM stiffening through interaction with integrins capable of stimulating important factors of these signaling pathways[86]. Systemically, the adrenergic system and renin-angiotensin-aldosterone system (RAAS) also contribute to fibroblast activation post cardiac injury[19, 87]. Relatively soft substrate (with low Young's modulus* and low mechanical stress) is an important factor promoting the quiescent fibroblast phenotype[13, 86], and other factors such as ALDH2, SKI, PPR-γ and IFN-γ demonstrated inhibition of myofibroblasts activation [90-93].

1.3.1 α-SMA

The *Acta2* gene contains 10 exons and encodes α-SMA, one out of six main mammalian actin isoforms, which is present in smooth muscles cells and non-muscle cells, such as astrocytes and myofibroblasts [94]. When cardiac fibroblasts activate to myofibroblasts, α-SMA is incorporated into cytoplasmatic stress fibers, which confers contractile properties [67, 95]. These stress fibers are formed by the association of focal adhesion sites with bundles of actin filaments and non-muscle myosin spread along the actin filaments, which constitutes the contractile organelle with contiguous communication to the extracellular matrix (ECM)[94-96]. Actin filaments are composed of the α-actin isoform, and the speed and level of α-SMA incorporation determines the degree of contractility[94, 97].

Myofibroblast contractions occur by lock-step mechanisms where strong and long-ranging contractions take place via RhoA/Rho kinase signalling, followed by calcium

* Young's modulus is defined as measurement of an object's elasticity/stiffness and calculated by the ratio of stress over strain[88, 89].

oscillations leading to short-ranging and low-amplitude contractions. As a result, long-term and irreversible contractions lead to tissue remodelling[98-100].

Several mechanisms are involved in modulating α-SMA synthesis and repression. The most known signalling is RhoA/Rho kinase signaling. Mechanical force activates RhoA and Rho kinase inducing phosphorylation of LIM-kinase, involving cofilin and finally promoting α-SMA synthesis and actin assembly[12, 13, 97, 101]. Along with RhoA/Rho kinase, TGF-β is also involved with α-SMA elevation through ERK 1/2 MAPK signaling and SMAD-dependent pathways[98]. ERK1/2 MAPK, through DDR2, promotes integrin β_1 elevation which stimulates α-SMA synthesis and induces mechanosensitive effectors and YAP to increase collagen production[37, 47, 96]. In a different mechanism, SMAD3 binding elements, such as serum response factor, directly stimulate α-SMA synthesis by binding to the *Acta2* promoter. Ultimately, α-SMA production is suppressed when PPAR-γ and Kruppellike factor-4 inhibit SMAD3 binding sites[99, 102, 103].

1.4 Cardiac Extracellular Matrix

The heart is a high cell density tissue which is enveloped by an intricate biomechanical component called extracellular matrix (ECM). In the past, the ECM was categorized as a structural substrate with the only purpose of giving support for the myocardium and maintaining the cardiac architecture[104]. More recent work, however, has shown the ECM to be a dynamic and active organizational component that interacts with different cells, especially during wound healing[10, 105].

Cardiac cells are in intimate contact with the ECM via integrins and cadherins, which influence cellular response to injury[10, 99, 106]. In cardiac injury, cardiac death and disruption of

ECM architecture regulate several ECM elements, such as collagen, fibronectin, periostin and MMP-14-mediating scar formation[50, 107].

1.4.1 Extra domain A fibronectin (EDA-Fn)

Fibronectin (FN) is a family of alternatively spliced glycoproteins present in soluble and insoluble forms in the plasma and in the ECM, respectively, and first discovered by Richard Hynes in 1973[108-110]. In humans, the gene locus is in chromosome 2 and in mouse, chromosome 1, counting for 46 exons. In both species, it is encoded by a single gene, but several variants are synthesized through alternative mRNA splicing. Fibronectin molecules are composed of covalently bound dimers, which are in turn formed by repeated sequences of fibronectin type I, type II, and type III[111, 112].

The protein diversity, however, is determined by the amount and variety of type III homologous units. This FN Type III consists in two extra-domains, determined by alternative splicing: A and B (ED-A-Fn and ED- B-Fn)[113, 114]. Both extra-domains are present and active during embryogenesis, but in adults they are only present in pathological conditions, where ED–A domain-Fn is elevated in fibrotic conditions while ED-B-Fn is related to tumorigenesis[115].

ED-A domain-Fn participates in the activation of TGF-β_1, and fibroblast activation to myofibroblasts especially in the heart. Several studies have demonstrated that through mechanotransduction[107, 116], ED-A domain-Fn interacts with integrins, such as $\alpha 4\beta 1$ and $\alpha 9\beta 1$, to regulate FN ability to bind to the latent transforming growth factor beta binding protein 1 (LTBP-1) and activate TGF-β_1 which is intimately related to cardiac myofibroblast activation[116, 117].

1.4.2 Fibrillar collagens in the heart

Collagens are abundant molecules in the ECM that maintain tissue structure and interact with different cells, especially during wound healing. They comprise of 28 members divided into two main groups: fibrillar and non-fibrillar molecules[118, 119]. Each collagen is distinct and is comprised of a triple-helix structural shape of repeated peptide sequences (Gly-X-Y), where X and Y are usually proline and hydroxyproline, forming α chains[119-121].

Fibrillar collagens are the most predominant collagen molecules and represented by collagen I, II, III, V and XI, in which fibrillar collagens I and III are the main collagen molecules in the cardiac interstitium[120, 122]. Collagen I is heterotrimeric, composed by two α1 chains and one α2 chain; and it represents the primary collagen in the heart, forming thick fibers configurating a stiffer environment, especially in the epimysium and perimysium [123, 124]. On the contrary, collagen III is homotrimeric with three α1 chains forming thin fibers characterized by its elasticity properties surrounding cardiomyocytes in the endomysium [120, 123, 125]. Non-fibrillar collagens, such as VI and VIII are also important components of the ECM, capable of interacting with collagen I and III to stimulate fibroblast activation and migration[9].

After a cardiac injury, cardiomyocytes cell death rapidly leads to collagen I and III degradation by matrix metalloproteinases (MMPs) such as MMP-1, -8, and -14. To counterbalance this process, tissue inhibitors of metalloproteinases (TIMPs) modulate collagen turnover by regulating MMPs degradation [126, 127].

The subsequent events occur in the granulation phase of the scar formation through myofibroblast secretion of *de novo* ECM, especially collagen III, to form a provisional and elastic matrix that supports cell migration and interaction with several cytokines and growth

factor[128, 129]. As the scar tissue moves to a more mature stage, collagen III is degraded and collagen I synthesis increases, producing a stiffer and more mature matrix[29, 129].

1.4.3 MMP-14

Matrix metalloproteinases (MMPs) are part of the endopeptidase family, which comprises 25 MMPs, of which 19 are soluble and 6 are anchored to the membrane. Some of the soluble and all of the membrane attached MMPs are translocated to the cytoplasm as active enzymes after a protease enzyme called furin cleaves the latent domain in the Golgi apparatus[130-132]. Among transmembrane MMPs, MT1-MMP (or MMP-14) was the first to be identified and it is found to have an important role in cardiac fibrosis[131, 132].

MMP-14 structure is made up of a N-terminus, a catalytic domain, and a C-terminus. The N-terminus contains the domain to maintain MMP-14 in the latent form; the catalytic domain is responsible for breaking down targeted proteins; and the C-terminus has a hemopexin domain which elevates target-specificity by the formation of structures called blades[131, 133, 134]. Blade II is specific to collagen I, creating a triple-helical communication with MMP-14; and blades I and IV create a dimer that supports the interaction with pro-MMP2, leading to its activation mediated by MMP-14 and tissue inhibitor of metalloproteinase 2 (TIMP-2) complex[134, 135]. In a concentration-dependent manner, TIMPs are responsible for MMPs degradation, while TGF-β promotes MMP-2 and MMP-14 synthesis and function[131, 132].

The primary function of MMP-14 is to target collagen I, II, and III, fibronectin, fibrin, laminin 1 and 5 for degradation. This proteolytic role is crucial for the maintenance of a physiological and pathophysiological cardiac substrate[107, 119, 130, 134]. After a myocardial injury, damaged cardiomyocytes and ECM are removed from the wounded area. For this, MMP-14 is

one of the proteases responsible for collagen degradation whereby leads to myofibroblast synthesis of a provisional matrix followed by matured ECM and cardiac remodelling[105, 136].

1.5 PDGFR-α

The platelet derived growth factor (PDGF) family presents four different ligands: PDGF-A, PDGF-B, PDGF-C, and PDGF-D which form five different dimers, PDGF-AA, PDGF-AB, PDGF-BB, PDGF-CC, and PDGF-DD[137, 138]. PDGF-A and PDGF-B are processed and secreted as active proteins, but PDGF-C and PDGF-D are secreted in a latent form. These dimers activate two separate classes of type III tyrosine kinase receptors: platelet derived growth factor receptor – alpha and – beta (PDGFR-α and PDGFR-β) by structural rearrangement followed by autophosphorylation[139, 140]. Once PDGFR-α is activated, cellular hemostasis is modulated by ECM deposition, cell migration, tissue remodelling, and cell differentiation through regulation of RAS/mitogen-activated protein kinase (MAPK) and AKT/phosphatidylinositol 3-kinase (PI3K) pathways[68, 140-144].

PDGFR-α appears to modulate fibroblast development, representing a biomarker along with TCF-21 and WT-1 to identify cardiac fibroblasts from epicardial origin [27, 56, 62, 63, 71, 125, 145, 146] . However, PDGFR-α is not exclusive to cardiac fibroblasts, being present in several other mesenchymal cells.

At the same time, PDGFR-α also was found to also play a role in cardiac fibrosis. Studies provoking PDGFR-α inhibition had shown reduction of cardiac scar formation in pressure overload animal models[8, 9, 74, 146-148]. Along with these studies, our own recent findings evaluating scar tissue from rats post-MI showed significant elevation of PDGFR-α protein and a modest (not statistically significant) elevation in viable tissue from post-MI hearts as well[149]. These

results are in accordance with the findings of elevated presence of PDGFR-α in activated fibroblasts, and it indicates PDGFR-α importance in cardiac fibrosis[28, 58, 73, 76, 149, 150].

1.6 Pro-fibrotic cytokine signaling pathways

1.6.1 TGF-β_1 pathway

The transcriptional growth factor beta (TGF-β) superfamily is comprised of approximately 33 genes transcribed within monocytes, cardiomyocytes, fibroblasts, and immune cells to synthesize several proteins, including TGF-β_1, TGF-β_2, TGF-β_3, bone morphogenetic proteins (BMP), growth differentiation factors (GDF), activins and inhibins[74, 79, 151]. This superfamily holds pleiotropic functions in embryos and in adults, modulating cell proliferation, migration, and differentiation, as well as promoting tissue remodeling such as cardiac fibrosis[42, 152, 153].

In the context of cardiac fibrosis, TGF-β_1 is the most studied isoform and while TGF-β_2 and TGF-β_3 have shown to be elevated following coronary reperfusion little is known about their specific function[77, 79, 80, 83]. TGF-β_1 which is known to promote collagen synthesis and fibroblast activation in hypercontractile myofibroblasts[154-156]. Initially, TGF-β_1 is synthesized in a latent form by being bound to latency-associated peptide (LAP), thereby constituting the small latent complex. Following its synthesis, TGF-β_1 secretion is regulated by the formation of the large latent complex by binding to latent TGF-β binding protein (LTBP) which assists TGF-β_1 folding and secretion into the EMC where it retains its latent form while anchored to ECM elements (Figure 1.7.1)[37, 84, 157].

After a cardiac injury, TGF-β_1 will be activated by chemical and mechanical stimuli. Heat, release of reactive oxygen species and consequent lowering of pH, as well as mechanical stress and proteolysis mediated by proteases such as MMP and matricellular proteins stimulate TGF-β_1 detachment from latency proteins[133, 158, 159].Once TGF-β_1 is activated, it binds to a complex of transmembrane serine/threonine receptors formed by two TGF-β receptor type II (TβRII) and two TGF-β receptor type I (known as ALK-5). Initially, the canonical pathway is triggered as TGF-β_1 binds to TβRII which later phosphorylates ALK-5[79, 105]. In the cytoplasm, ALK-5 interacts and induces the phosphorylation of receptor-activated Smads (Sma and mothers against decapentaplegic (Mad) proteins, known as R-Smads) represented by Smad 2 and Smad3. Subsequently, phosphorylated R-Smads form a complex with common Smad (Smad4 known as Co-Smad) in the cytoplasm which is translocated via MH2 domain activity[79, 160, 161]. Once in the nucleus, MH1 domain binds to Smad-binding elements (SBE), promoting transcription of gene targets, including α-SMA, EDA-Fn, and collagens, modulating cardiac fibrosis (Figure 1.7.1)[93, 99, 153].

This process can be inhibited by several proteins, including SKI and inhibitory Smads (Smad 6 and 7)[72, 91, 162, 163]. SKI supressing function will be described in the next sections, but it is known that Smad7 competes for ALK-5 binding sites with Smad2 and Smad3, repressing R-Smads phosphorylation, as well as promoting degradation of the same complex (ALK-5-Smad2/3) through ubiquitination[72, 80].

TGF-β_1 also interacts with other non-Smad-dependents pathways, represented by MAPK-ERK, p38/MAPK, PI3K-AK-mTOR, Rho/RhoA kinase, Jun kinase, Wnt and Hippo pathways[50, 84, 164, 165]. The last two have been more extensively studied, showing that TGF-β_1 overexpression increases β-catenin stability and translocation to the nucleus, while stimulation of TAZ and

WNT3a induces TGF-β_1 elevation by inducing Smad complex to be shuttled to the nucleus[164, 166].

1.6.2 Hippo Pathway

The Hippo pathway signaling was initially studied in *Drosophila* to modulate organogenesis. Later, it was found to also be involved in tumorigenesis and fibrosis[62, 146, 149]. The activation of this pathway starts with macrophage stimulating 1 and 2 (MST1/2) phosphorylation, which recruits Salvador-like homolog (SAV1) to form a complex, followed by phosphorylation of large tumor suppressor (LATS1/2), specially LATS2[167, 168]. Activated LATS1/2 forms a complex by binding to Mps One Binder kinase (MOB1) which then phosphorylates yes-associated protein (YAP), and transcription co-activator with a PDZ motif (TAZ, also called WW domain-containing transcriptional regulator 1 – WWTR1) to be sequestrated to the cytoplasm, undergo ubiquitination and proteasomal degradation[164, 168]. This pathway is deactivated by LIM proteins, such as LIMD1, which binds to LATS1/2 and inhibits YAP/TAZ phosphorylation. Instead, they are translocated to the nucleus, to bind to TEA domain and promote transcription of targeted genes[164, 169].

In the heart, YAP and TAZ have been demonstrated to promote cardiac fibrosis [15, 145]. YAP and TAZ translocation to the nucleus seems to be directly involved to the level of stiffness of the substrate[55, 73, 170]. During wound healing, YAP/TAZ mechanically sense ECM stiffening along with mechanical tension by interacting with integrins, F-actin, and Rho/GTase[76, 106, 171]. This interaction stimulates them to be shuttled to the nucleus to regulate pro-fibrotic transcriptional factors, such as connective tissue growth factor (CTGF)[172].

The Hippo pathway interacts with several other pathways and molecules. As Wnt signaling interacts with β-catenin, TAZ is induced to translocate to the nucleus and promote cardiac fibrosis and cardiac fibroblast activation[149,85, 173, 174,162]. Alongside, TAZ appears to interact with Smad2/3-Smad4 complex to enhance collagen transcription in the canonical TGF-β_1 pathway. [149,153,85, 173, 174]. On the other hand, TAZ activity seems to be repressed as SKI interacts and promotes the Hippo pathway. SKI modulates LIMD1 function, which inhibits its repressive role in the Hippo pathway, leading to TAZ degradation[70, 85, 164, 168, 175-177].

1.7 SKI

Ski (Sloan-Kettering Institute) is a proto-oncogene first discovered in avian sarcoma virus in the Sloan-Kettering Institute in the late 80's, where it was identified to promote oncogenic transformation of chicken fibroblasts[178-180]. SKI protein belongs to a superfamily of transcription co-regulators with 13 members along with SKI-related novel protein N (SnoN) as SKI's closest "relative"[162, 163, 181].

The *Ski* gene locus is found on chromosome 1 in humans and 4 in mouse, being encoded by 7 exons and translating approximately 728 amino acids. The protein half-life is approximately 100 minutes in lung epithelial cells and is 90 kDa in size[182-184]. The majority of SKI is translated by the full-length of the DNA sequence, being called *Ski* transcript variant 1 (*Ski tv1*). However, a minority of SKI protein copies do not possess exon 2 (*Ski tv2*), they represent a shorter variant with 60 kDa, but remain functional. However, there is a lack of studies evaluating the functionality of this splicing variant and confirming their presence in different cells and tissues[85].

SKI is a ubiquitous protein, being present in most tissues, and participating in the embryological formation of skeletal muscle and neurodevelopment. Its primary functions are

related to cell proliferation and differentiation, depending on its subcellular location, which cell type and if in healthy or injured tissues[185-187]. SKI is considered a predominantly nuclear protein, as most studies demonstrate SKI to play the role of a nuclear repressor[181, 182]. However, SKI has been found in the cytoplasm in invasive and metastatic melanoma cells and may serve to retain Smads in the cytoplasm[182, 184, 188]. SKI has also shown to be promote and repress several cancers, such as esophageal squamous cell carcinoma, estrogen receptor-positive breast carcinoma, colorectal carcinoma, melanoma, as well as metastatic conditions. On the other hand, SKI has been found to modulate lung, renal, and cardiac fibrosis[175, 182, 187, 189-194].

In cardiac fibrosis, SKI inhibits TGF-β_1 pathway through Smad-dependent and independent mechanisms; and represses fibrotic tissue deposition[195, 196]. In the nucleus, SKI forms homodimers/trimers or heterodimers/trimers with itself or with SnoN through C-terminus dimerization sites[197, 198]. These oligomers interact with R-Smad/Co-Smad complex via the I-loop in the SAND-like domain and N-terminus recognition sites; recruiting nuclear co-repressors (Ncor) and histone deacetylases (HDAC) to form a complex that disrupts R-Smad/Co-Smad complex (Figure 1.7.1) [175, 183, 194, 199-201].

Despite initial studies only focusing on the nuclear role of SKI, recent studies have demonstrated SKI function in the cytosol. SKI can inhibit Smad 2/3 phosphorylation in the cytoplasm, as well as blocking TGF-β_1 receptor I[181, 200].

TGF-β_1 is also repressed by different pathways: SKI interacts with c-Jun N-terminal kinase (JNK) and forms a complex with c-Jun to inhibit Smad 2 activity[202]. SKI also supresses Zeb2 to stimulate Meox2 and promote fibroblast phenotype[202, 203]. Likewise, the Hippo pathway is regulated by SKI interaction with LIMD1 whereby increasing LATS2 reduces TAZ protein activity in rat cardiac fibroblasts overexpressing SKI[85, 162, 168, 175].

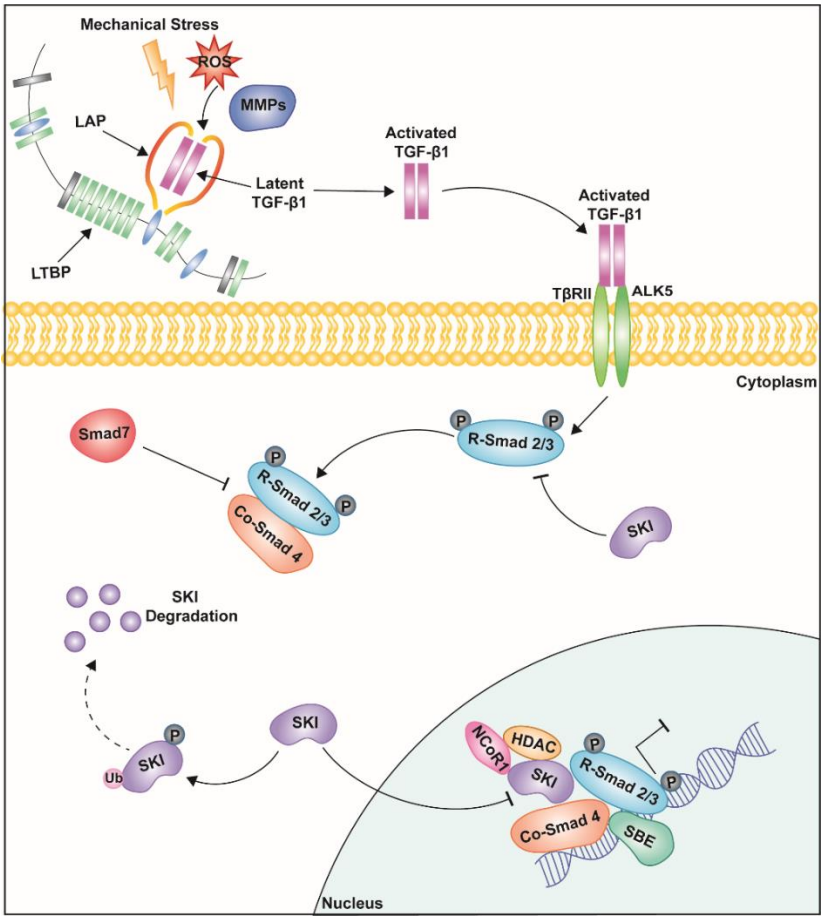

Figure 1.7.1 ***Role of SKI in TGFβ_1 signalling.***
TGFβ_1 is present in latent form and is bound to LAP and LTBP. Several factors including mechanical stress, low pH, the release of ROS and MMPs stimulate TGFβ_1 activation. Following its activation, it binds to two receptors (TβRII and ALK5) which induces R-Smad2/3 phosphorylation in the cytoplasm. Phosphorylated R-Smad 2/3 forms a complex with Co-Smad 4 which is translocated to the nucleus where it binds to SBE to promote transcription of fibrotic co-factors. This process can be repressed by Smad 7 (and Smad 6) inhibiting the Smad complex in the cytosol and by SKI which inhibits R-Smad 2/3 phosphorylation in the cytoplasm. In the nucleus SKI recruits NCoR1 and HDAC to form a complex and disrupt R-Smad 2/3/Co-Smad 4 complex. TGFβ_1: Transforming Growth Factor Beta 1; LAP: Latency-Associated Peptide; LTBP: Latent TGFβ Binding Protein; ROS: Reactive Oxygen Species; MMPs: Matrix Metalloproteinases; TβRII: TGF-β Receptor II; ALK5: Activin Receptor-like Kinase 5; R-Smad

2/3: Receptor Smad 2/3; Co-Smad 4: Common Smad 4; SKI: Sloan-Kettering Institute; NCoR1: Nuclear Receptor Corepressor; HDAC: Histone Deacetylase.

Previous studies with SKI overexpression in rat cardiac fibroblasts have shown to reduce myofibroblast contractility and promote apoptosis through inhibition of autophagy[204]. One of the most relevant findings about SKI function is related to its ability to revert cardiac myofibroblasts to fibroblasts by reducing α-SMA, EDA-Fn, and synthesis of collagen I[91, 205, 206]. In these same studies, SKI protein size varied from 95 kDa, 105 kDa and 115 kDa, as well its function in these different sizes. 95 kDa SKI showed to be elevated in the nucleus after 48h TGF-β_1 stimulation[90]. In the contrary, 105 kDa appeared to be increased in the cytoplasm from 48h to 4 weeks post-MI in rats[90, 149]. In this context, SKI is suggested to be elevated by being entrapped in the cytoplasm during cardiac wound healing while the variation in protein size and localization is believed to be caused by post-translational modifications such as phosphorylation, ubiquitination, and/or interaction with proteins such as C184M[54]. In addition, *Ski* gene expression has been demonstrated to be downregulated by the interaction of miR-21 with the p38/MAPK pathway in vascular smooth muscle cells, as well as in leukemia by miR-29 activity and in vascular endothelial cells by miR-155[91, 207-210].

SKI knockdown has also been explored in some recent published research. In humans, mutations deleting a12 base pair mutation in the R-Smad binding domains in exon 1 cause Shprintzen-Goldberg syndrome, a rare autosomal-dominant disease marked by craniofacial and neural malformations[153, 211, 212]. The clinical presentation is characterized by facial dysmorphism with exophatlmos, micrognathia or retrognathia; craniosynostosis, recurrent hernias, Marfan-like features such as arachnodactyly, hypertelorism, pectus deformity and scoliosis[85, 212]. Intellectual disability and epileptic seizures are also present, as well as some cases of valvular and aortic

malformations[168, 213, 214]. Unfortunately, treatment is limited, which results in life expectancy of approximately 40 years old.

Murine studies inducing *Ski* deletion or mutation are limited because *Ski* embryonic manipulation is lethal due to severe neural, craniofacial, and muscular malformations[169, 212]. For that reason, *in vitro* studies are largely used to study SKI knockout. *Ski* deletion in intervertebral disc degeneration mediated by lentivirus demonstrated inhibition of MMPs and apoptosis through regulation of Wnt/β-catenin pathway. Induction of apoptosis was also found in cancer, whereby osteosarcoma cell migration and proliferation were supressed by *Ski* knockdown[215 216]. Moreover, in vascular smooth muscle cell lines, *Ski* knockdown via RNAi induces autophagy and repression of α-SMA[207, 208]. However, other studies that employed the tactic of supressing *Ski* through shRNA showed reduction of rat cardiomyocyte cell line proliferation or induction of transformation to myofibroblasts with elevated α-SMA[217]. While these studies are encouraging, they only begin to address the broad impact of SKI's function and thus further study is needed to understand the effects of SKI loss in various mammalian cells.

1.8 Cre-LoxP

Genetic engineering has existed for more than half a century. Since then, a great depth of knowledge has been acquired[218, 219]. The Cre-LoxP system was discovered in bacteriophage P1 and developed in the early 1990s to promote specific gene manipulation, causing activation or deletion of targeted genes[220, 221]. Initially, the focus was the construction of embryonic stem cell mutations, which demonstrated to be successful, however roughly 30% of those mutations led to neonatal death[220, 222]. Over time, conditional and inducible models added more complexity to this system. The conditional component refers to cell or tissue-specificity, where Cre recombinase

sequence is incorporated to a unique promoter to target only a particular cell population; while the inducible portion controls the temporal aspect of the mutation[223, 224].

In a conditional-inducible knockdown model using Cre-LoxP system, the cassette sequence containing Cre recombinase sequence which represents a 38 kDa protein is inserted to a cell-specific promoter in a mouse line and bound to an estrogen-receptor (ER) ligand-binding domain at the C-terminus and N-terminus (MerCreMer). This cassette remains inactive, until 4-hydroxytamoxifen (4TH) or tetracycline (Tc) is added to the system to release Cre recombinase[225, 226]. In a different mouse line, locus of X-over P1 (LoxP) palindromic sequence constitutes a 34bp sequence, formed by two 13bp repeated inverted sequences linked by an 8bp unique sequence[223, 225, 227, 228]. LoxP sites should be inserted in the introns before and after the critical exon to be flanked (floxed-gene). The critical exon is usually chosen based on the size and position in the gene sequence. This exon is frequently the next one after exon 1 which provides enough space in the intron for the cassette containing LoxP sequence to be inserted[229, 230].

The following step is breeding these two different mouse lines, one containing MerCreMer related to a cell-, tissue-specific promoter and the second one, flanking the target gene with LoxP sites[231, 232]. These animals, then, present two different mutations, but with a normal embryogenic development. Once, 4TH or Tc is administrated by intraperitoneal injections, gavage, water, or food, it recognizes ER sites which activates Cre recombinase, thus recognizing LoxP sequence sites, and triggering the excision or inversion of the flanked exons[224, 233]. The outcome is determined by the direction of both LoxP sequences. If they are positioned in the same direction, the critical exon will be completely excised from the genome and form a circular DNA, which will be dissipated and further degraded[234, 235]. If LoxP sites are in opposite

positions, the targeted exon will be inverted. Both scenarios result in frameshift and creation of a stop codon, which results in absence of protein synthesis or translation of a truncated, non-functional protein[225, 232].

Another known technique to deliver Cre-recombinase, without the use of 4TH or Tc, is the overexpression of Cre recombinase via a viral vector[235-238]. This method skips a few steps and is easily manipulated in cell culture[239]. However, both drug- or viral- Cre recombinase induction are not without risks and side effects. Cre recombinase and tamoxifen are recognized for their cell and tissue toxicity. Both interfere with gene expression, cell viability and heart function [236, 237, 240-245].

Chapter 2: Rationale, Hypothesis, and Objectives

2.1 Study Rationale

Heart failure is defined as a complex clinical syndrome emerging from a major adverse cardiac event, such as myocardial infarction, chronic hypertension, and valvular disease. Cardiac damage in these disease aetiologies is closely associated with cardiac fibrosis which (since the late 2000's) is included among the primary underlying cause of HF[22, 246-248]. According to the Heart & Stroke Foundation, HF affects more than 6.2 million Americans and close to 600,000 Canadians, with an incidence of 21 cases per 1000 people[23, 24, 249]. Globally, the prevalence varies between 1-2%, however, some regions such as Sub-Saharan Africa and the Middle East are underrepresented[21, 250]. In North America, minority groups such as Canadian and American First Nations, African Americans are considered higher risk groups for developing the disease when compared to Caucasians[251-253]. In addition, sex appears to interfere with risk of HF, males are at higher risk of developing HF until 65 years old, whereas women start being at risk at 65 years old (paralleling that in men at the age of 80)[253, 254].

Despite advances in drug-therapy, implementation of novel cardiac devices, and transplantation technology, the mortality rate one year from diagnosis is at 7.2% while the 5-year mortality rate from moment of diagnosis is still 50% [255, 5, 254]. Patients with HF are hospitalized on a recurring basis, present high incidence of depression, isolation, and missing workdays[256, 257]. Annually, HF costs approximately 30 billion dollars for the health system with a predicted increase of 127% by 2030 [24, 258]. In the future, these costs are likely to be increase further because of elevated cases of HF among young people as a sequalae of SARS-CoV2

infection[259-262]. This scenario will increase societal and fiscal burdens for the government managed health system as well as patients, caregivers, and employers[246, 263].

To begin to address this knowledge gap, we began to investigate the role of SKI protein in cardiac fibrosis[54]. SKI overexpression in rat cardiac fibroblasts has been demonstrated to inhibit cardiac fibrosis by negative regulation of TGF-β_1/Smad signalling and deactivation of myofibroblasts (to fibroblasts) [90, 169]. SKI is known to suppress cardiac fibrosis by activation of the Hippo pathway which has also been shown to reduce cellular contractility[85, 168]. However, there is a lack of knowledge about SKI knockdown in cardiac fibrosis.

2.2 Hypothesis

Ski knockdown in primary cardiac myofibroblasts increases gene transcription of Hippo pathway component proteins and fibrosis marker gene transcription. Further, we hypothesize that SKI may exist in two exon splice variants in mouse heart.

2.3 Study Objectives

Objective 1: To establish a reproducible protocol for Ski conditional knockdown.

Unconditional global *Ski* gene knockdown in mice has been shown to cause embryonic lethality. Therefore, we sought to optimize a mouse model wherein *Ski* is conditionally knocked down after normal development in young adult mice. To accomplish this, transgenic mice were produced by the Cre-LoxP system, promoting conditional knockdown through viral overexpression of Cre-recombinase. To monitor the effectiveness, qPCR, PCR and DNA sequencing were performed. By providing a reliable *Ski* knockdown methodology, the goal of determining a novel anti-fibrotic target can be expanded.

Objective 2: To confirm the existence of Ski splice variant in mouse cardiac myofibroblasts.

Ski splice variants have been confirmed in chicken and their presence has been predicted in mammals. However, there is no documentation of distinguished splice variants in mouse cardiac myofibroblasts. To interrogate this, wild-type (non-transgenic) and mice with floxed *Ski* exons 2 and 3 (Ski-floxed mice group, e.g. transgenic mice) were used to analyze the presence/absence of exon 2 through PCR and DNA sequencing. This model represents a first step to allow us to interrogate the issue of *Ski* knockdown and thus derive an understanding of SKI function in the regulation of cardiac fibroblasts cultured *in vitro*.

Chapter 3: Materials and Methods

3.1 *Animal Ethics*

All animal experiments were approved by the University of Manitoba's Office of Research Ethics and followed the regulations of Compliance followed the Canadian Council on Animal Care (CCAC). All protocols were based on standard of operation adopted by our research laboratory, as previously described [90, 168, 264, 265].

3.2 *Transgenic Mouse Model*

Our laboratory obtained two different transgenic mouse lines: a knock-in mouse from Dr. Molkentin's laboratory at Children's Hospital in Cincinnati. This first mouse line has Cre-recombinase tagged to estrogen-like receptor using the periostin promoter to target myofibroblasts. The second component was obtained from Dr. Dietz's laboratory at John Hopkins University and has two LoxP sequences flanking *Ski* exons 2 and 3 (Figure 4.1.1) to cause the knockdown. This model was developed primarily for *in vivo* studies where Cre-recombinase is activated in myofibroblasts upon tamoxifen treatment. However, in the current study we focused on the *in vitro* studies using cultured primary cardiac fibroblasts, and this was to simplify the model system and allow us to focus on fibroblast function *per se*. Ideally, this approach would eliminate the need to treat mice with tamoxifen in vivo to initiate *Ski* knockdown *in vitro*. Thus, to achieve *Ski* knockdown in plated cardiac fibroblasts, we overexpressed Cre-recombinase in vitro using an adenoviral vector for Cre. Therefore, we did not need to invoke the periostin-dependency component of this knockdown model, as we relied upon Cre to directly provide the signal for excision of *Ski* exons 2 and 3 flanked by LoxP

sequences. The transgenic (Ski-floxed) colony started with two females MerCreMer homozygous mice, two males MerCreMer hemizygous mice, and two male Ski-floxed hemizygous mice, which were bred to reach double homozygosity.

3.3 *Study groups*

Cardiac fibroblasts from 8-20 weeks female and males of an independent in-house colony of C57/BL6J mice (initially purchased from JAX laboratories) were labeled as wild-type mice (non-transgenic), as they did not carry the cassette with LoxP flanking *Ski* sequence. These mice were divided into three groups including adenoviral GFP treated, adenoviral Cre treated and untreated. In this manner, we sought to obtain 100% penetrance of the signal for *Ski* knockdown in primary fibroblast cells obtained from our transgenic mouse model. Again, treated samples were transfected with either Ad-GFP (a control group) or Ad-Cre (experimental group) at a multiplicity of infection (MOI) of 50 and harvested 48h, 72h, 96h and 120h post-transfection. Untreated samples (a second control group) were not transfected, and only received fresh medium replaced by serum-free (starvation condition) medium and harvested 24h (designated control for the untreated group), 48h, 72h, 96h and 120h after medium change to evaluate the influence of stiff (e.g., plastic) substrate, which induces mechanical stress and starvation medium on mRNA expression. Primary cardiac fibroblasts from 8 to 20 weeks old from both sexes mixed of C57/BL6J Ski-floxed mice (transgenic mice, double homozygous), have the cassette with LoxP flanking *Ski* sequence, and these cells were transfected with Ad-GFP or Ad-Cre MOI 50 and harvested after 72h post-transfection. Final analysis consisted in three separated analysis: untreated wild-type timepoints relative to 24h post-starving conditions; treated wild-type timepoints relative to sample treated with Ad-GFP as control; and 72h treated wild-type versus

72h Ski-floxed, which included Ad-GFP and Ad-Cre 72h for both groups. Sample sizes varied between 3 and 9 biological replicates per group, with the exception of wild-type Ad-Cre 48h with n of 2.

3.4 *Isolation of Mouse Primary Cardiac Fibroblasts*

Mouse primary cardiac fibroblasts were isolated from C57/BL6J mice 8-20 weeks old with randomized sex. The same procedure was performed for wild-type (non-transgenic) and Ski-floxed (transgenic) animals. They were anesthetized with 3% inhaled isofluorane, and sternotomy was performed after signs of sedation, such as loss of rear foot reflex. Next, the hearts were excised and placed in DMEM/F12 (#11330-032, Gibco) and sterile 1X PBS (Phosphate-buffered saline, pH 7.4). Subsequently, in a 10 cm polystyrene (plastic) plate each heart was infused with 10ml of EDTA buffer (5 mM EDTA, 130 mM NaCl, 5 mM KCl, 500 nM NaH2PO4, 10 mM HEPES, 10 mM Glucose, 10 mM 2,3-Butanedione 2-monoxime, and 10 mM Taurine, pH 7.8), followed by 3 ml of perfusion buffer (1mM MgCl2, 130 mM NaCl, 5 mM KCl, 500 nM NaH2PO4, 10 mM HEPES, 10 mM Glucose, 10 mM 2,3-Butanedione 2-monoxime, and 10 mM Taurine, pH 7.8) and finally 30-40 mL of collagenase buffer (S-MEM (#11380-037, Gibco) supplemented with collagenase type II (330 U/mL, # CLSS-2 Worthington Biochemical Corporation). In this last step, the tissue was triturated using two forceps and incubated in 25 mL of collagenase buffer at 37°C and 5% CO_2 for 30 minutes.

After incubation, the cell suspension was further minced by aspirating it several times with a 10 mL serological pipette, then transferred to a 50 mL conical tube containing 10 ml of DMEM/F12 (#11330-032, Gibco), supplemented with 10% fetal bovine serum (FBS) (#090150, Multicell), 100 U/mL penicillin-streptomycin (#15140-122, Gibco), and 1μM ascorbic acid to

neutralize the collagenase buffer. Once no large tissue fragments were visible, the suspension was strained using a sterile 40 μm strainer (#22-363-547, Fisherbrand). Next, the cells were centrifuged at 200 x g for 7 min at room temperature. The supernatant was aspirated, and cell pellet resuspended in appropriate volume – usually enough volume to pipette 6-7 mL of cell suspension to each polystyrene cell culture plate. After 3 hours, the medium was replaced by new solution. Following that, the cells were washed once or twice with 1X PBS (pH 7.4), supplemented with 100U/mL anti-anti (10,000 units/mL of penicillin, 10,000 μg/mL of streptomycin, and 25 μg/mL of Amphotericin B, #15240-062, Gibco) and had their medium replaced every day for 2-3 days.

3.5 *Cell Culture and Adenoviral Transfection*

After 6-7 days of isolation, the medium was replaced by serum-free (starving) medium composed of DMEM/F10 (#11550-043, Gibco) supplemented with Insulin-Transferrin-Selenium-Sodium Pyruvate (ITS-A; #51300-044, Thermo Fisher), and 100U/mL penicillin-streptomycin, without FBS supplement. Finally, unpassaged cells (P0) from the treated groups were transfected with Ad-GFP (as control) or Ad-Cre (as experimental group) with multiplicity of infection (MOI) 50. Treated wild-type cardiac fibroblasts were harvested at 24h, 48h, 72h, 96h and 120h post- transfection, considering 72h as standard for most comparisons, while Ski-floxed cardiac fibroblasts were solely harvested at 72h post-transfection.

Both adenoviral vectors were designed using CMV promoter in *E. coli.* Our lab generated Ad-eGFP using Adeno-X Expression System (Takara Bio Inc., Kusatu, Japan) while adenoviral construct overexpressing Cre was generated by VectorBuilder Inc. (Chicago, IL). Both constructs were sequenced at The Centre for Applied Genomics (TCAG, Hospital for Sick

Children, Toronto, ON) and titrated by Adeno-X Rapid Titer Method (#PT3651-1, Takara Bio Inc., Kusatsu, Japan). This method uses HEK293A monolayers to be infected through adenoviral hexon protein and detected by an indirect cell-based ELISA. The antibodies used were mouse anti-Adenovirus Type 1 Hexon (Invitrogen, #MA1-82982) and peroxidase goat anti-mouse (Jackson ImmunoResearch, #115-035-003); chromogenic detection was performed using DAB substrate (Thermo Scientific, #34002). All constructs and their sources are listed below:

Table 3.5 1: List of Adenoviral Constructs

Construct	Gene Product	Source
Adeno-X-eGFP	*E. coli GFP* (NP_414878.1)	Dixon Lab
Ad-eGFP-Cre [SV40NLS]	*E. coli* Cre (NP_414878.1)	Vector Builder Inc.

A.

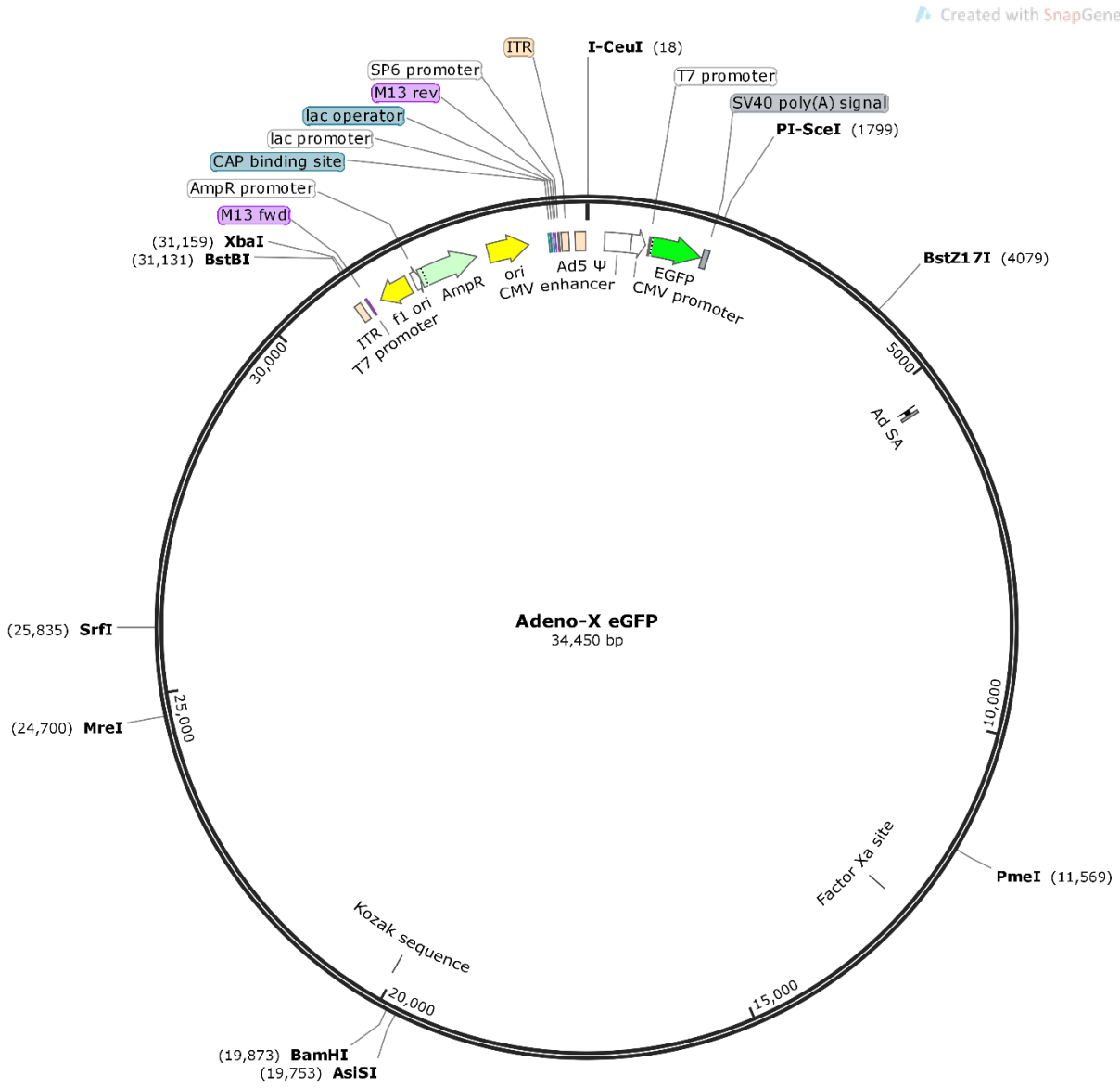
Created with SnapGene®
ITR
I-CeuI (18)
SP6 promoter
T7 promoter
M13 rev
SV40 poly(A) signal
lac operator
PI-SceI (1799)
lac promoter
CAP binding site
AmpR promoter
M13 fwd
(31,159) XbaI
(31,131) BstBI
BstZ17I (4079)
ITR
T7 promoter
f1 ori
AmpR
ori
CMV enhancer
Ad5 Ψ
EGFP
CMV promoter
30,000
5000
Ad SA
Adeno-X eGFP
34,450 bp
(25,835) SrfI
(24,700) MreI
25,000
10,000
Factor Xa site
PmeI (11,569)
Kozak sequence
20,000
15,000
(19,873) BamHI
(19,753) AsiSI

B.

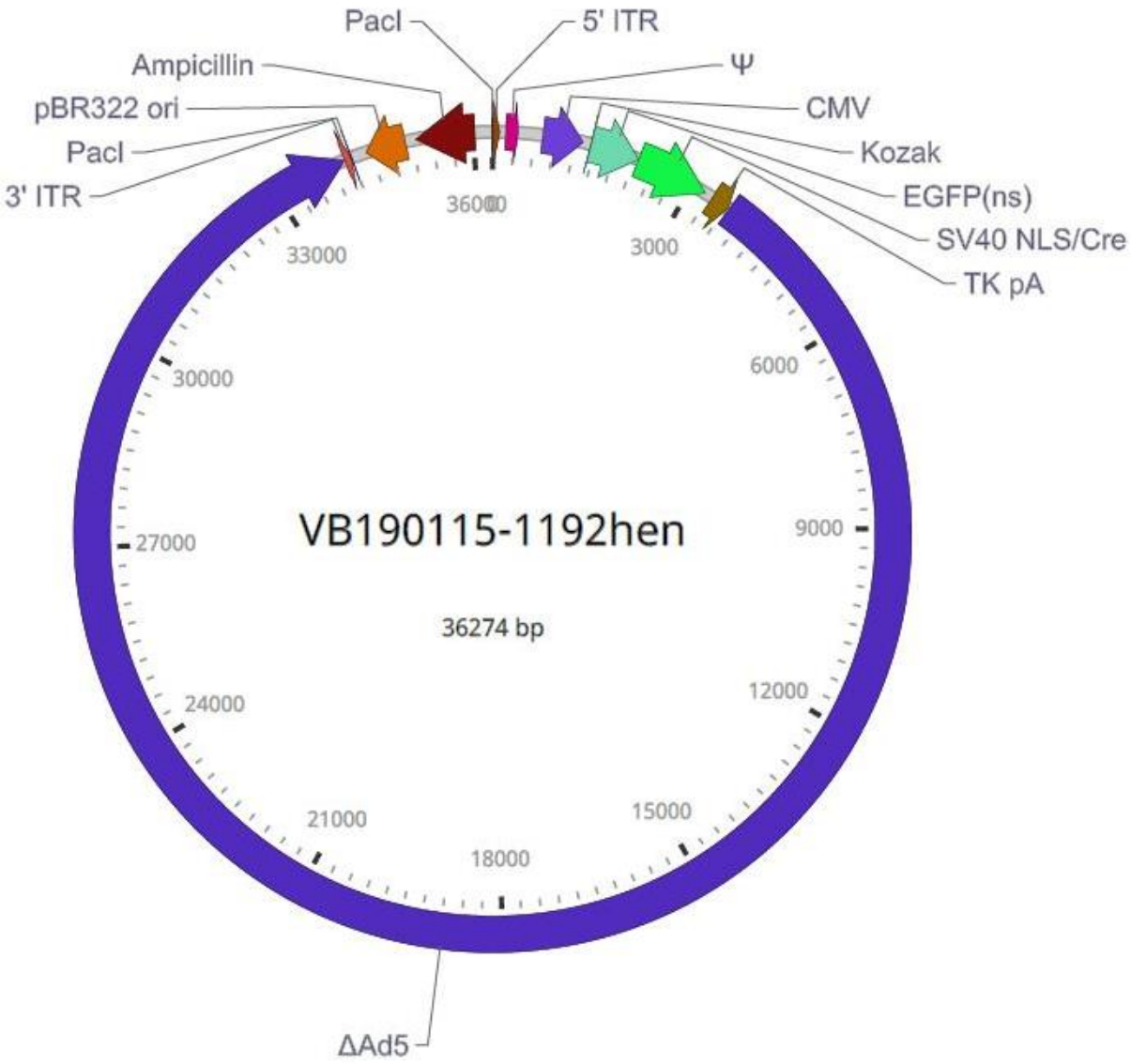

Figure 3.5.1 ***Vector Maps***
A. The vector map represents Adeno-X eGFP structure. The image was created using SnapGene® software (from Insightful Science; available at snapgene.com). **B.** The vector map represents Ad-eGFP-Cre [SV40NLS]. The image was created by VectorBuilder Inc.

After 72h of transfection, all Ski-floxed cells were harvested and wild-type cells were harvested 24h, 48h, 72h, 96h and 120h after transfection or simply change to cell starvation media (serum-free media), to assess Cre toxicity or solely the effects of plating cells in plastic culture plates and starvation conditions, according with their assigned experimental group. After a second wash with sterile 1X PBS; 3 mL of 0.25% Trypsin-EDTA (#25200-072, Gibco) was pipetted unto the cells and incubated at 37℃ and 5% CO2 for 1-1.5 minute followed by neutralization with 7 mL of DMEM/F12 (#11330-032, Gibco), supplemented with 10% FBS (#090150, Multicell). The cells were pipetted to a 10 mL conical tube and centrifuged at 200 x g for 7 min at room temperature. The supernatant was aspirated, leaving approximately 0.5 mL. Next, the pellet was resuspended in 500 μL of sterile 1X PBS and transferred to a 1.5mL tube to be centrifuged at 200 x g for 10 min at 4℃. The supernatant was vacuumed, and the pellet was stored at -80℃ before being used for RNA and gDNA isolation.

3.6 *RNA and gDNA isolation*

All RNA and DNA experiments were performed after sanitization of materials and bench with 100% ethanol and RNase away buffer. RNA extraction was performed using Total RNA Miniprep Kit (#T2010, New England Biolabs) and following manufacture's protocol. All centrifugation spins were performed at 16,000 x g. Initially cell pellets were resuspended in 600 μL of RNA lysis buffer and then transferred to gDNA removal column to be centrifuged for 30 seconds. Following that, 600 μL of 100% sterile anhydrous ethanol was added and mixed by pipetting. The mix was transferred to an RNA purification column and span for 30 seconds. Next, the column was washed with 500 μL RNA wash buffer and centrifuged for 30 seconds, discarding the supernatant. A mix of 5 μL of DNase I and 75 μL DNase reaction buffer for each

sample as added directly to the column and incubated for 15 minutes at room temperature. The samples were primed by pipetting 500 μL RNA priming buffer, followed by centrifugation for 30 seconds. Next, 500 μL RNA wash buffer was added for 30 seconds, followed by a second wash and 2 minutes of centrifugation. Finally, between 30-100 μL nuclease-free water (#AM9937, Ambion™) was directly added to the column and incubated for 5 minutes at room temperature. Samples for immediate use were stored at 4℃ and for long-term storage at -80℃.

Complementary DNA (cDNA) was synthesized using Maxima First Strand cDNA Synthesis Kit for RT-qPCR (which contains Oligo$(dT)_{18}$ and hexamer primers, #K1672, Thermo Scientific) and following manufacture protocol. Initially, RNA extracts were quantified through NanoDrop™ Lite Spectrophotometer (Thermo Scientific). In a 1.5 mL sterile microcentrifuge tube, 1μL of 10x dsDNase buffer, 1μL of dsDNase, volume corresponding to 100 ng of RNA for each sample and nuclease-free water (#AM9937, Ambion™) to reach 10 μL were added. The mix was briefly centrifuged and incubated for 2 minutes at 37℃. Next, 4μL of 5x Reaction Mix, 2 μL of Maxima enzyme mix and 4 μL of nuclease-free water (#AM9937, Ambion™) were added, centrifuged, and then incubated for 10 minutes at room temperature, 15 minutes at 50℃ and finally 5 minutes at 85℃. Samples were eluded in 180 μL of sterile TE buffer (10 mM Tris-HCl, 1 mM EDTA, pH 8.0) and stored at 4℃ for immediate use and at -80℃ for long-term storage.

gDNA extraction was performed using DNeasy® Blood & Tissue Kit and following manufacture protocol (#69504, QIAquick). Cells were centrifuged for 5 minutes at 300 x g, and the pellet resuspended in 200 μL 1X PBS. Next, 20uL of Proteinase K and 100 mg/mL RNase A were added and incubated at room temperature for 2 minutes. Subsequently, 200 μL Buffer AL was added, then mixed and incubated at 56℃ for 10 minutes. Following, 200 μL 100% sterile

ethanol was added, vortexed and centrifuged at 20,000 x g for 1 minute, discarding the flow-through. Then, 500 μL Buffer AW1 was added, centrifuged at 20,000 x g for 1 min, followed by adding 500 μL Buffer AW2 and centrifugation for 3 minutes at 20,000 x g, discarding the flow-through. The column was transferred to a 1.5 mL microcentrifuge tube, and the samples were eluted by adding 50 μL nuclease-free water (#AM9937, Ambion^{TM}) directly to the column membrane and incubated for 5 minutes at room temperature. Absorbance and concentration were verified using GeneQuant III, Biochrom.

3.7 *Quantitative PCR*

Two-step qPCR was performed using QuantStudio 3 Thermo Fisher thermocycler (Applied Biosystems, Foster City, CA). Settings were changed to use comparative-Ct-SYBR, in the fast-cycling mode. qPCR reactions were prepared following Luna® Universal qPCR Master Mix (#M3003S, New England Biolabs, Ipswich, MA) protocol, using approximately 20 ng of cDNA as template, and 200 nM of each forward and reverse primers to achieve a final volume of 10μL. The qPCR program was set up as follows: initial denaturation at 95℃ for 60 seconds, followed by 40 cycles of denaturation at 95℃ for 15 seconds/each, and extension at 60℃ for 30 seconds. A continuous melt curve was then produced from 60℃ to 95℃ for approximately 20 seconds. The relative gene expression (fold-change) was calculated following $2^{-\Delta\Delta Ct}$ method[266] using Tyrosine 3-monooxygenase/ Tryptophan 5-monooxygenase Activation protein Zeta (*Ywhaz*) and Hypoxanthine-Guanine Phosphoribosyltransferase (*Hprt1*) housekeeping genes for normalization, and relative to the designated group controls. Below is a list of primer pairs and respective gene/exon targets.

Table 3.7 1: List of primer pairs used in quantitative PCR and regular PCR.

Gene/Exon	Accession	Forward Primer (5'-3')	Reverse Primer (5'-3')
Hprt1	NM_013556.2	CTCATGGACTGATTATGGACAGGAC	GCAGGTCAGCAAAGAACTTATAGCC
Ywhaz	NM_011740.3	TTGAGCAGAAGACGGAAGGT	GAAGCATTGGGGATCAAGAA
Ski Exon 1	NM_011385.2	TGTGAGACCGTGCTGGAAG	ATCGCACACGGAGTTGATCT
Ski Exon 1-2	NM_011385.2	TGTGAGACCGTGCTGGAAG	GTGTCGTCTGTTTTGGGTCT
Ski Exon 1-3	NM_011385.2	TGTGAGACCGTGCTGGAAG	CGAATCAAAGCTGGGAGGTG
Ski Exon 1-4	NM_011385.2	TGTGAGACCGTGCTGGAAG	GGGCCTCAGAATCCTTGTC
Ski Exon 2-3	NM_011385.2	AGCAGTCCACTTGGCTGCG	CGAATCAAAGCTGGGAGGTG
Ski Exon 4-5	NM_011385.2	GGGCACCAGAGCCTCTTAC	TTGCCGCAGGTGCTCCAAC
Ski Exon 6	NM_011385.2	AGGCCAAGCGCAGTTTGAG	CTGAGTACTTGGCACGCAG
Ski Exon 7	NM_011385.2	GAGCAGCTTCGAGCTGACC	CCAGCTCAGCGTTGCTCTC
Col1a1	NM_007742.4	TGCTCCTCTTAGGGGCCA	CGTCTCACCATTAGGGACCCT
Col3a1	NM_009930.2	GGTTTCTTCTCACCCTGCTTC	GGTTCTGGCTTCCAGACATC
Pdgfra	NM_001083316.2	TCCTTCTACCACCTCAGCGAG	CCGGATGGTCACTCTTTAGGAAG
Acta2	NM_007392.3	GTCCCAGACATCAGGGAGTAA	TCGGATACTTCAGCGTCAGGA
Fn-1	NM_010233.2	ACTGCAGTGACCAACATTGATC	CACCCTGTACCTGGAAACTTGC
Mmp14	NM_008608.4	CCCTAGGCCTGGAACATTCT	TTTGGGCTTATCTGGGACAG
Yap1	NM_001171147.1	CAGACAACAACATGGCAGGAC	CTTGCTCCCATCCATCAGGAAG
Taz	NM_001168281.1	CAGCAACATGGACGAGATGG	AGGTTAGAAAGGGCTCGCTT
Limd1	NM_013860.2	GAGAGATGGATGCTCACCCC	GTAGAGATCTCCCATGGCCT
Lats2	NM_015771.2	GGACCCCAGGAATGAGCAG	CCTCGTAGTTTGCACCACC
Postn Wt	PMID: 27447449	TCTGTAAGGCCATCGCAAGCT	AATAAGTAAAACAGCTCCCCT
Postn Mut	PMID: 27447449	GGTGGGACATTTGAGTTGCT	AATAAGTAAAACAGCTCCCCT
Ski Flox	MGI: 98310 Project ID: 71569	GAGGTGTGTCATGATCCTTCAAGC	ACTGGATCATCGTAACTCCACAGC

3.8 *PCR and DNA Sequencing*

Regular PCR was performed using QuantStudio 3 Thermo Fisher thermocycler (Applied Biosystems, Foster City, CA). Cycling settings were adjusted as follows: 35 cycles of denaturation for 40 seconds, followed by 20 seconds of annealing and 30 seconds for extension phase. Each reaction had a final volume of 25 μL, composed of 1X Q5 DNA Polymerase Buffer (#B9027S, New England Biolabs) and Enhancer (#B9028A, New England Biolabs) , 50 ng of gDNA and 1 μg of cDNA as template, 200 μM of dNTP (Deoxynucleotide Solution Mix, #N0447S, New England Biolabs), 0.5U of Q5 DNA Polymerase (#M0491S, New England

Biolabs) and 250 nM of each forward and reverse primers, and enough nuclease-free water (#AM9937, Ambion™) to reach 25 μL.

Following PCR, an electrophoresis tank, bench, and materials were sterilized with hydrogen peroxide and/or ethanol. Electrophoresis buffer was prepared using 1x TAE buffer (40 mM Tris-acetate, 1 mM EDTA, pH 8) and sterile water. The gel was prepared by using a Bunsen burner to boil 70-120 mL of electrophoresis buffer and powdered agarose (#16500-500, Invitrogen) for 30 seconds to achieve 1-2% agarose gel. 1X SYBR™ Safe DNA Gel Stain (#S33102, Invitrogen) was added at boiling. The solution was poured into the gel molder with proper comb and let it set on the tray for 30-40 minutes. A 6X gel-loading solution was prepared with 18% Ficoll (type 400, #F-2637, Sigma), 0.1% 10% SDS, and 0.25-0.5% xylene cyanol FF (#BP565-10, Fisher BioReagents®) or Orange G (#J62743, Alfa Aesar); and added to each sample. Once set, the gel was loaded with 5-10 μL of DNA ladder (#DM010-R500, Bio-Helix), and sample mix. Electrophoresis was performed at 120V for 50 min to 3 hours. Next, the gels were imaged using ChemiDoc™ Imaging System (BioRad) or prepared to have the band isolated to send the product for DNA sequencing at TCAG.

Using a 11-size scalpel, the bands were excised using UV light to visualize the bands. The products were then sliced, placed in a DNA extraction column (#42600, Millipore) and centrifuged for 10 minutes at 5,000 x g at room temperature. Next, the samples were purified using PCR Purification Kit (#28104, QIAquick) protocol and had their absorbance analyzed through spectrophotometry (GeneQuant III, Biochrom). Finally, the sequencing reactions were prepared for four different conditions by adding only forward, only reverse primers with and without enhancer DMSO (Dimethylsulfoxide). The products were sent to The Centre for Applied

Genomics (TCAG, Hospital for Sick Children, Toronto, ON) for chemical analysis, followed by report analysis using FinchTV software version 1.4.0 (Geospiza. Inc.).

3.9 *Cell Viability Assay*

After 72h of viral transfection, cell viability was analyzed using Live/Dead Viability/ Cytotoxicity Kit (#MP03224, Invitrogen). The cells were washed twice with sterile 1X PBS, followed by addition of 2 μM Calcein-AM (C3100, Invitrogen) and 4 μM ethidium homodimer (E1169, Invitrogen) in 1X PBS for 45 minutes at room temperature and protected from light. Next, 150 μL of sterile 1X PBS was added and the cells were analyzed using FITC (475 to 650 nm emission wavelength) and Texas Red (580 to 604 nm emission wavelength) fluorescence detection channels from Zwiss LSM 5 Pascal microscope and Axio Vison version 4.8.2.0 software.

3.10 *Statistical Analysis*

All statistical analysis and graphs were created using GraphPrism 9.1.2. The graphs are presented as the mean ± standard deviation. Each N value represents experiments performed from one animal. All grouped data was analysed using one-way, two-way ANOVA with Tukey test for multiple comparisons, or multiple unpaired Students t test. All data with one control and one testing condition was analysed using Student's t-test wherein $P \geq 0.05$; *: $P < 0.05$; **: $P < 0.01$; ***: $P < 0.001$; ****: $P < 0.0001$.

Chapter 4: Results

4.1 *Conditional knockdown of Ski is verified at the gene level in our model*

To confirm the position of the cassette in the genomic DNA, mouse *Ski* genomic DNA and mRNA sequences (NC_000070.7 and NM_011385.2) was extracted from NCBI database to identify introns and exons via comparison of genomic DNA and mRNA sequences (Fig. 4.1.1.A). At the same time, the genomic DNA sequence for the cassette containing LoxP sequences inserted in the *Ski* sequence was also identified, as well as each component of this cassette (MGI:98310, Project ID: 71569, Design ID: 270055) (Fig. 4.1.1.B). Initially, the Ski-floxed cassette sequence contained FRTs, LacZ, Neo, and LoxPs, inserted in intron 1 until intron 3 as illustrated in the first line of Figure 4.1.1.B. As these animals were first developed within Dr. Dietz' laboratory, the first two steps showed in Figure 4.1.1, consisting in the insertion of the cassette to flank *Ski* sequence in embryonic cells and the use of flipase to cause the removal of LacZ and Neomycin sequences were already performed before the acquisition of these transgenic mice. Therefore, our experimental group (Ski-floxed mice) only included cardiac fibroblasts from mice with two LoxP sequences, located before exon 2 and immediately after exon 3 (step 3 on Figure 4.1.1.B), which had the deletion activated by overexpression of Cre via adenoviral transfection (step 4) (Fig. 4.1.1.B). However, the complete model also uses a knock-in model with the insertion of Cre recombinase bound to an estrogen-like receptor (MerCreMer) using the periostin promoter to target myofibroblasts. Thus, *in vivo* studies would induce *Ski* knockdown under Cre recombinase activity which would be activated by tamoxifen treatment.

The genotype was analyzed by PCR analysis (Fig. 4.1.2.A), in addition to the penetrance of the mutation in different organs (Fig. 4.1.2.B), using primer sequences provided by Dr.

Molkentin's and Dr. Dietz's laboratories revealed a double homozygous genotype, which means homozygous genotypes for MerCreMer and for Ski-floxed animals. To confirm the position of the Ski-floxed cassette, several PCR reactions were performed that targeted different positions of the cassette, followed by DNA sequencing. The sequencing reports were compared with the genomic sequence for the cassette, which confirmed the location of the cassette: the first LoxP was localized at the end of intron 1 (just before exon 2), and the second LoxP just after exon 3, in the intron 3 as expected.

A.

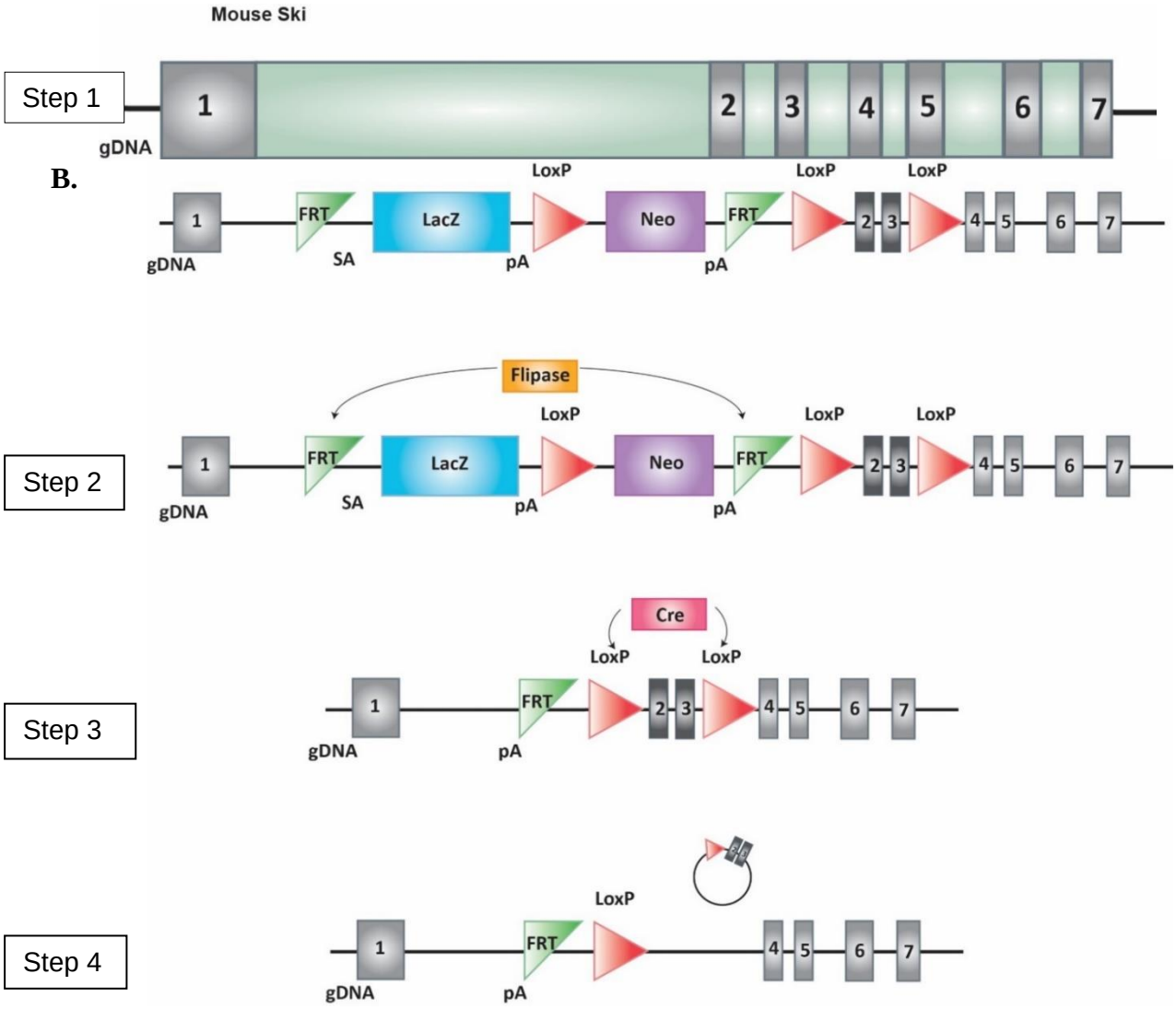

Figure 4.1.1. ***Mouse Ski representative genomic sequence and knockdown model.***
Gray represents exons and green, introns of genomic mouse *Ski* sequence. **B**. **Mouse Ski-Floxed cassette**. Flipase is added to bind and excise the region in between FRTs. Subsequently, Cre recombinase is activated or produced in transgenic mouse cells, binding to LoxP, excising exons 2 and 3. Finally, the excised exons form a circular fragment maintaining one LoxP within it.

A.

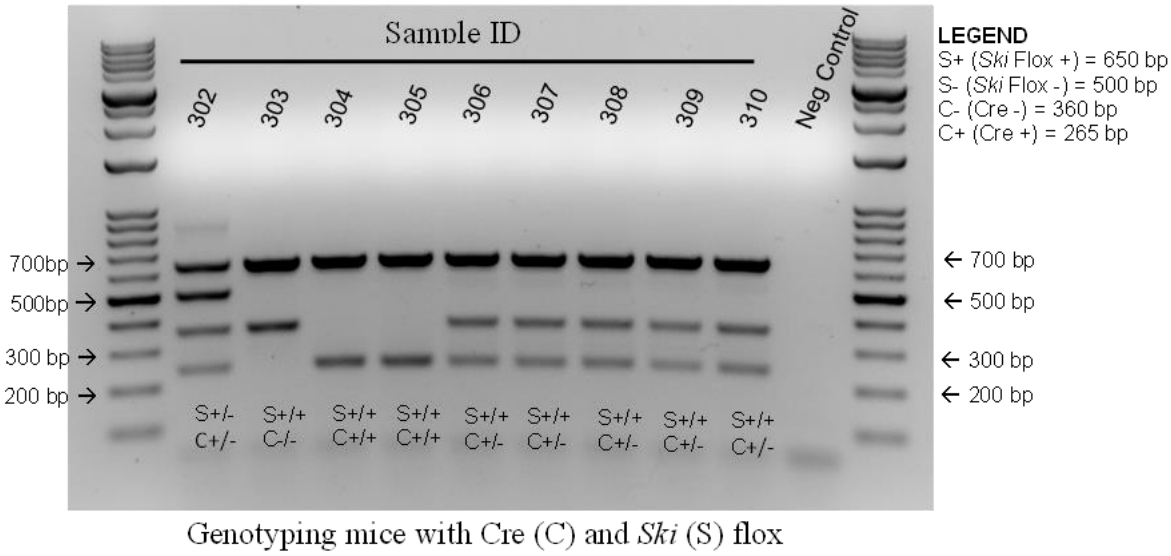

Genotyping mice with Cre (C) and *Ski* (S) flox

B.

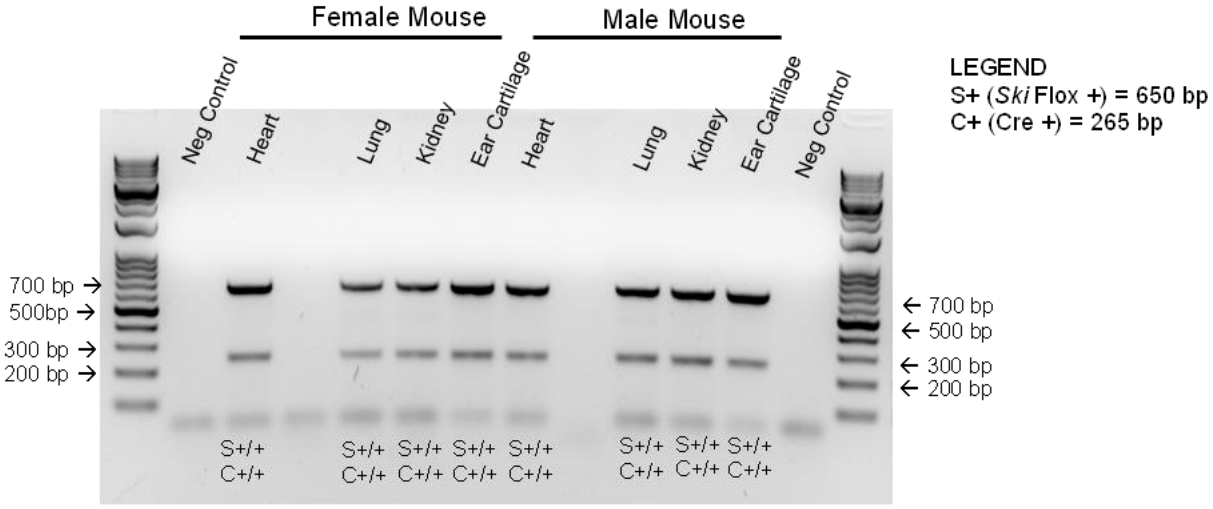

Figure 4.1.2 ***Ski knockdown genotyping.***
A. Genotyping mouse *Ski* knockdown mice from ear cartilage samples**.** Initially, we began our cross with two different mouse lines: MerCreMer with the Cre recombinase site using the periostin (POSTN) promoter; and *Ski* flox. After several generations of breeding, we were able to maintain the double homozygous genotype. The presence of four bands (lane #302) that corresponds to the double hemizygous loci, whereas the presence of three bands represented those animals that were homozygous

for *Ski* flox loci and hemizygous for the Cre loci. Finally, the presence of only two bands indicates the presence of the double homozygous (*Ski* flox/Cre) genotype. Explanation of coded lettering in the Legend to Figure: S = *Ski* flox, C = Cre. **B.** The double homozygous Cre/*Ski*-Floxed genotype is present in the heart, lung, kidney, and ear cartilage tissue from female and male transgenic mice before treatment. Explanation of coded lettering in the Legend to Figure: S = *Ski* flox, C = Cre

4.2 *Assessment of adenoviral Cre toxicity in cell viability and mRNA expression*

Cre recombinase has been shown to have toxicity for tissues and cells[237, 267]. Cre recombinase reduces cardiac function *in vivo*; and *in vitro* affects cell viability and gene expression[241, 267]. To analyze cell viability, transgenic (Ski-floxed) and non-transgenic (wild-type) passage zero (P0) primary cardiac myofibroblasts were transfected with Ad-GFP (control) or Ad-Cre (experimental group) MOI 50 in serum-free medium and assessed three days post-transfection with Calcein and Eth-1. It was found that cell death was slightly elevated in Ski-floxed cells treated with Ad-Cre versus control. However, neither this elevation not the direct comparison of wild-type cells versus Ski-floxed cells treated with Ad-Cre which analyzes the interaction between treated groups reached statistical significance (*p = 0.6942 and p = 0.5354, respectively*) (Fig. 4.2.1). Cre toxicity was further analyzed in mRNA expression through qPCR, which will be dealt with in the following sections. All following mRNA expression experiments compared the interaction of Cre recombinase effects in wild-type versus Ski-floxed treated cardiac myofibroblasts.

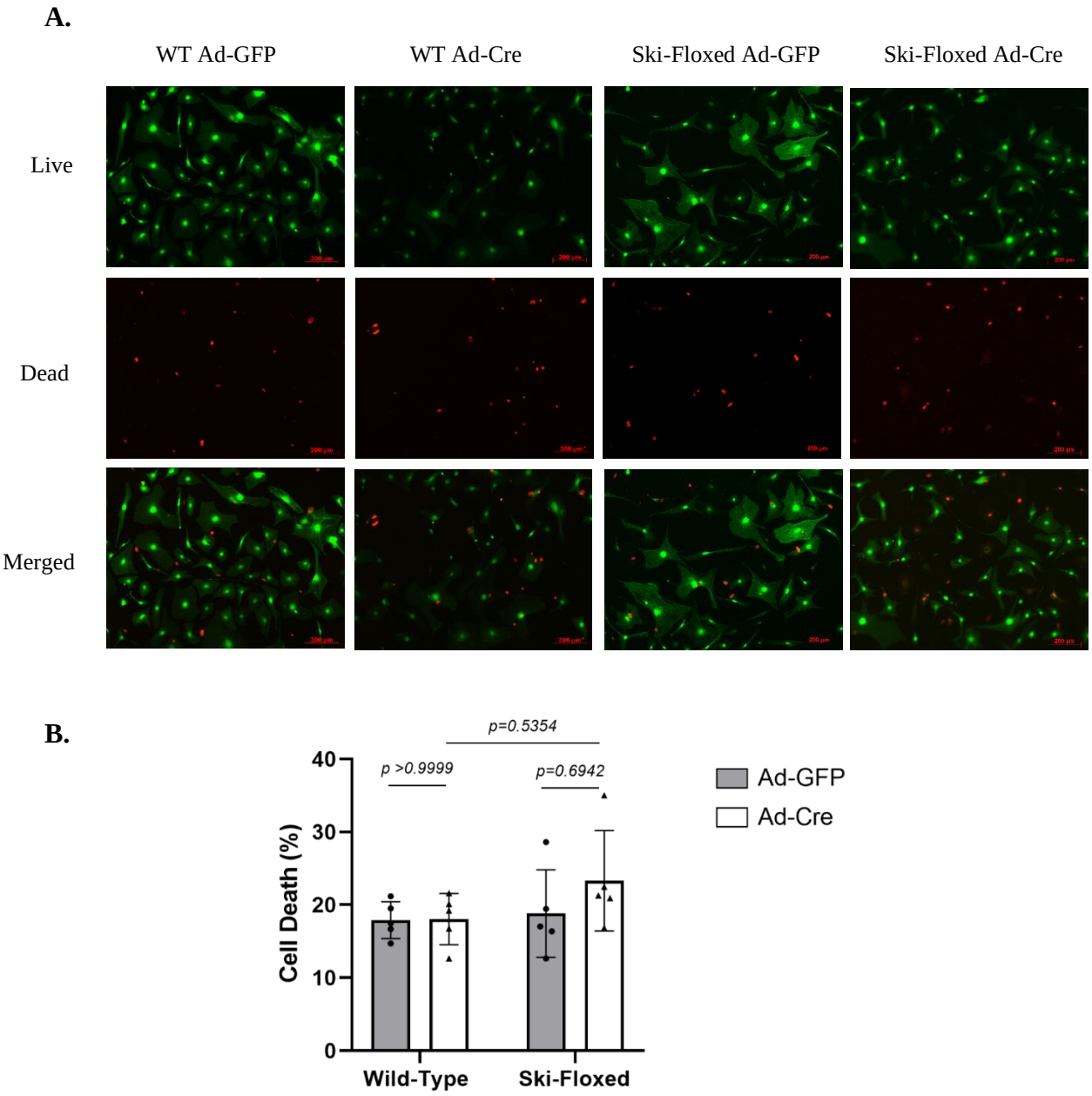

Figure 4.2.1 ***Cell Viability Assay in primary cardiac fibroblasts.***
Treatment of cardiac myofibroblasts did not affect cell death after 72h of Ad-Cre treatment. A. Cell viability was assessed by Calcein-AM (green) staining, representing live cells, and ethidium homodimer (red), representing dead cells. B. Graphic representation of cell count, indicating no significance in cell death, despite relative elevation in Ski-Floxed Ad-Cre treated cells. Total of biological replicates: n=5. Each biological replicate was evaluated by at least 3 random fields at 10X.

4.3 *Mouse Ski Exons 2 and 3 are completely excised post-transfection with Adenoviral Cre in cardiac myofibroblasts and evidence of Ski splice variants*

Among all mouse *Ski* exons, exon 1 is the longest (with 971 bp) and most important, where the SMAD-binding sites are located, and most mutations occur. The peptide product corresponding to exons 2 and 3 have phosphorylation, ubiquitination and nuclear localization predicted sites, but none of them are unique to these exons only. Thus, the most probable reason for positioning LoxP sequences before and after these two exons was practicality. These exons are relatively short, consisting of 121 and 116 bp respectively, as well as intron 2 (between them), with 138 bp. Their size and location (after exon 1) facilitated the insertion of the cassette as well as the creation of a stop-codon (TGA) after the excision, which caused a frameshift and interruption of the transcription process.

To assess *Ski* deletion, primary cardiac fibroblasts were isolated from Ski-floxed and wild-type mice followed by transfection with Ad-GFP (control) or Ad-Cre at MOI 50 for three days. Harvested cells had their mRNA isolated, and cDNA synthesized for analysis. Through qPCR, using specific primers for exons 2 and 3 showed significant reduction of these exons in Ski-floxed Ad-Cre cells, as well as in wild-type Ad-Cre animals compared to their respective controls. However, the direct comparison between transgenic and non-transgenic treated cells excluded Cre toxicity effect and confirmed downregulation of exons 2 and 3 (Fig. 4.4.1.B) ($p < 0.0001$). Visually, through PCR electrophoresis targeting exons 1 through exon 4, we covered areas before and after the insertion of the cassette to confirm the deletion of exons 2 and 3 as predicted by the theorical model. We also verified if three days treatment with adenoviral Cre was sufficient to cause the excision. The full product length (*Ski tv1*) for exons 1 to 4 was

estimated to be 1044 bp; as products with absence of exons 2 and 3 were expected to be 807 bp as demonstrated in Fig 4.3.1.C.

In these same experiments to confirm excision of *Ski* exons 2 and 3, it was evidenced an unpredicted band in the control groups below the primary band corresponding to full length from exon 1 to 4. This band was isolated, excised and analyzed through DNA sequencing; confirming a 923 bp band size which matched the sequence from exon 1 to exon 4 without exon 2 (*Ski tv2*) (Fig. 4.3.1.A). This incidental finding is a predicted splice variant for *Ski* in mammals, but with no prior identification in mouse cardiac fibroblasts. To further analyze these different variants, the tertiary protein structure was determined using Phyre2 software and visualized by EzMol 2.1 by inserting the predicted reading gDNA sequences (Fig. 4.3.1.B)[268, 269]. These structures represent a theorical model, where *Ski tv1* is slightly longer than *Ski tv2* and *Ski* KO even shorter. However, it is unknown if *Ski* KO protein is not formed because of frameshift caused by exons 2 and 3 excision, or a truncated protein is synthesized instead.

Despite evidence of downregulation of *Ski* exons 2 and 3, and confirmation of their deletion through PCR electrophoresis, when PCR was performed targeting only exons 2 and 3, there was still evidence of a faint band in the predicted size of those exons (Fig. 4.3.2). This shows reminiscent mRNA of full-length *Ski*, despite excision of exons 2 and 3 at the genomic level. This is a relevant finding because it points to the role of transcriptome in knockdown models. Because *Ski tv2* does not have exons 2 and our knockdown model targets both exon 2 and 3, it was important to define if the presence of low levels of exons 2 and 3 in qPCR were due to presence of *Ski* transcript variants. To analyze this, PCR electrophoresis was performed with three different targets: from exon 1 to exon 2; exon 1 to exon 3; and exon 1 to exon 3. We found that control samples (wild-type Ad-GFP, wild-type Ad-Cre, and Ski-floxed Ad-GFP) showed

only *Ski tv1* when probing for exons 1 to 2 but that *Ski tv2* was present for exons 1 to 3 and exons 1 to 4. It was also noted that bands wild-type Ad-Cre targeting exons 1 to 4 were visibly less intense than the other samples, indicating possible Cre toxicity. For Ski-floxed lanes, no visible bands were found when probing for exons 1 to 2 and exons 1 to 3 as expected due to excision of critical exons; and finally, the band for exons 1 to 4 was, as mentioned before, below the band for the other groups in accordance with the complete excision of exons 2 and 3 (Fig. 4.3.3).

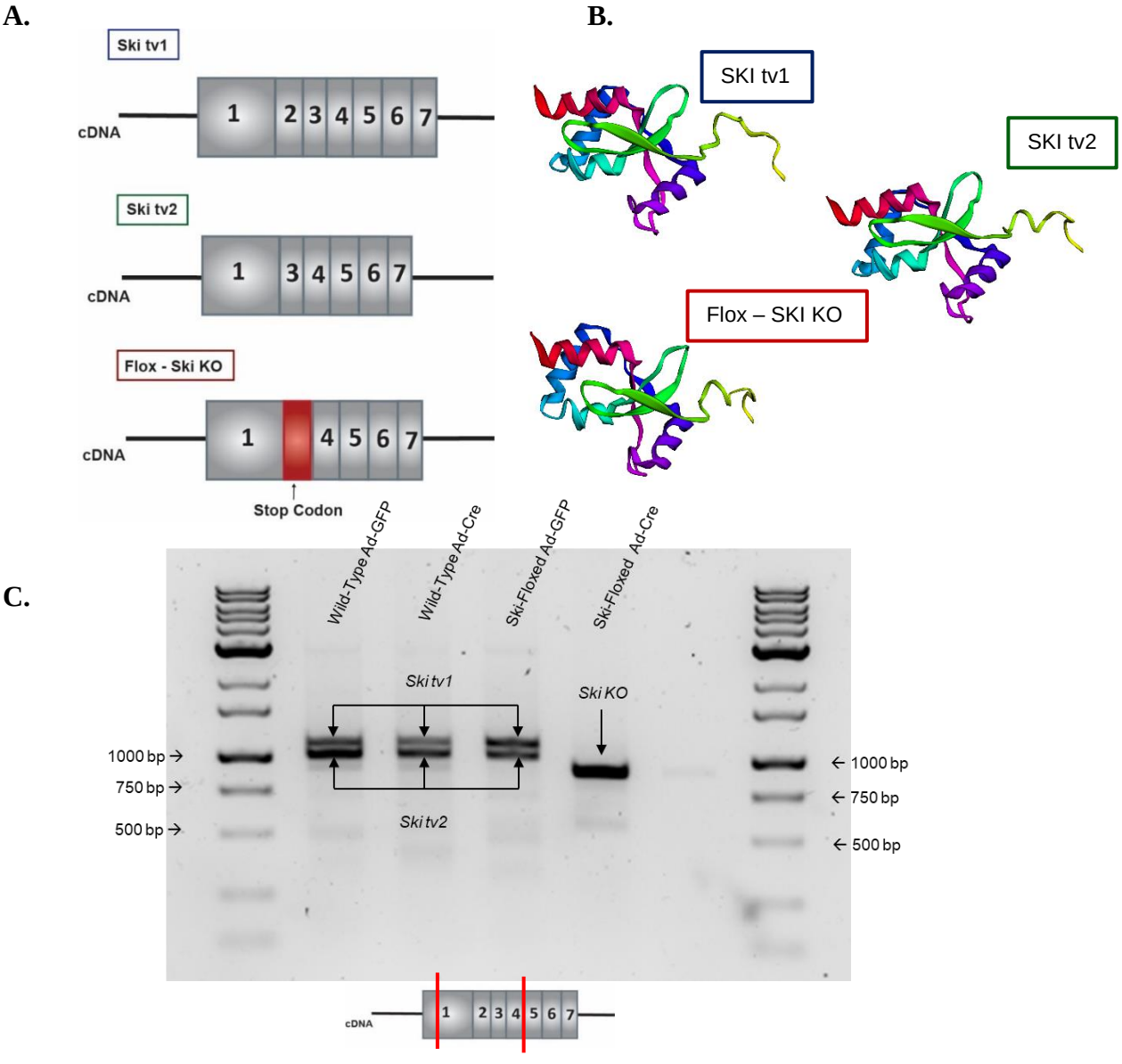

Figure 4.3.1 ***Evidence of Ski splice variants and knockdown.***
A. Mouse *Ski* representative complementary DNA (cDNA) sequence. Gray represents exons. *Ski* tv1 presents all seven exons, while *Ski* tv2 is a physiological variant without exon 2. *Ski* KO represents cDNA after excision of exons 2 and 3 with the creation of a stop codon because of frame-shift post-excision. **B. Prediction of SKI tertiary structure**. From top to bottom: SKI tv1 and 2, and theorical representation of SKI KO until the stop codon. **C. Discovery of *Ski* tv2 in mouse primary cardiac myofibroblasts and confirmation of deletion of exons 2 and 3 in floxed animals.** PCR data from WT and Flox mouse primary cardiac myofibroblasts cultured in plastic and treated with viral control or Cre-treated (MOI 50). *Ski* tv1 is represented by the upper band at 1044bp, *Ski* tv2 at 923bp and *Ski* KO 807bp. The remaining low intensity bands represent background, as this experiment was repeated to isolate bands representing transcript variants.

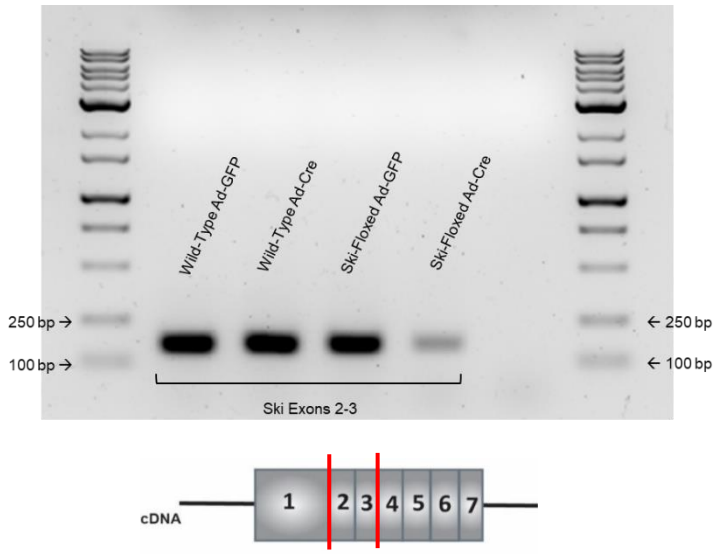

Figure 4.3.2 ***Confirmation of Ski knockdown and residual transcriptome in Ski-Floxed primary cardiac myofibroblasts treated with adenovirus-Cre.***
PCR data from cultured cells in plastic treated with viral control or Cre-treated (MOI 50). Residual transcriptome is confirmed by the presence of residual band in Ski-floxed adenovirus-cre treated cells, despite confirmation through DNA sequencing of excision of exons 2 and 3 after 72h of infection.

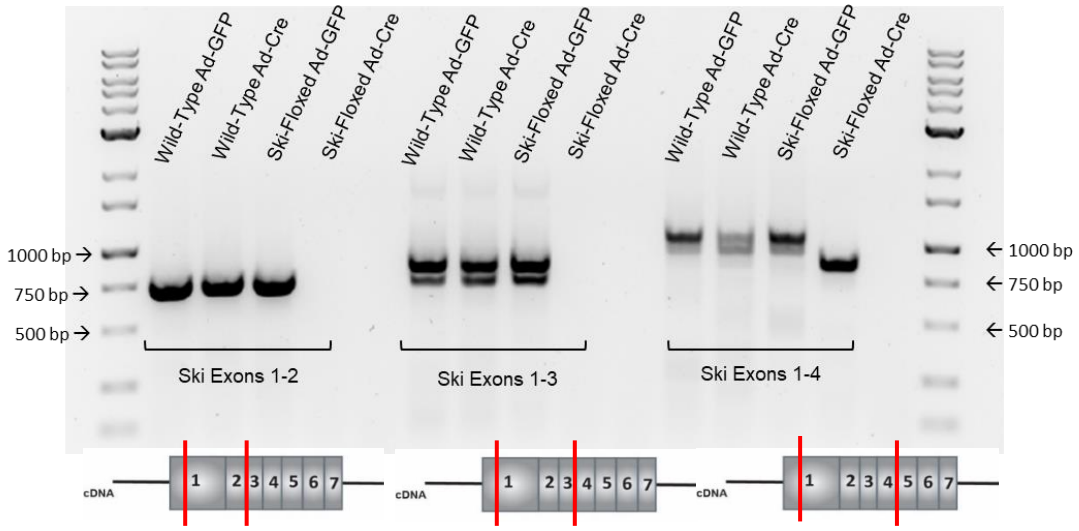

Figure 4.3.3 ***Assessment of mouse Ski exons 1-2, exons 1-3 and exons 1-4 in wild-type and Ski-Floxed primary cardiac myofibroblast treated with adenovirus-Cre.***
PCR data from cultured cells in plastic treated with adenovirus-GFP or adenovirus-Cre (MOI 50) harvested 72h after infection. The absence of a band representing exons 1-2 and 1-3 in Ski-floxed adenovirus-cre treated cells confirms that the residual band of mouse *Ski* exons 2-3 found in Figure 27 is a result of residual transcriptome after deletion of exons 2 and 3 in Ski-floxed adenovirus-Cre treated cells and not *Ski* transcript variant 2 (without exon 2).

4.4 *Deletion of Ski exons 2 and 3 interfere with mRNA expression of remaining Ski exons*

As *Ski* exons 2 and 3 were found to be completely excised from the genomic DNA and consequent mRNA, DNA sequencing confirmed the creation of a stop codon (TGA, an ochre stop-codon) following the excision. With that in mind, the mRNA expression for the remaining exons was also analyzed through qPCR. Mechanical stress did not show to play a role in this context, as *Ski* exons mRNA levels were neither elevated nor reduced in treated samples (Supplemental Fig 1). However, Cre treated cells appeared to have lower levels of mRNA expression for all *Ski* exons. The immediate comparison between transgenic and non-transgenic Ad-Cre treated cells revealed significant reduction of exons 2 and 3 in Ski-floxed cells (Fig.

4.4.1.A, C, D and E) ($p < 0.0001$), confirming that excision of exons 2 and 3 also interfere with *Ski* exons 1, 4, 5, 6, and 7 expressions.

A.

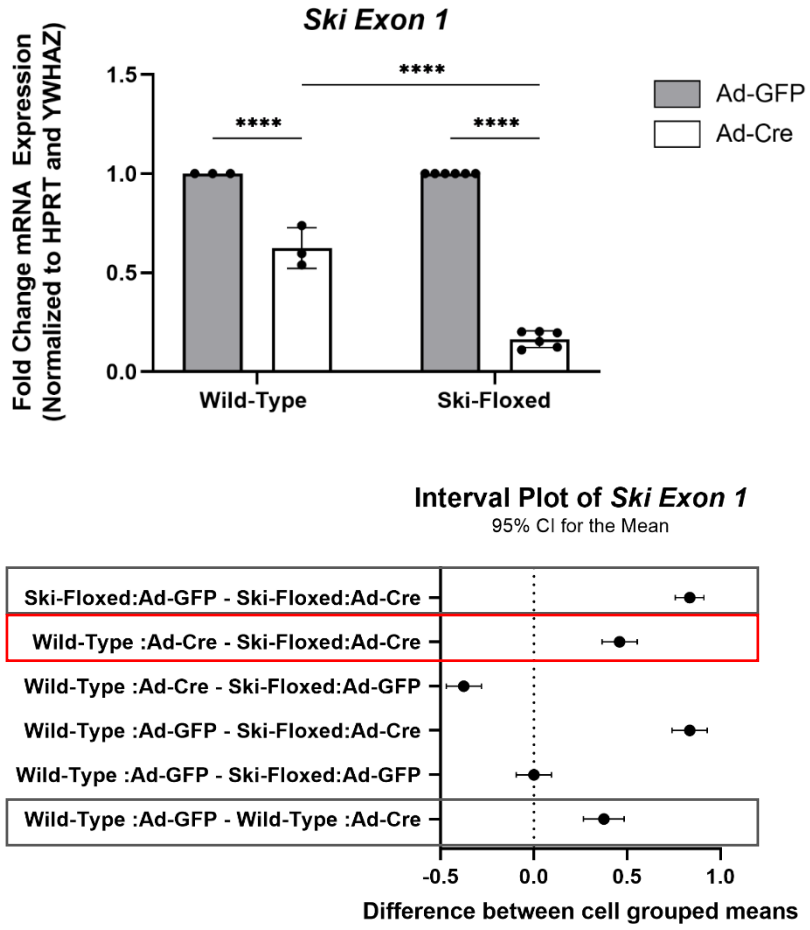

B.

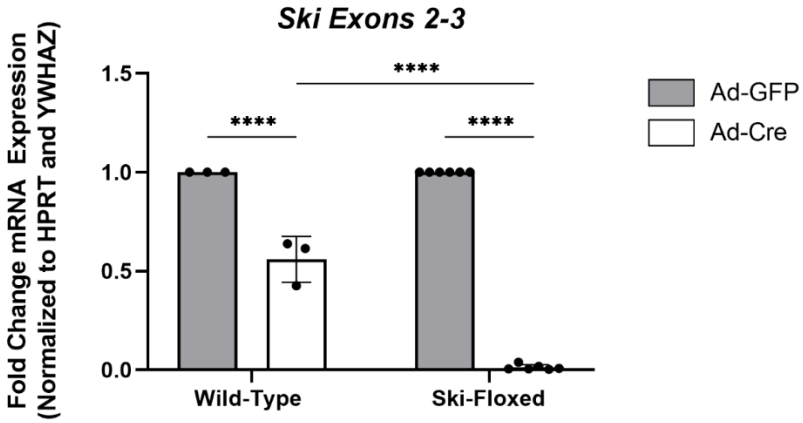

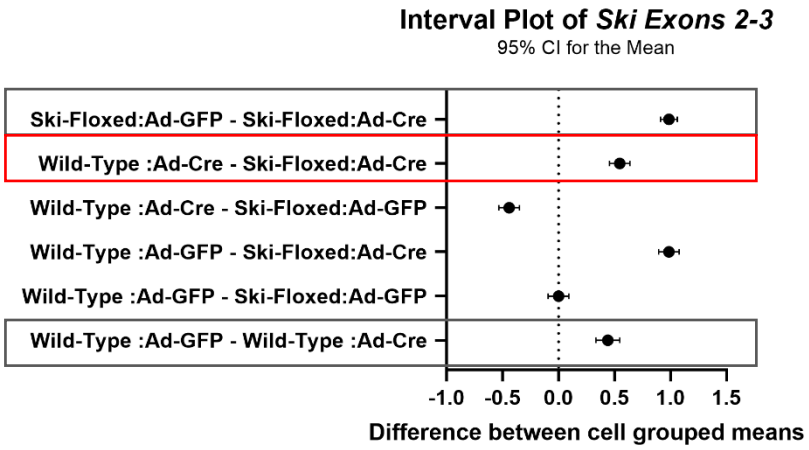
Interval Plot of Ski Exons 2-3
95% CI for the Mean
Ski-Floxed:Ad-GFP - Ski-Floxed:Ad-Cre
Wild-Type :Ad-Cre - Ski-Floxed:Ad-Cre
Wild-Type :Ad-Cre - Ski-Floxed:Ad-GFP
Wild-Type :Ad-GFP - Ski-Floxed:Ad-Cre
Wild-Type :Ad-GFP - Ski-Floxed:Ad-GFP
Wild-Type :Ad-GFP - Wild-Type :Ad-Cre
-1.0 -0.5 0.0 0.5 1.0 1.5
Difference between cell grouped means

C.

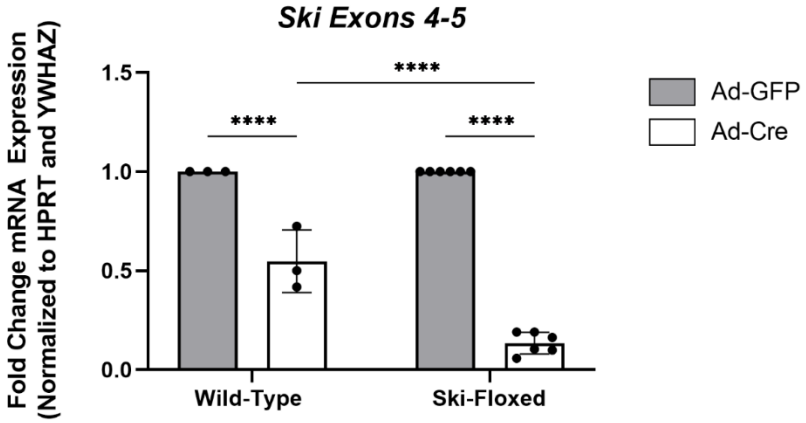
Ski Exons 4-5
Fold Change mRNA Expression
(Normalized to HPRT and YWHAZ)
1.5
1.0
0.5
0.0
****
****
****
Ad-GFP
Ad-Cre
Wild-Type
Ski-Floxed

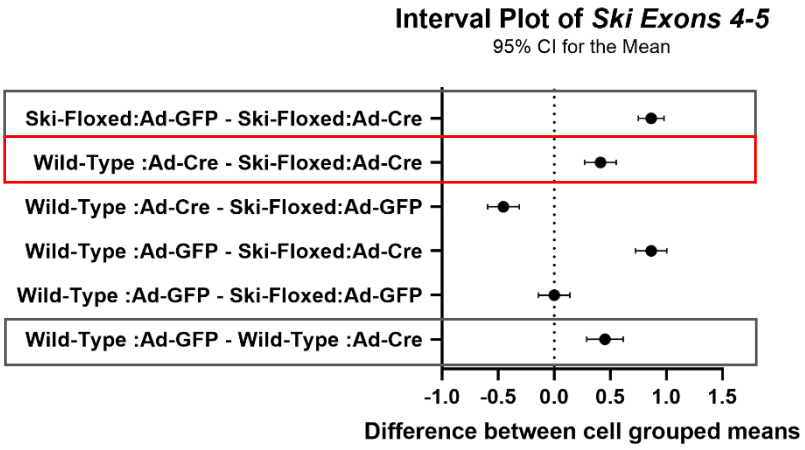
Interval Plot of Ski Exons 4-5
95% CI for the Mean
Ski-Floxed:Ad-GFP - Ski-Floxed:Ad-Cre
Wild-Type :Ad-Cre - Ski-Floxed:Ad-Cre
Wild-Type :Ad-Cre - Ski-Floxed:Ad-GFP
Wild-Type :Ad-GFP - Ski-Floxed:Ad-Cre
Wild-Type :Ad-GFP - Ski-Floxed:Ad-GFP
Wild-Type :Ad-GFP - Wild-Type :Ad-Cre
-1.0 -0.5 0.0 0.5 1.0 1.5
Difference between cell grouped means

D.

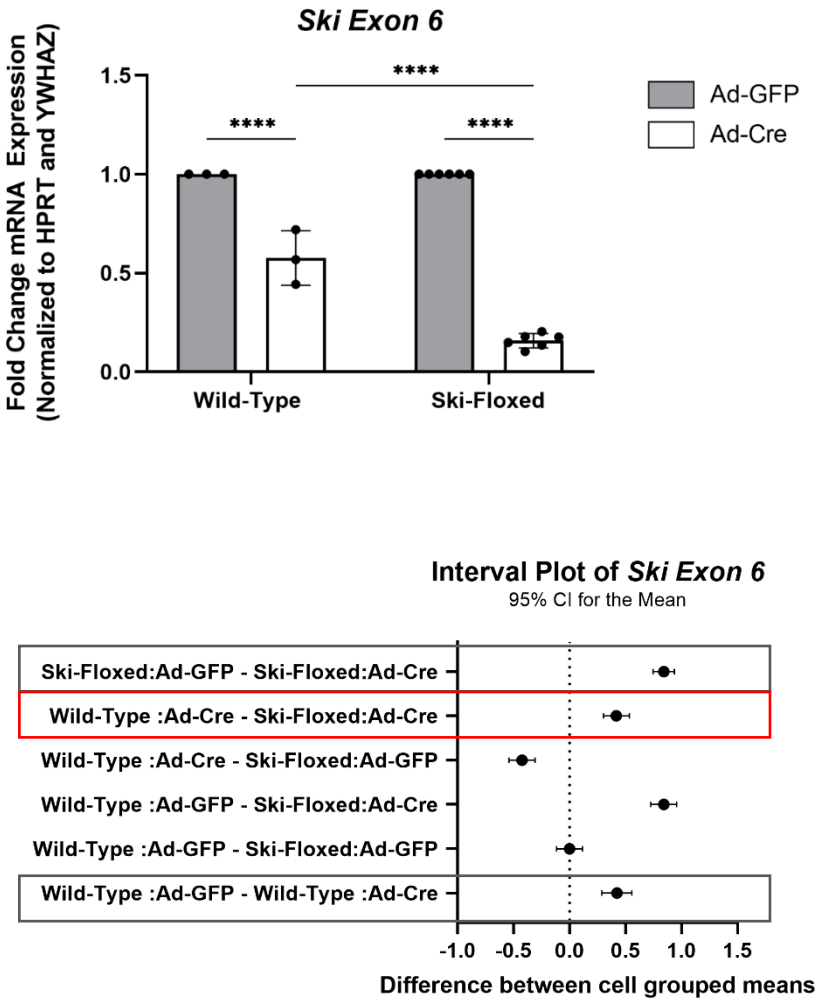
Ski Exon 6
Fold Change mRNA Expression
(Normalized to HPRT and YWHAZ)
1.5
1.0
0.5
0.0
****
****
****
Wild-Type
Ski-Floxed
Ad-GFP
Ad-Cre
Interval Plot of Ski Exon 6
95% CI for the Mean
Ski-Floxed:Ad-GFP - Ski-Floxed:Ad-Cre
Wild-Type :Ad-Cre - Ski-Floxed:Ad-Cre
Wild-Type :Ad-Cre - Ski-Floxed:Ad-GFP
Wild-Type :Ad-GFP - Ski-Floxed:Ad-Cre
Wild-Type :Ad-GFP - Ski-Floxed:Ad-GFP
Wild-Type :Ad-GFP - Wild-Type :Ad-Cre
-1.0 -0.5 0.0 0.5 1.0 1.5
Difference between cell grouped means

E.

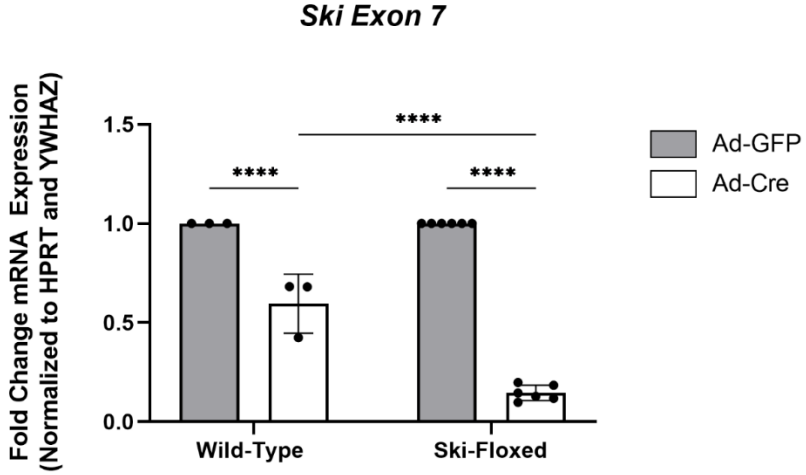
Ski Exon 7
Fold Change mRNA Expression
(Normalized to HPRT and YWHAZ)
1.5
1.0
0.5
0.0
****
****
****
Wild-Type
Ski-Floxed
Ad-GFP
Ad-Cre

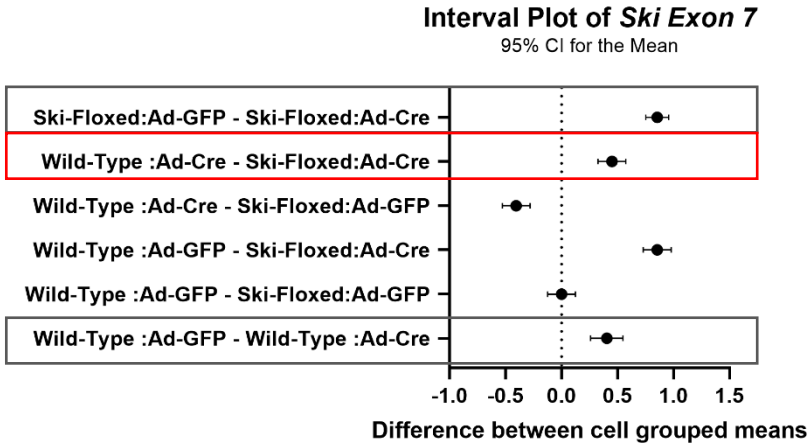

Figure 4.4.1. ***Mouse Ski knockdown in primary cardiac myofibroblasts.***
mRNA was extracted from wild-type and Ski-floxed murine primary cardiac myofibroblasts cultured on plastic and analyzed by qPCR. All samples were infected with Ad-GFP or Ad-Cre and harvested after 72h. Each gene expression graph reveals significant reduction of *Ski* exons 1 to 7, especially exons 2 and 3, confirming *Ski* gene knockdown. The confidence interval plots further support the significance level of the comparison between both treated samples. Total biological replicates n=3-6. Each biological replicate was evaluated by 3 technical replicates. ****: $P < 0.0001$. Ad-GFP = Adenoviral-GFP (control virus); Ad-Cre = Adenoviral-Cre; HPRT = hypoxanthine phosphoribosyltransferase 1; YWHAZ = tyrosine 3-monooxygenase/tryptophan 5-monooxygenase activation proteins zeta, both housekeeping genes used for normalization.

4.5 *In vitro Ski knockdown does not directly affect ECM components mRNA expression*

SKI overexpression is known to revert cardiac myofibroblasts to fibroblasts and reduce cardiac fibrosis[90, 203]. To evaluate the effects of *Ski* knockdown on ECM component protein and other regulatory protein regulation, mRNA expression for *collagen type I alpha 1* and *III*, *Mmp-14* and *ED-A domain-Fn (Eda-Fn)* was analyzed. qPCR studies were performed in cardiac myofibroblasts from wild-type and Ski-floxed animals infected with Ad-GFP or Ad-Cre MOI 50. To verify mechanical input and serum-starved medium interference, untreated wild-type cells were also evaluated by being cultured in plastic plates using starvation media. Mechanical input significantly reduces *collagen type I alpha 1 and type III alpha 1* mRNA expression (Supplemental Fig. 2). This downregulation was also found in wild-type Ad-Cre treated as well

as Ski-floxed cells (Fig. 4.5.1 and 4.5.2), being not significant when comparing both treated groups (*p = 0.7914 and p = 0.6599,* respectively). Thus, *Ski* knockdown does not significantly affect *collagen I α 1and III* α 1 mRNA expression. *Mmp-14* is found to be slightly reduced in untreated wild-type cells, but this reduction only reaches significance after 120h in serum-free medium (Supplemental Fig. 3). At 72h post-transfection, *Mmp-14* is reduced in both wild-type and Ski-floxed cells, showing that the direct comparison between these two groups was not significant (*p = 0.1069*) (Figure 4.5.3). This suggests that Cre expression is responsible for the reduction of *Mmp-14* expression in Ski-Floxed cells (Fig. 4.5.3). Mechanical stress and starving medium significantly reduced *Eda-Fn* in untreated wild-type cardiac fibroblasts (Supplemental Fig. 4). This was not found in wild-type or Ski-floxed treated samples (Fig. 4.5.4). Therefore, maintenance of cells in polystyrene plates and serum-free medium negatively interfered with *Eda-Fn* mRNA expression but treating these cells with Ad-Cre elevates to a non-significant level (*p = 0.5238*), which indicates that *Ski* reduction does not influence *Eda-Fn* mRNA expression in Cre treated cultured primary mouse fibroblasts.

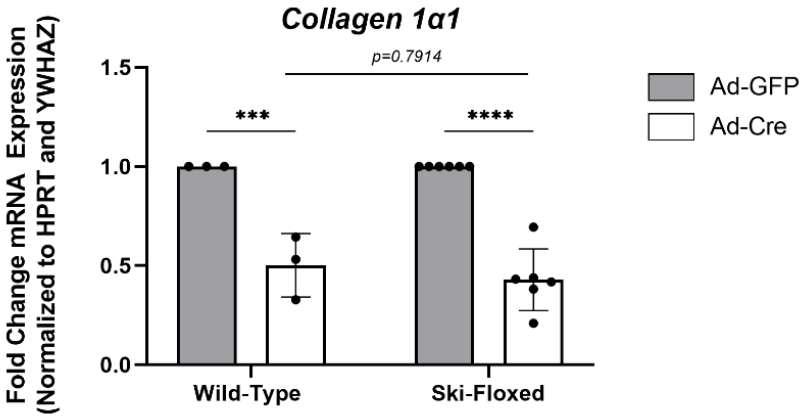

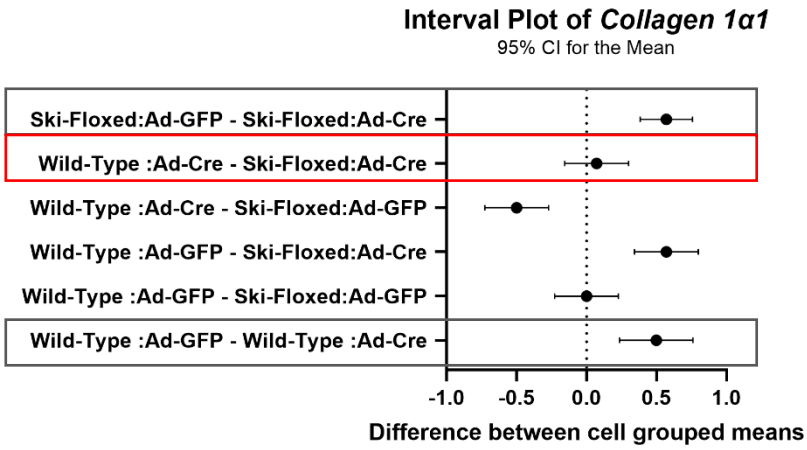

Figure 4.5.1 ***Fibrillar collagen 1 α1 mRNA expression is not significantly affected by Ski knockdown in primary cardiac myofibroblasts.***
P0 primary cardiac myofibroblasts from two different groups (non-transgenic – wild-type; and transgenic – Ski-floxed) were cultured on polystyrene plates, infected with Ad-GFP or Ad-Cre MOI 50. After 72h post-transfection, mRNA was extracted, and cDNA was analyzed by qPCR. *Collagen 1α1* mRNA expression is significantly reduced in both wild-type and Ski-floxed cells treated with Ad-Cre, but not significantly reduced when directly comparing both groups. The confidence interval plot demonstrates the significance level of these comparisons. Total biological replicates n=3-6. Each biological replicate was evaluated by 3 technical replicates. Ns: $P \geq 0.05$; ***: $P < 0.001$; ****: $P < 0.0001$. Ad-GFP = Adenoviral-GFP (control virus); Ad-Cre = Adenoviral-Cre; HPRT = hypoxanthine phosphoribosyltransferase 1; YWHAZ = tyrosine 3-monooxygenase/tryptophan 5-monooxygenase activation proteins zeta, both housekeeping genes used for normalization.

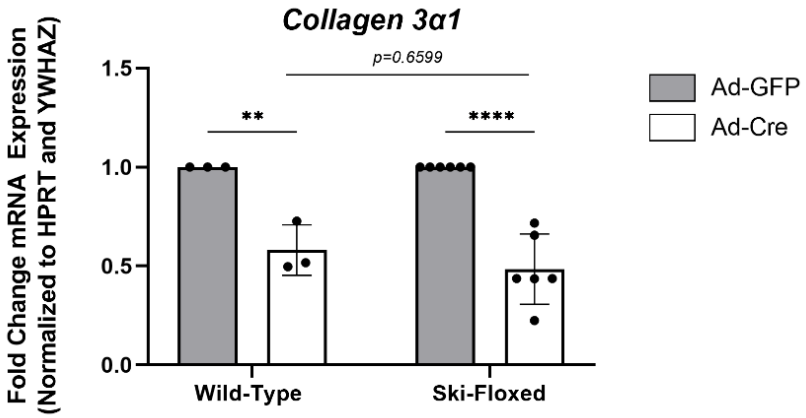

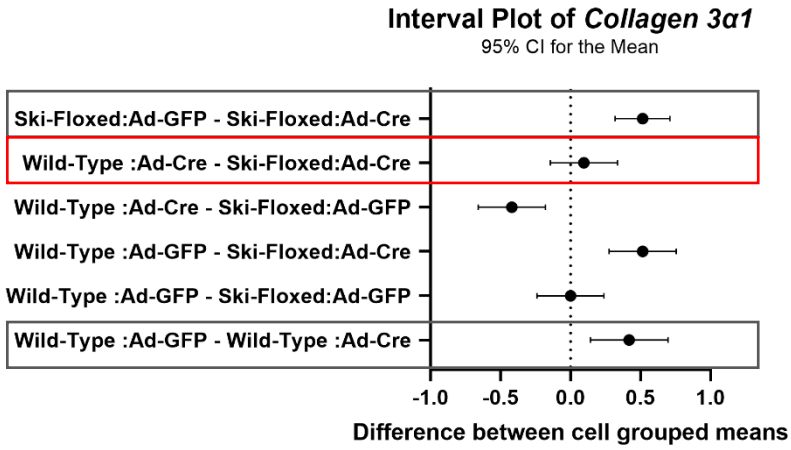

Figure 4.5.2. ***Ski knockdown does not significantly influence fibrillar collagen 3 α1 mRNA in primary cardiac myofibroblasts.***
mRNA extracted from non-transgenic (wild-type) and transgenic (Ski-floxed) murine P0 primary cardiac myofibroblasts cultured on polystyrene (plastic) culture dishes and analyzed by qPCR. Cells from both groups were transfected with Ad-GFP or Ad-Cre MOI 50 for 72h. Collagen 3 α1 mRNA expression appears to be significantly reduced in both wild-type and Ski-floxed cells treated with Ad-Cre compared to control samples, However, the direct comparison between treated samples from both experimental groups was not significant. The confidence interval plot demonstrates the significance level of these comparisons. Total biological replicates n=3-6. Each biological replicate was evaluated by 3 technical replicates. Ns: P ³ 0.05; **: P < 0.01; ****: P < 0.0001. Ad-GFP = Adenoviral-GFP (control virus); Ad-Cre = Adenoviral-Cre; HPRT = hypoxanthine phosphoribosyltransferase 1; YWHAZ = tyrosine 3-monooxygenase/tryptophan 5-monooxygenase activation proteins zeta, both housekeeping genes used for normalization.

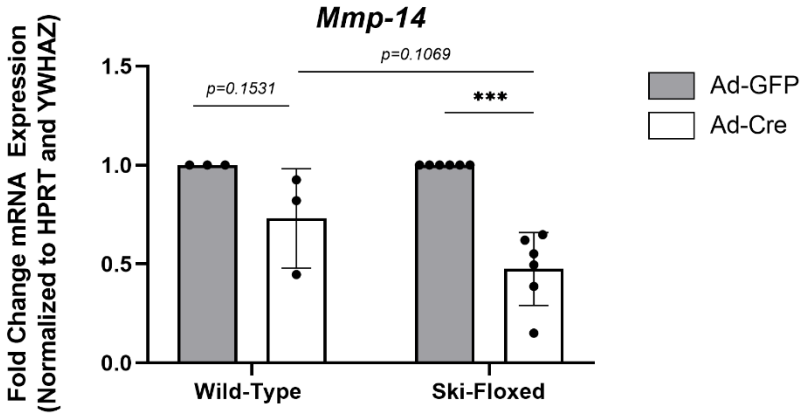

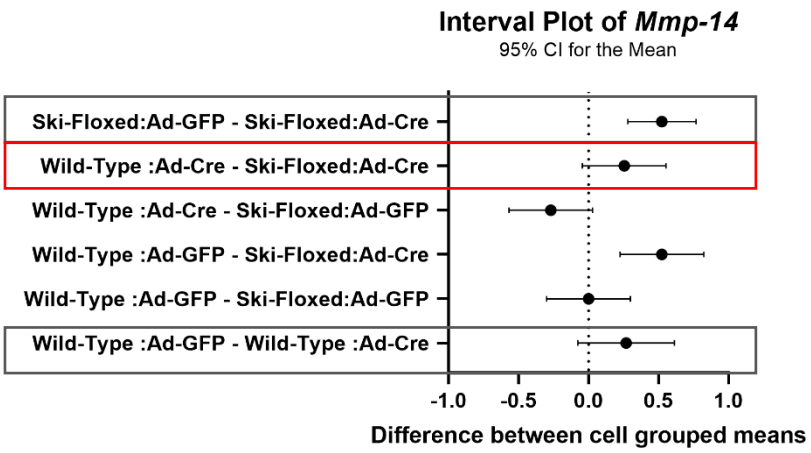

Figure 4.5.3 ***Ski knockdown does not significantly influence Mmp-14 mRNA expression in primary cardiac myofibroblasts.***

P0 primary cardiac myofibroblasts from transgenic (Ski-floxed) and non-transgenic (wild-type) were cultured on polystyrene plates and transfected for 72h with Ad-GFP (control) and Ad-Cre MOI 50. mRNA was extracted analyzed by qPCR. *Mmp-14* mRNA expression is significantly reduced in Ski-floxed cells treated with Ad-Cre, However, comparing Ad-Cre from both groups to exclude Cre toxicity effect revealed that *Ski* knockdown did not significantly reduced *Mmp-14* mRNA expression. The confidence interval plot confirms the significance level of these comparisons. Total biological replicates n=3-6. Each biological replicate was evaluated by 3 technical replicates. Ns: $P \geq 0.05$; ***: $P < 0.00$. Ad-GFP = Adenoviral-GFP (control virus); Ad-Cre = Adenoviral-Cre; *Mmp-14* = matrix metalloproteinase 14; HPRT = hypoxanthine phosphoribosyltransferase 1; YWHAZ = tyrosine 3-monooxygenase/tryptophan 5-monooxygenase activation proteins zeta, both housekeeping genes used for normalization.

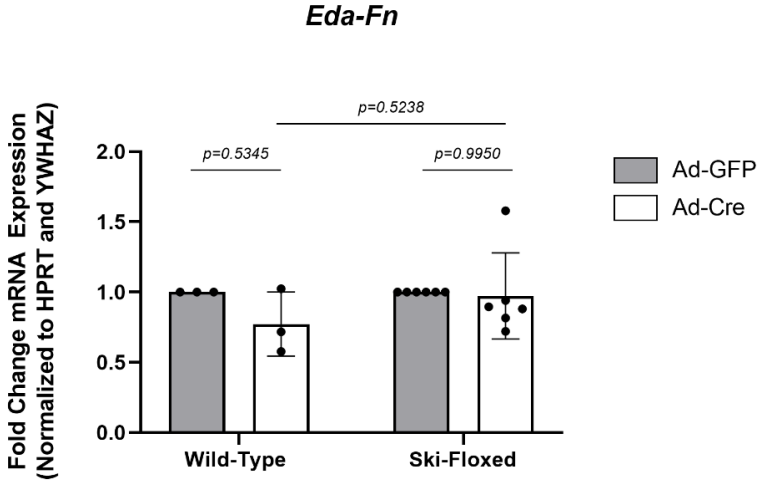

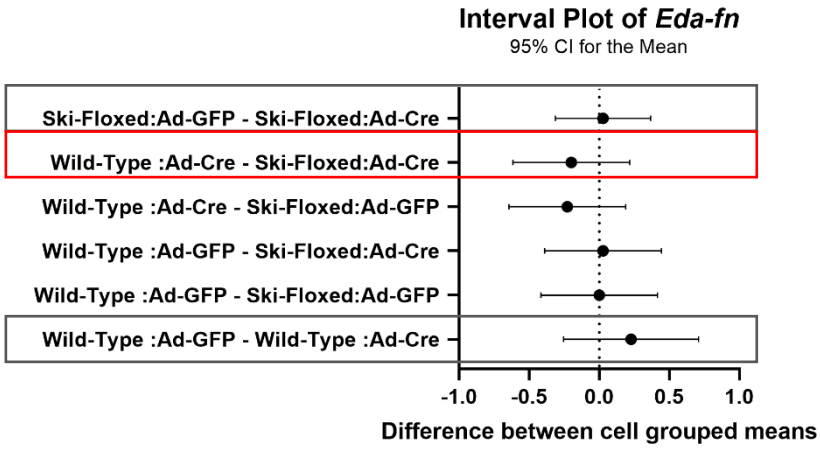

Figure 4.5.4 ***Ed-a domain Fn gene expression is not altered in Ski knockdown P0 myofibroblasts in Cre-treated wild-type and floxed (transgenic) primary cardiac myofibroblasts.***
qPCR was performed using mRNA from transgenic (Ski-floxed) and non-transgenic (wild-type) murine P0 primary cardiac myofibroblasts cultured on plastic. All samples were harvested at 72h post-transfection with Ad-GFP or Ad-Cre MOI 50. *Eda-Fn* gene expression is not significantly elevated in any of the sample sets or comparisons. The confidence interval plot confirms the significance level of these comparisons. Total biological replicates n=3-6. Each biological replicate was evaluated by 3 technical replicates. Ns: $P \geq 0.05$. Ad-GFP = Adenoviral-GFP (control virus); Ad-Cre = Adenoviral-Cre; *Eda-Fn* = Extra Domain A Fibronectin; HPRT = hypoxanthine phosphoribosyltransferase 1; YWHAZ = tyrosine 3-monooxygenase/tryptophan 5-monooxygenase activation proteins zeta, both housekeeping genes used for normalization.

4.6 *Ski deletion does not influence myofibroblast effector markers*

Myofibroblasts are known to express *Pdgfr*-α and have incorporated stress fibers marked by α-SMA. While *Pdgfr*-α mRNA expression is not significantly changed in cultured untreated cardiac myofibroblasts plated in serum-free medium for several days (Supplemental Fig. 5.), when wild-type or Ski-floxed cells were treated with Ad-Cre, there is a substantial reduction in its mRNA expression compared with respective controls (Fig. 4.6.1). However, this significant reduction is parallel across both groups ($p = 0.9311$), which is evidence of Cre toxicity to these cells.

Acta2 (α-SMA gene), on the other hand, is found to gradually increase in untreated cells, without reaching significance (Supplemental Fig. 6). The same is observed in treated wild-type cells ($p = 0.9595$), but not in Ski-floxed cells which reached significance ($p < 0.01$) (Fig. 4.6.2). However, as Cre toxicity also had to be addressed, the direct comparison between wild-type and Ski-floxed Ad-Cre samples showed an elevation in transgenic treated cells, but without significance (*p = 0.1554*). This may be explained because of α-SMA intrinsic variance in each sample, as α-SMA is found to be unevenly expressed in myofibroblasts.

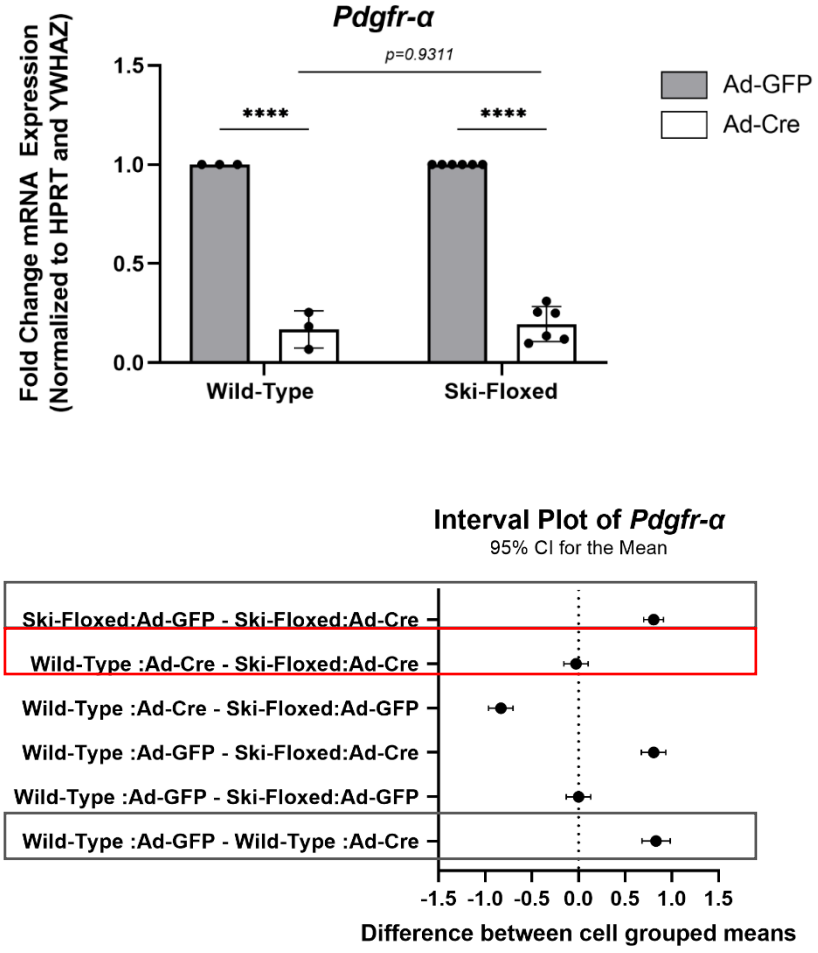

Figure 4.6.1 ***Pdgfr-α mRNA expression is not significantly impacted by Ski knockdown in primary cardiac myofibroblasts.***
Wild-type (non-trasngenic) and Ski-floxed (transgenic) murine P0 primary cardiac myofibroblasts cultured on polystyrene were transfect with Ad-GFP (control) or Ad-Cre MOI 50 for 72h. mRNA was extracted and analyzed by qPCR. *Pdgfr-α* gene expression is significantly reduced in both wild-type and Ski-floxed cells treated with Ad-Cre compared to control. However, not significance when directly comparing both groups reveal that Cre toxicity affects *Pdgfr-α* mRNA expression. The confidence interval plot demonstrates the significance level of these comparisons. Total biological replicates n=3-6. Each biological replicate was evaluated by 3 technical replicates. Ns: $P \geq 0.05$; ****: $P < 0.0001$. Ad-GFP = Adenoviral-GFP (control virus); Ad-Cre = Adenoviral-Cre; *Pdgfr-α* = Platelet-derived growth factor receptor alpha; HPRT = hypoxanthine phosphoribosyltransferase 1; YWHAZ = tyrosine 3-monooxygenase/tryptophan 5-monooxygenase activation proteins zeta, both housekeeping genes used for normalization.

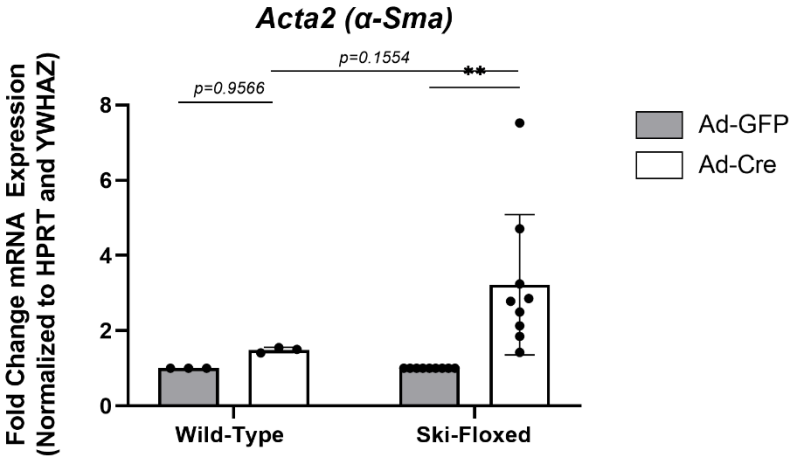

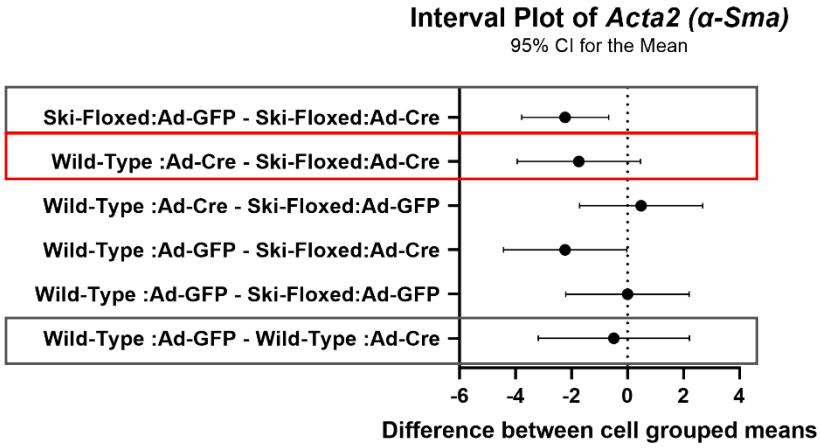

Figure 4.6.2 *α-Sma (Acta2) mRNA expression is not significantly altered with Ski knockdown in primary cardiac myofibroblasts.*
mRNA was extracted from murine P0 primary cardiac myofibroblasts cultured in plastic and analyzed in qPCR. All samples were infected with Ad-GFP or Ad-Cre MOI 50 and harvested after 72h. It is noted that exposure of P0 myofibroblasts to Ad-Cre resulted in significant increase in α-Sma expression from Ad-GFP infected Ski-floxed myofibroblasts. Comparing Cre treated groups among wild-type and myofibroblasts derived from floxed mice revels an upward trend, but no significant elevation in the *Ski* knockdown group. The confidence interval plot demonstrates the significance level of these comparison. Total biological replicates n=3-9. Each biological replicate was evaluated by 3 technical replicates. Ns: P ≥ 0.05; **: P < 0.01. Ad-GFP = Adenoviral-GFP (control virus); Ad-Cre = Adenoviral-Cre; *Acta2* = Actin alpha-2; HPRT = hypoxanthine phosphoribosyltransferase 1; YWHAZ = tyrosine 3-monooxygenase/tryptophan 5-monooxygenase activation proteins zeta, both housekeeping genes used for normalization.

4.7 *Ski knockdown in Cre treated primary cardiac fibroblasts directly modulates Hippo pathway signalling*

The Hippo pathway is an important signalling pathway related to mechanical input and cardiac fibrosis. As SKI is known for interacting with LIMD1 to promote this pathway and consequently inhibit YAP and TAZ function; *Yap*, *Wwtr* (*Taz*), *Limd1* and *Lats2* mRNA expression were analyzed. Mechanical stress and starving medium did not show to interfere with mRNA expression of these genes over the course of 5 days (Supplemental Fig. 7, 8, 9 and 10). Individually, Ad-Cre reduced *Yap* and *Lats2* expression in both wild-type and Ski-floxed treated cells compared with their own controls (Ad-GFP) (Fig. 4.7.1 and 4.7.2), while *Limd1* was not altered by Cre toxicity or *Ski* knockdown ($p = 4057$) (Fig. 4.7.3). However, *Taz*, showed to be significantly elevated in Ski-floxed ($p < 0.01$), as well as in the interaction between wild-type and Ski-floxed cells ($p < 0.01$) (Fig. 4.7.4). This finding is consistent with the knowledge that SKI overexpression downregulates TAZ function, and it suggests that *Ski* is directly involved in *Taz* mRNA expression, as *Ski* knockdown elevates *Taz* expression.

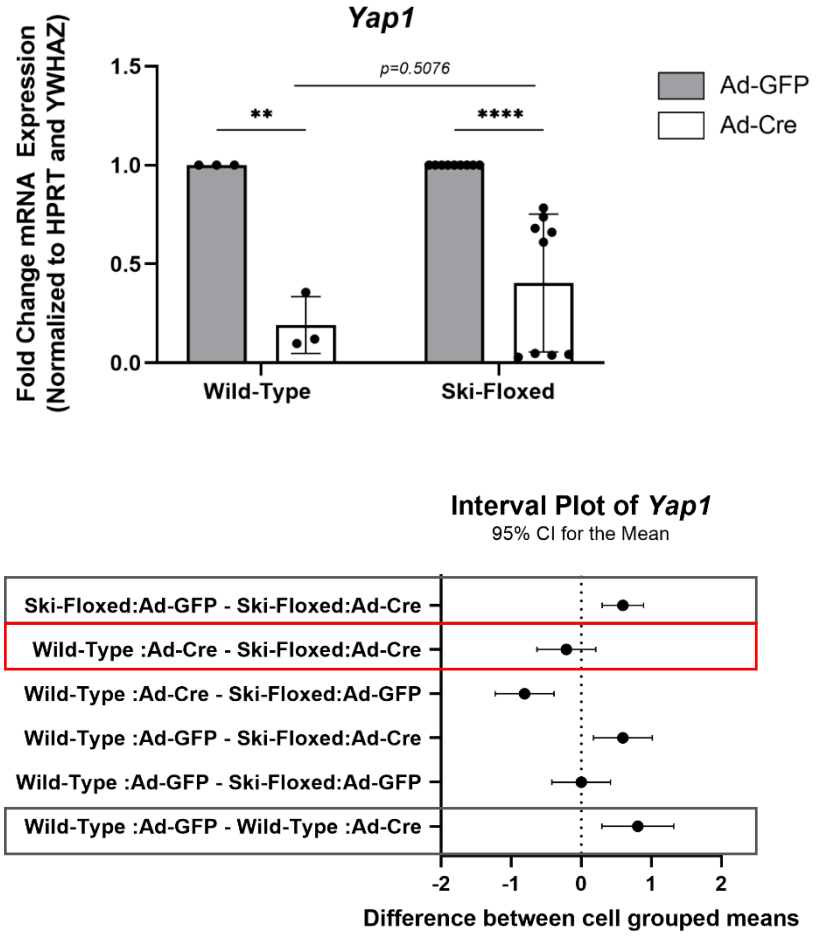

Figure 4.7.1 ***Yap1 gene expression is not significantly affected by Ski knockdown in primary cardiac myofibroblasts.***

mRNA was extracted from murine P0 primary cardiac myofibroblasts cultured on plastic and analyzed by qPCR. All samples were infected with Ad-GFP or Ad-Cre and harvested after 72h. *Yap1* gene expression was significantly reduced in both sets of samples treated with Ad-Cre, but not significantly reduced when comparing treated wild-type and Ski-floxed. The confidence interval plot confirms the significance level of these comparisons. Total biological replicates n=3-9. Each biological replicate was evaluated by 3 technical replicates. Ns: $P \geq 0.05$; **: $P < 0.01$; ****: $P < 0.0001$. Ad-GFP = Adenoviral-GFP (control virus); Ad-Cre = Adenoviral-Cre; *Yap1* = Yes-associated protein 1; HPRT = hypoxanthine phosphoribosyltransferase 1; YWHAZ = tyrosine 3-monooxygenase/tryptophan 5-monooxygenase activation proteins zeta, both housekeeping genes used for normalization.

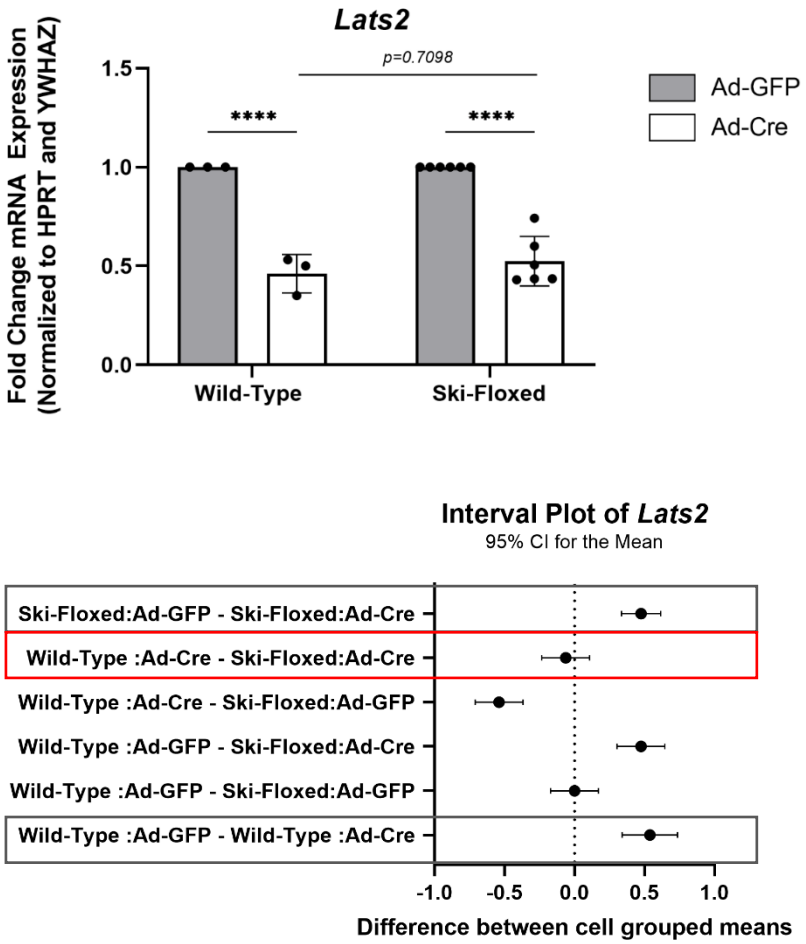

Figure 4.7.2 ***Lats2 mRNA expression is not significantly affected by Ski knockdown in primary cardiac myofibroblasts. qPCR analyzed.***

mRNA was extracted fromwild-type and Ski-floxed murine P0 primary cardiac myofibroblasts cultured. Samples from both groups were transfected with Ad-GFP or Ad-Cre MOI 50 and harvested after 72h. *Lats2* gene expression was significantly reduced in both sets of samples treated with Ad-Cre vs control. On the other hand, the direct comparison between treated groups was not statistically significant, confirming Cre toxicity effects. The confidence interval plot confirms the significance level of these comparisons. Total biological replicates n=3-6. Each biological replicate was evaluated by 3 technical replicates. Ns: $P \geq 0.05$; ****: $P < 0.0001$. Ad-GFP = Adenoviral-GFP (control virus); Ad-Cre = Adenoviral-Cre; *Lats2* = Large Tumor Suppressor Kinase 2; HPRT = hypoxanthine phosphoribosyltransferase 1; YWHAZ = tyrosine 3-monooxygenase/tryptophan 5-monooxygenase activation proteins zeta, both housekeeping genes used for normalization.

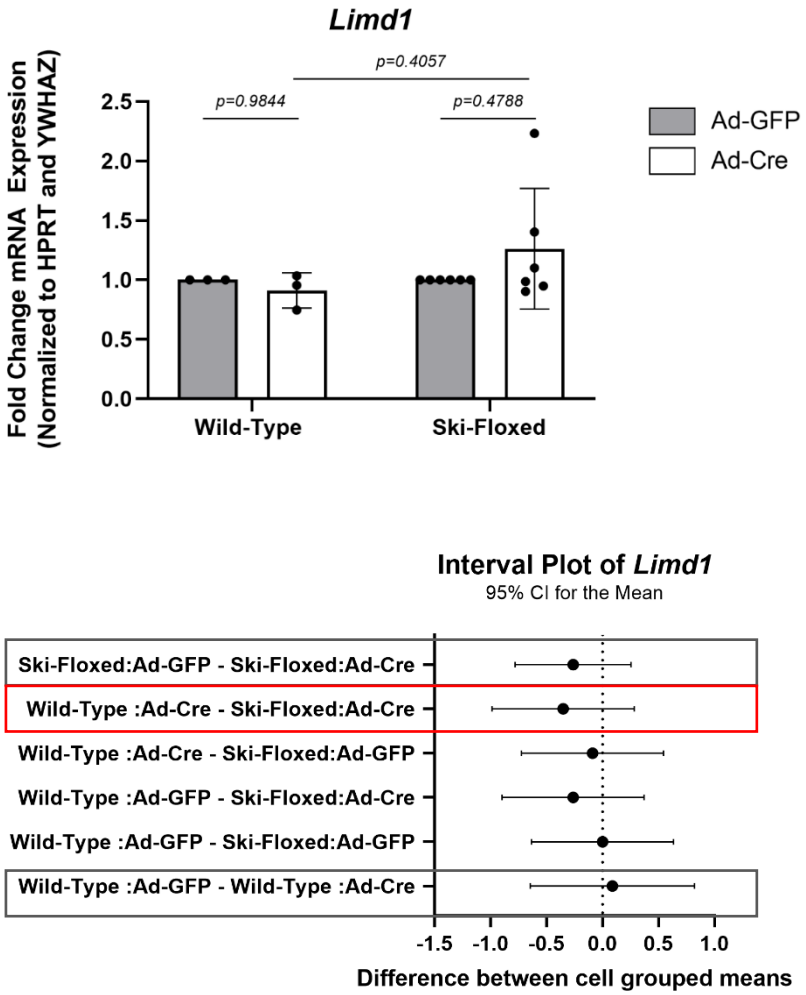

Figure 4.7.3 ***Ski knockdown does not significantly alter Limd1 mRNA expression in primary cardiac myofibroblasts.***

mRNA was extracted from transgenic (Ski-floxed) and non-transgenic (wild-type) murine P0 primary cardiac myofibroblasts cultured on polystyrene plates and analyzed by qPCR. All samples were infected with Ad-GFP or Ad-Cre and harvested after 72h. *Limd1* mRNA expression revealed an elevation trend in Ski-floxed treated cells but did not reach statistical significance. The significance was also not confirmed when comparing treated wild-type and Ski-floxed. The confidence interval plot confirms the significance level of these comparisons. Total biological replicates n=3-6. Each biological replicate was evaluated by 3 technical replicates. Ns: $P \geq 0.05$. Ad-GFP = Adenoviral-GFP (control virus); Ad-Cre = Adenoviral-Cre; *Limd1* = LIM Domain Containing 1; HPRT = hypoxanthine phosphoribosyltransferase 1; YWHAZ = tyrosine 3-monooxygenase/tryptophan 5-monooxygenase activation proteins zeta, both housekeeping genes used for normalization.

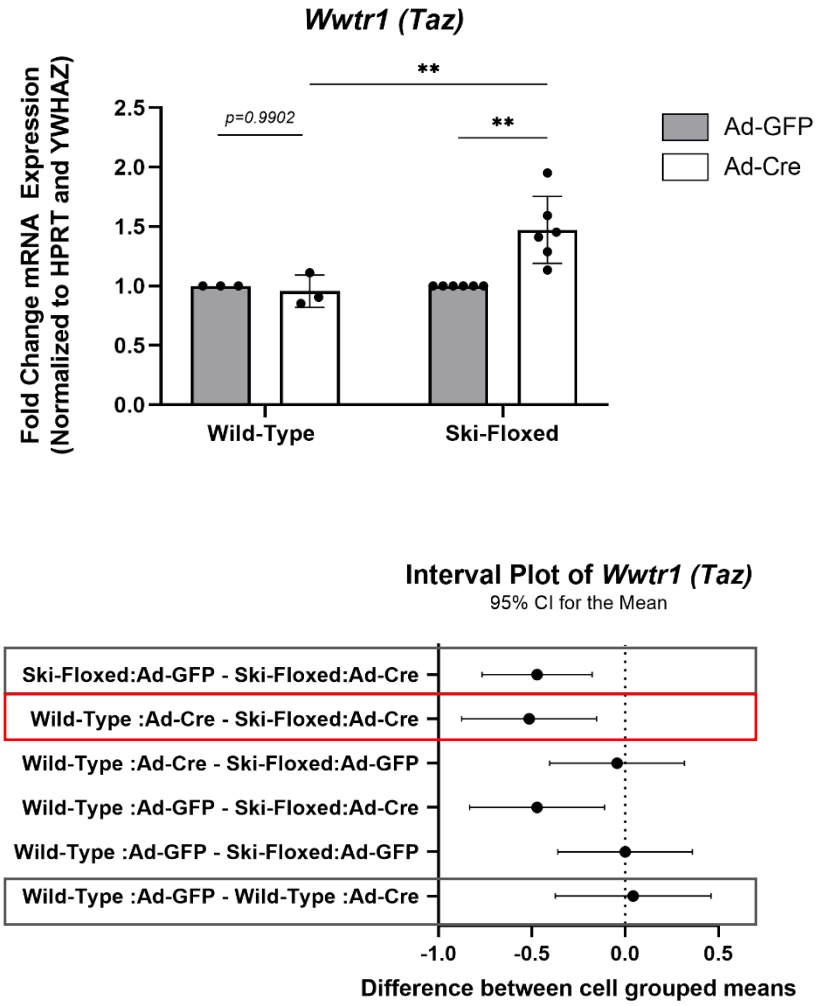

Figure 4.7.4 ***Elevation of Wwtr1 (Taz) mRNA expression with Ski knockdown in primary cardiac myofibroblasts.***

In vitro studies in cultures of primary myofibroblasts (transgenic (Ski-floxed) and non-transgenic (wild-type) mice P0 cells) we compared the influence of *Ski* knockdown performed by transfecting cells with Ad-GFP (control) or Ad-Cre. The cells were harvested at 72h post-transfection, and mRNA was analyzed by qPCR. Wwtr1 mRNA expression is significantly elevated in Ski-floxed cells treated with Ad-Cre compared to control. Cre toxicity was assessed by comparing treated wild-type and Ski-floxed groups. The confidence interval plot reveals significance of these comparisons. Total biological replicates n = 3-6. Each biological replicate was evaluated by 3 technical replicates. P □ 0.05; **: P < 0.01. Ad-GFP = Adenoviral-GFP (control virus); Ad-Cre = Adenoviral-Cre; Wwtr1 = WW Domain Containing Transcription Regulator (i.e., TAZ); HPRT = hypoxanthine phosphoribosyltransferase 1; YWHAZ = tyrosine 3-monooxygenase/tryptophan 5-monooxygenase activation proteins zeta, both housekeeping genes used for normalization.

Chapter 5: Discussion

In the adult mouse healthy heart, cardiac fibroblasts represent 10-37% of all cardiac cells[14, 56, 63, 270, 271]. Cardiac ECM components such as fibronectin, fibrillar collagens I and III, and glycosaminoglycans may undergo relatively slow turnover with degradation and removal by MMPs followed by directed synthesis by cardiac fibroblasts for the maintenance of ECM homeostasis [57, 107]. Conversely any major cardiac event leading to myocardial damage such as ischemic injury, chronic pressure, volume overload, diabetes, or viral myocarditis may lead to myocyte death and subsequent disruption of normal homeostasis of cardiac ECM, which influences and usually accelerates matrix turnover[46, 129]. As cardiomyocytes are unable to spontaneously regenerate following necrosis or apoptosis, myocardial wound healing is activated, which is marked by cardiac fibroblast activation to myofibroblasts which participate in subsequent scar formation which may be punctate or as an infarct scar depending upon the etiology of cardiac injury [52, 272]. Myofibroblasts feature a relatively large cytosol, Golgi apparatus, endoplasmic reticulum, incorporation of stress fibres in the cytoplasm, marked by α-SMA proteins contiguous with stress fibres, as well as PDGFR-α expression [93, 150, 273]. In the heart, the acute benign wound healing process following inflammation response becomes pathogenetic when myofibroblasts remain chronically activated, or enter a chronically senescent state; ergo the excessive deposition of fibrotic or hypertrophic ECM spills over to peripheral areas (previously healthy tissues) surrounding the site of injury [71, 75, 169].

Two of the major molecular pathophysiological pathways implicated in cardiac fibrosis are the TGF-β_1/Smad signalling pathway and the Hippo signalling pathway [149, 170, 274, 275]. When ECM is disturbed by cell death, abnormal or excessive mechanical shearing force (mechanical stress)[276], or by the release of oxygen species, TGFβ_1 is released and activated, initiating a

canonical cascade where co-Smads and R-Smad form complexes, migrating to the nucleus to promote cardiac fibrosis effector genes[9 277]. The Hippo pathway induces LATS2 to promote YAP and TAZ phosphorylation which is inhibited by LIMD1[169] (Figure 5.1). YAP/TAZ signalling is "off" with phosphorylation, as this leads to cytosolic degradation[85, 168]. Activation of LATS1/2 allows for phosphorylation and retention of YAP/TAZ in the cytosol, whereas if the LATS1/2 complex is inhibited, then YAP/TAZ can move to the nucleus and influence gene transcription, including the modulation of fibrillar collagens. In this context, mechanical stress has been shown to inhibit this pathway which then facilitates YAP and TAZ translocation to the nucleus and stimulation of transcription of pro-fibrotic factors[171]. SKI protein has been found to modulate both pathways, including its role as a negative repressor of TGFβ_1/Smad signalling[162]. When activated, SKI moves to the nucleus and binds to the Smad complex and the entire complex and SKI's inclusion forms a disrupting bridge which halts transcription of fibrotic factors[197, 278]. In the cytoplasm SKI has been shown by our group to inhibit LIMD1 leading to TAZ phosphorylation and reduction of cardiac fibrosis [168]. One of the main findings of the current work is *Taz* (*Wwtr1*) mRNA expression is significantly elevated with *Ski* knockdown *in vitro*. An implicit underlying corollary hypothesis relevant to this investigation is that *Ski* knockdown may facilitate the activation of cardiac fibroblasts to myofibroblasts. An extension of this hypothesis is that more myofibroblasts may promote the progression of cardiac fibrosis *in vivo*. As this study is strictly focused on cell culture and target marker gene mRNA abundance, we do not directly address the overarching hypothesis. If knockdown of *Ski* is associated with elevation of *Taz* mRNA expression, we may extrapolate by suggesting that this intervention may lead to cellular elevation of TAZ protein and/or translocation of TAZ to the cellular nucleus – which correlates to switching Hippo signaling off[168]. Landry et al. have shown that with SKI

protein localized in the cytoplasm (i.e., SKI is not activated to inhibit R-Smads) that TAZ-dependent pro-fibrotic signaling occurs[168]. With activation of SKI, it inhibits LIMD1 protein which derepresses LATS2 kinase which allows for subsequent phosphorylation and degradation of TAZ, removing it from any stimulation of the fibroblast to induce fibrosis. the context of the current study does not allow us to draw any conclusion about TAZ protein expression under these conditions, but rather represents a first step toward implementation of the mouse transgene and use of Cre treatment *in vitro*.

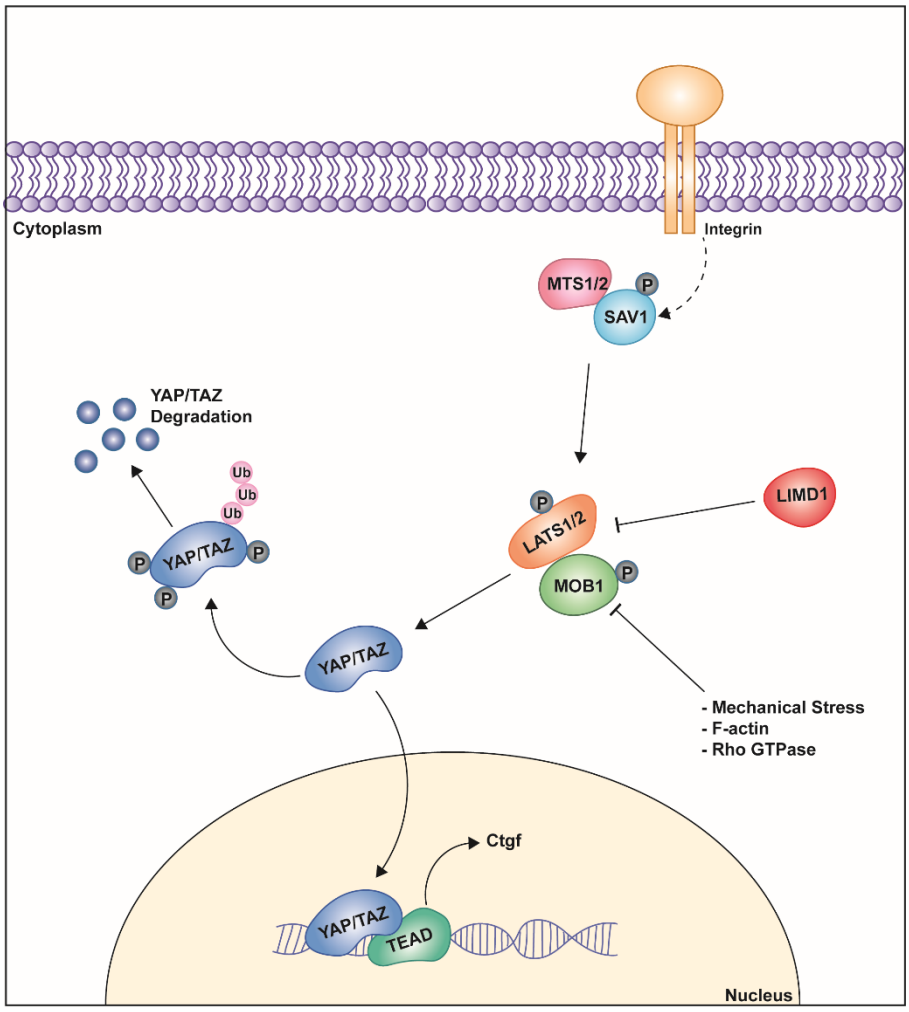

Figure 4.7.1 The Hippo Signalling Pathway

Activated Hippo Pathway: activated MTS1/2 forms a complex with Sav1, which phosphorylates LATS1/2 /MOB1 complex. This last complex induces YAP and TAZ phosphorylation which leads to YAP/TAZ cytoplasmic retention followed by degradation.

Deactivated Hippo Pathway: LIMD1, mechanical stress, F-actin and Rho GTPase inhibit YAP/TAZ phosphorylation by inhibiting LATS1/2/MOB1 complex. Thus deactivation allows to YAP/TAZ translocate to the nucleus, binding to TEAD to promote transcription of pro-fibrotic genes such as CTGF. (Adapted from Landry NM and Dixon IMC. Fibroblast mechanosensing, SKI and Hippo signaling and the cardiac fibroblast phenotype: Looking beyond TGF-beta, Figure 2. *Cell Signal*. 2020;76:109802).

In vivo studies with myocardial infarction (chronic or short duration ischemia) or reperfusion injury associated with tamoxifen treatment will certainly complement our *in vitro* findings using Cre treated fibroblasts isolated from transgenic mouse heart. Further, the inclusion of Western blot experiments from cellular extract, from tamoxifen treated transgenes or immunofluorescence studies *in vivo* will also answer questions about downstream effects on marker proteins with *Ski* knockdown. Furthermore, it is likely that SKI contributes to other pathways that may influence ECM component proteins or matrikines that are relevant to cardiac fibrosis. Finally, we expect that additional studies to address other members of the SKI superfamily including SnoN may reveal their importance in the negative repression of TGFβ_1/Smad signaling be knocked down in the presence or absence of *Ski* knockdown. These topics are discussed briefly below in the section devoted to Future Directions (Chapter 6).

A number of previous studies from our lab were focused on SKI (or I-Smad7) overexpression and how that event is linked to myofibroblast deactivation to quiescent fibroblasts[90, 203, 279]. The current thesis data addresses complementary *Ski* knockdown to investigate SKI's putative role in regulation of fibroblast function and cardiac fibrosis. As the global silencing of *Ski* early in development is lethal to mice (as it is required for normal development), we used a conditional knockdown model implementing the Cre-LoxP system. The

highlights of the current thesis include the confirmation of a *Ski* splice variant in mouse cardiac myofibroblasts, establishment of a reliable method to confirm a knockdown model and analyzing gene specific effects (eg, mRNA abundance) of *Ski* knockdown in Cre treated primary cardiac myofibroblasts.

Taguchi et.al. (2019) and Bonnon et.al. (2012) have shown that SKI is elevated in cancer and metastasis[192, 200]. Their results are presented in the context of SKI's negative repression of TGF-β_1 which in cancer cells has been shown to prevent cell death, leading to dissemination of cancer cells. Tecalco-Cruz et.al (2018) and Xie et.al (2017) reveal SKI inhibiting progression of other types of cancer[162, 175]. These apparent contradictory findings may be explained by the pleuripotency of SKI (a phylogenetically ancient protein) and the cellular location of SKI in different diseases. Our current work indicates the existence of SKI transcript variants and thus it is possible that differential function of transcript variants also contributes to these disparate findings; however, there are no studies in the literature that address alternative SKI splice variant function, including cardiac fibrosis. According to GENCODE 39, there are close to 20,000 recognized protein-coding genes, with approximately 90,000 known isoforms in humans[280]. This wide range encompasses considerable biovariability, configurating a broader scope of protein function, increasing the system complexity[281]. Thus, it is unknown whether SKI tv1 (full length) and SKI tv2 (without exon 2) exert different functions or act in different stages in cardiac fibrosis. Thus, we have completed the first step in the characterization of SKI isoforms by isolating those isoforms and being able to recognize each exon and their presence/absence is mouse cardiac myofibroblasts.

Another goal within the outline of the thesis was to establish a reliable protocol for SKI knockdown *in vitro* for mouse cardiac myofibroblasts. The use of an adenoviral vector

overexpressing Cre recombinase is a practical method to cause the deletion of critical exons (exon 2 and 3). This is not to say that this is a method without complications, indeed Rezai Amin et.al (2019) and Frahsek et.al (2019) have underscored the toxicity of Cre and we fully acknowledge that this consideration is a potential pitfall within our data analysis[267, 282]. In an attempt to control for Cre toxicity, non-transgenic (wild-type or WT) mouse cardiac myofibroblasts were also transfected with Ad-Cre. In this manner, we confirmed roughly parallel effects in WT murine cells as observed Ski-floxed cells subjected to the same treatment. Another consideration within our experimental design during this investigation was culture plate substrate stiffness and starved-serum media conditions to influence mRNA expression, which was evaluated by using untreated non-transgenic cells. Thus, we strove to discern the extent of influence on mRNA expression variation was due to *Ski* knockdown *per se*, as well as Cre toxicity and biomechanical stress input. The control (Ad-GFP) for wild-type timepoints for data contained in the Supplemental Figures was harvested only at 72h and was then compared to other timepoints. While each timepoint should ideally be compared to the same duration (e.g., 48h Ad-GFP vs 48h Ad-Cre) we were limited in our ability to do so, due to animal viability and limited cell amount and thus cell groups were split into a maximum of five 10 cm^3 polystyrene (plastic) plates. As 72h post-transfection was considered to be the standard duration for more than 75% of cells being infected, this was the timepoint used for most comparisons. Finally, we note that the impact of mechanical stress and serum-free media in untreated cells cannot be distinguished in these experiments. To approach that, several other controls could have been added: by plating cells in 5 kPa (Young's modulus "heart-soft") plates to evaluate the mechanical component and having cells in starved-serum media and supplemented media. Nonetheless Ski-floxed cells were plated out on relatively stiff polystyrene (plastic) plates and

the media was changed to low nutrient (starved) media and thus the untreated samples were considered adequate controls for this project.

Prior to assessing *Ski* knockdown in our mouse model, we resolved to confirm the genotype of these mice at the DNA level. Thus, we sought to identify the components of the Cre-LoxP system within this mouse model (*Ski* KO). The first step consisted of verifying the genotype and penetrance of the mutation in different tissues in untreated *Ski* KO animals. The genotype represented the presence of the cassette sequence in the genomic DNA. This step is established if Ski-floxed cassette was homozygous as expected or if further breeding manipulation was required for efficient deletion. Takebayashi et.al. (2008) observed that homozygous MerCreMer animals were associated with a modicum of embryonic toxicity, with cell death upon Cre activation through tamoxifen[283]. Despite the current genotype in our hands (homozygous), we did not see elevated levels of mortality or malformation in transgenic mice. Further, we sought to confirm the location and effectiveness of *Ski* exon 2 and 3 excision. Thus, we carefully analyzed DNA sequences to compare each theoretical base-pair to experimental samples and we observed a differential form to be distinguished from the physiological splice variants. That is, the physiological splicing is noted to skip one exon in-frame which we interpreted to be when genomic DNA folds to expose the reading frame, only exon 2 was skipped so that the rest of the reading sequence remains intact. However, in this knockdown model, exons 2 and 3 are excised, and this excision leads to a frameshift, which creates a stop-codon – TGA – interrupting the reading. This finding confirmed that three days treatment of primary murine cardiac fibroblasts from *Ski* KO mice with Ad-Cre led to excision of exons 2 and 3. Nonetheless we observed that only targeting exons 2 and 3 would still show presence of these exons and we suggest that this is due to remanence of transcriptome[227, 284]. Despite gDNA having

the excision, a pool of mRNA pre-excision is still present in a low amount. To avoid this scenario prolonged exposure to Ad-Cre treatment would be necessary but this is balanced by potential elevation of Cre toxicity. However, further investigation to interrogate this theory is still required.

SKI has been studied for more than three decades since the time of its discovery[178], and for approximately 15 years in our lab, since the discovery of its repressor function of TGFβ_1/Smad signalling. In heart, SKI overexpression is associated with modulating the repression of TGF-β_1 pathway directly while promoting the deactivation of the cardiac myofibroblast (i.e., promotion of the quiescent fibroblast) phenotype[54]. It is well known that plating of fibroblasts on stiff plastic substrates is associated with rapid activation of fibroblasts to myofibroblasts[90]. Cunnington *et al* demonstrated that overexpression of exogenous SKI is sufficient to deactivate cardiac myofibroblasts to fibroblasts[90]. Our recent work, by Landry et.al (2021) indicates that SKI interacts with LIMD1 to promote the Hippo pathway, inhibiting TAZ pro-fibrotic role in cardiac fibrosis[85, 168]. We hypothesized that in the absence of *Ski*, mRNA abundance of fibrotic marker genes and associated genes would be elevated *in vitro* due to the cardiac fibrosis repressor role of SKI. In a model of intervertebral disc degeneration, the role of SKI knockdown in nucleus pulpous cells was attempted (centre of intervertebral disc[216]) and it was shown that SKI knockdown inhibited apoptosis induced by IL-1β and reduced ECM degradation in those cells by inhibiting Wnt/β-catenin pathway[216]. Our lab had previously shown that adenoviral mediated SKI overexpression is associated with significant fibroblast apoptosis when administered in high titre[169]. Zhao et.al. (2020) carried out a study of *Ski* knockdown in osteosarcoma and observed that *Ski* knockdown reduced cell proliferation and migration by inhibiting PI3k/Akt pathway[215]. In human cardiomyocytes cell line (H9C2), Ling et.al (2019)

carried *Ski* knockdown, which supressed cell proliferation, but increased cell invasion and TGF-β_1 epithelial-mesenchymal transition without altering α-SMA and FN-1[217]. Moreover, Landry et.al (2021), from our laboratory, also studied *Ski* knockdown as part of a larger project. *Ski* knockdown in cardiac fibroblasts plated in soft substrate (5 kPa) further treated with TGF-β_1 practically removed all F-actin but did not increase myofibroblast activation and did not significantly affect *Ctgf* and *Taz* (i.e., *Wwtr1*) mRNA expression. A stiff substrate (polystyrene culture plates) did not cause any significant changes when compared to control[168]. All of these studies, however, used small interfering RNA (siRNA) or short hairpin RNA (shRNA) knockdown models. These models use vectors containing up to 80 nucleotides of RNA sequences to cause gene silencing. siRNA transfection peak is reached after 4h and at 48h, approximately 99% is degraded[285]. siRNA and shRNA systems differ mechanistically, as siRNA uses the RNA-induced Silencing Complex (RISC) to knockdown the target gene, while shRNA is incorporated into the genomic DNA and creates a hairpin to silence the critical gene[286, 287]. For this reason, shRNA tends to be more efficient and specific with prolonged knockdowns. However, Rao et.al (2009) and Acharya R. (2019) highlighted that both systems present elevated levels of off-target effects, increasing non-specific transcription[285, 286]. Mismatches may be placed in the sequences to avoid this toxic effect, but it may compromise the specificity of the knockdown. Another issue observed by Gavrilov et.al. (2012) is instability of siRNA sequences, reducing its efficiency[288]. Thus, these effects may explain some of the obtained results within our dataset, as using the Cre-LoxP system provides a direct manipulation of gene deletion, albeit with the associated cellular toxicity invoked by Cre itself. One promising alternative to cause *Ski* knockdown is the use of clustered regularly interspaced palindromic repeats (CRISPR)-Cas9 system to avoid siRNA, shRNA and Cre recombinase off-target effects. This genome-editing

tool was developed by Dr. Charpentier and Doudna (Nobel Prize in Chemistry 2020), which is based on *E. coli* immune system machinery to specifically edit the genome[289]. The specificity and efficiency of this system with lower off-target effects may provide accurate method to edit and knockdown *Ski.*

This project is marked by limitations in control group sample size, and, as is alluded to above, in the investigation of the influence of *Ski* knockdown at the level of protein expression. This is an important limitation as it is well known that transcriptional asynchrony may exist at the level of mRNA and proteins, especially in constitutively expressed genes including fibrillar *collagen 1α1* and *3α1*, *Ski* itself, *α-Sma* and *Eda-Fn*.

With respect to variations in sample size among groups, we note that while at least six different mice were used for Ski-floxed experiments this number of samples was not reached for wild-type groups, and this limited the power of our comparisons. For example, α-SMA (*Acta2*) (Fig. 4.6.2) Ski-floxed Ad-Cre samples (n = 9) was marked by relatively high standard deviation, which will naturally reduce the statistical significance for the comparison with wild-type Ad-Cre. We speculate that a source of abnormally elevated standard deviation is provided by Younesi et.al (2021), as α-SMA is increased in myofibroblasts in varying levels during fibroblast activation. Fibroblasts activate to myofibroblasts at different rates and stages, leading to a high cellular variability, increasing the standard deviation among samples[290]. This may be due to the high degree of fibroblast phenotype variation, even at basal levels[8].

The *Yap1* mRNA abundance expression deserves a comment in the context of this discussion (Fig. 4.7.1). We analyzed this gene using qPCR analysis; however, in some samples, specifically wild-type and Ski-floxed Ad-GFP cardiac myofibroblast, we noted that the melting curve produced two peaks. Possible sex-specific results were excluded as we found that two

peaks were present in both sexes. Technical errors were also excluded by repeating qPCR with fresh reagents (nuclease-free water, Luna Master Mix, *Yap*1 primers, and samples aliquots), sterile conditions (use of 100% Ethanol on the bench area, equipment, gloves, and bottles), as well as performing electrophoresis with qPCR products to confirm the predicted size, and to exclude presence of primer dimerization. We found that while qPCR electrophoresis showed a single band at the predicted size (133 bp), the melting curve for *Yap1* still produced two peaks for some Ad-GFP samples, and we felt that this work legitimized the result. One possible explanation for the duality of the melting curve is the likelihood of a transcriptional variant in the samples specific for *Yap1*. In this case, some Ad-GFP samples would have different proportions of splice variants which would be shown by the presence of two peaks in the melting curve and while Ad-Cre could be affecting only one of the variants, showing only one peak in the melting curve. The presence of a single band in electrophoresis in the presence of splicing variants could be explained by insufficient time to separate splice variants. Further investigation is necessary with use and optimization of PCR by adjusting the number of cycles, choosing different agarose gel percentages to better distinguish possible splicing variant bands, as well as prolonged electrophoresis to promote band dissociation, in addition to selection of a diversified number of primers that would allow us to analyze different portions of *Yap1* DNA sequence with following comparative DNA sequencing to confirm this finding.

As mentioned above, a limitation within the design of this study is the lack of accompanying investigation of protein products of the listed fibroblast and myofibroblast target genes to lend credence to Cre-based knockdown of *Ski* knockdown in our transgenic mouse model. Despite *Ski* knockdown failing to show direct effects to fibrillar *collagen 1α1 and 3α1, ED-A Fn, Pdgfr-α, Mmp-14, α-SMA, Yap1, Lats2, Limd1* mRNA expression, the effects on the

protein levels were not addressed. For example, α-SMA protein detection in transgenes' cultured myofibroblasts using immunofluorescence and Western analysis would be useful in confirming phenotype activation/deactivation by directly addressing α-SMA incorporation into the cellular stress fibres (see below in Future Directions – chapter 6). We also note that this study did not address other members of the SKI superfamily including SnoN, which has been demonstrated to dimerize with SKI in non-cardiac cells – we suggest that SKI/SnoN dimerization may be an additional means used by fibroblasts to repress normal TGFβ_1/Smad signaling.

Chapter 6: Future Directions

Since the initial discovery and recognition of the various stages of heart failure, therapy for this condition has improved life expectancy and quality of life[291]. Since roughly 2008[26], a major paradigm shift has occurred in basic cardiovascular sciences to include cardiac fibrosis as a *de facto* driver of heart failure [292]. However, despite the advances in cardiac devices, pharmacological treatments and transplantation technology and implementation, there are still no specific drugs that may target cardiac fibrosis[125] and the current study was designed to take a small step toward the investigation of SKI as a putative antifibrotic protein, following up on previous work from this laboratory. The following areas of investigation may be achieved in the future to complement the current work:

1. *Studies of target gene proteins vs mRNAs*. Our investigation is limited to the study of *Ski* transgenic myofibroblast cultures treated with Cre (to initiate *Ski* knockdown), and then to address one aspect of transcription (steady state mRNA abundance). As asynchronous expression of constitutive genes (i.e., fibrillar *collagen types I and III*) is well known to occur in heart and other organs, it may be that while mRNAs are unchanged, the similar pattern of expression for the protein product of the genes that we interrogated. Thus, a complementary dataset could be generated which would address protein abundance of target genes listed in the current thesis. This could be achieved via the use of standard Western blot technology or immunofluorescence of cells cultured *in vitro*. The caveat in these studies includes the reliability of the primary antibodies. This notwithstanding, it would be an optimal and feasible way to assess the synchronous or asynchronous mRNA/protein expression patterns of the list of target genes in these experimental conditions.

2. *Alternative means to knock down Ski in vitro.* One of the findings of the current exploratory work was indication of the relative impact of nonspecific Cre induction had upon the target genes used in the current study. While it was beyond the scope of the current project, we could use wild type myofibroblasts in culture to reassess target gene expression (i.e., markers of cardiac fibrosis) using alternative methods to inhibit transcription of *Ski* thereby knocking it down. This might include CRISPR-Cas9, siRNA, shRNA, or bifunctional shRNA techniques[285, 289].
3. *Use of experimental antifibrotic drugs to address mRNA abundance of target genes*. One of the latest drugs to be studied as a modulator of cardiac fibrosis is pirfenidone, a small molecule designed to treat idiopathic pulmonary fibrosis (IPF)[293]. Another drug to be considered is verteporfin which is a novel inhibitor of fibroblast mechanosensation and is also known to mimic the knockdown of the YAP[294]. While verteporfin is strictly an experimental agent, pirfenidone has been found to reduce fibrosis in the lungs and heart[293, 295]. Pirfenidone has been implemented in a phase 2 trial clinical trial (PIROUETTE) [296, 297]. The patients in this trial have heart failure with preserved ejection fraction and it also shown that these patients undergo a reduction of cardiac fibrosis[298]. Despite pirfenidone being classified as a TGF-β inhibitor, the molecular mechanisms are still not completely understood, as some researchers also add modulation of RAAS system and tumour necrosis factor alpha as possible mechanisms of action[299, 300]. We would examine the effects of either pirfenidone or verteporfin in a dose-dependent or time-dependent manner (or both) to determine their effects (if any) on *Ski* expression. If *Ski* is knocked down, then a follow up study to assess those drugs' influence on fibrotic marker genes would be of considerable interest.

4. *Investigation of the effects of Ski mRNA isoform variants*. SKI protein appears to be highly involved in cardiac fibrosis suppression and may be targeted for heart failure therapy[90]. We observe that *Ski* presents with two different mRNA isoforms (splice variants), with and without exon 2. To study their functions, we would like to isolate both variants and insert them into a vector to study their function by overexpressing them separately using cell culture *in vitro*. The endpoints would be to assess whether fibroblast activation would proceed normally in the presence of either variant to determine the net influence of each form on fibroblast phenotype. Our lab has shown that full length SKI protein overexpression regulates myofibroblast phenotype (it deactivates myofibroblasts subjected to mechanical stress by plating on stiff substrates) with an association of ECM component proteins.

Chapter 7: Appendices

A.

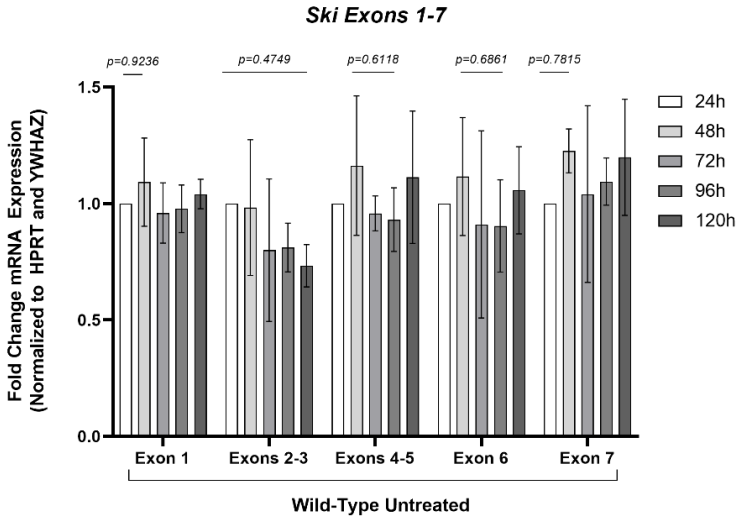

B.

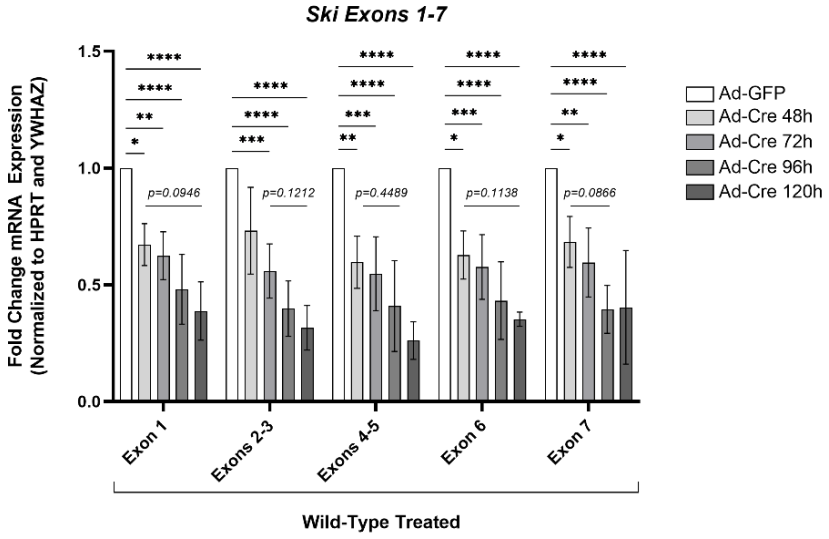

Supplemental Figure 1. ***Ad-Cre treatment knocks down Ski mRNA expression in wild-type primary cardiac myofibroblasts.***

mRNA was extracted from murine primary cardiac myofibroblasts cultured in plastic and analyzed by qPCR. A. Untreated serum-starved control cells cultured in plastic and harvested every 24h. B. Non-transgenic (wild-type) cells infected with Ad-GFP (control) or Ad-Cre. Ad-GFP cells were harvested at 72h and Ad-Cre were harvested at 48h, 72h, 96h and 120h after infection in starving conditional media. Ad-Cre infection alone was seen to reduce *Ski* gene expression over time. Total biological replicates n=3, except for Wild-Type Ad-Cre 48h with n=2. Each biological replicate was evaluated by 3 technical replicates. Ns: $P \geq 0.05$; *: $P < 0.05$; **: $P < 0.01$; ***: $P < 0.001$; ****: $P < 0.0001$. Ad-GFP = Adenoviral-GFP (control virus); Ad-Cre = Adenoviral-Cre; HPRT = hypoxanthine phosphoribosyltransferase 1; YWHAZ = tyrosine 3-monooxygenase/tryptophan 5-monooxygenase activation proteins zeta, both housekeeping genes used for normalization.

A.

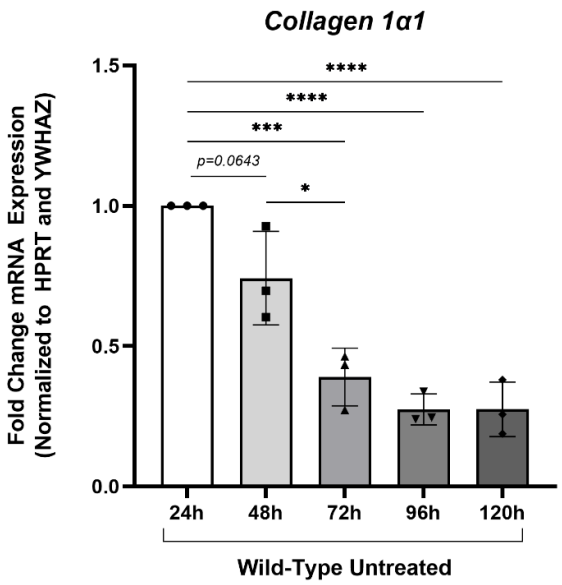
Collagen 1α1
Fold Change mRNA Expression (Normalized to HPRT and YWHAZ)
1.5
1.0
0.5
0.0
****
****
***
p=0.0643
*
24h
48h
72h
96h
120h
Wild-Type Untreated

B.

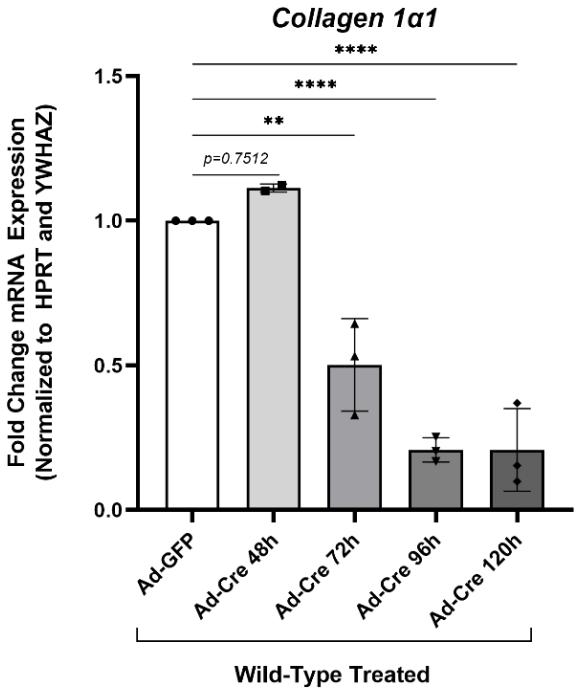
Collagen 1α1
Fold Change mRNA Expression (Normalized to HPRT and YWHAZ)
1.5
1.0
0.5
0.0
****
****
**
p=0.7512
Ad-GFP
Ad-Cre 48h
Ad-Cre 72h
Ad-Cre 96h
Ad-Cre 120h
Wild-Type Treated

C.

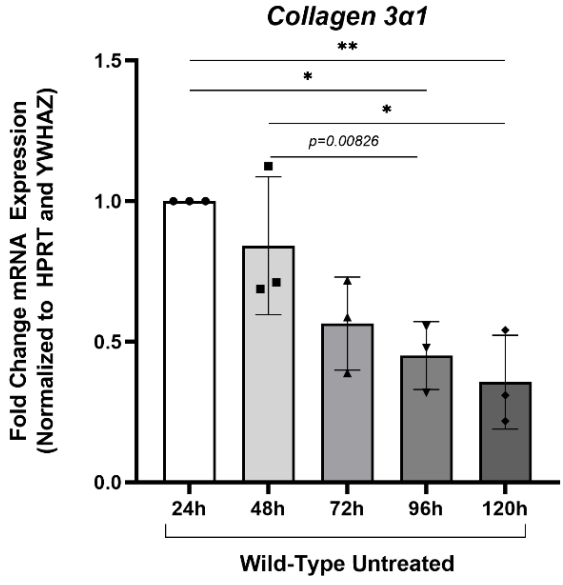
Collagen 3α1
Fold Change mRNA Expression (Normalized to HPRT and YWHAZ)
1.5
1.0
0.5
0.0
**
*
*
p=0.00826
24h
48h
72h
96h
120h
Wild-Type Untreated

D.

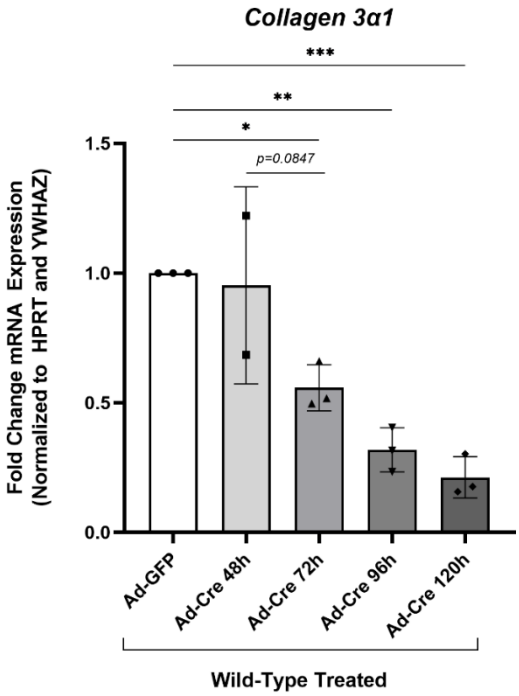
Collagen 3α1
Fold Change mRNA Expression (Normalized to HPRT and YWHAZ)
1.5
1.0
0.5
0.0
***
**
*
p=0.0847
Ad-GFP
Ad-Cre 48h
Ad-Cre 72h
Ad-Cre 96h
Ad-Cre 120h
Wild-Type Treated

Supplemental Figure 2. ***Time-dependent loss of Collagen 1α1 and Collagen 3α1 mRNA expression in Ad-Cre treated and untreated wild-type primary cardiac myofibroblasts.***

mRNA was extracted from murine P0 primary cardiac myofibroblasts, cultured and analyzed by qPCR. **A. and C.** Untreated serum-starved control cells cultured in plastic and harvested every 24h. **B. and D.** Non-transgenic (wild-type) cells infected with Ad-GFP (control) or Ad-Cre. Ad-GFP cells were harvested at 72h and Ad-Cre were harvested at 48h, 72h, 96h and 120h after infection in starving conditional media. Significant over time reduction of *Collagen 1α1* and *Collagen 3α1* gene expression in both sets of samples. Total biological replicates n=3, except for Wild-Type Ad-Cre 48h with n=2. Each biological replicate was evaluated by 3 technical replicates. Ns: P ≥ 0.05; *: P < 0.05; **: P < 0.01; ***: P < 0.001; ****: P < 0.0001. Ad-GFP = Adenoviral-GFP (control virus); Ad-Cre = Adenoviral-Cre; HPRT = hypoxanthine phosphoribosyltransferase 1; YWHAZ = tyrosine 3-monooxygenase/tryptophan 5-monooxygenase activation proteins zeta, both housekeeping genes used for normalization.

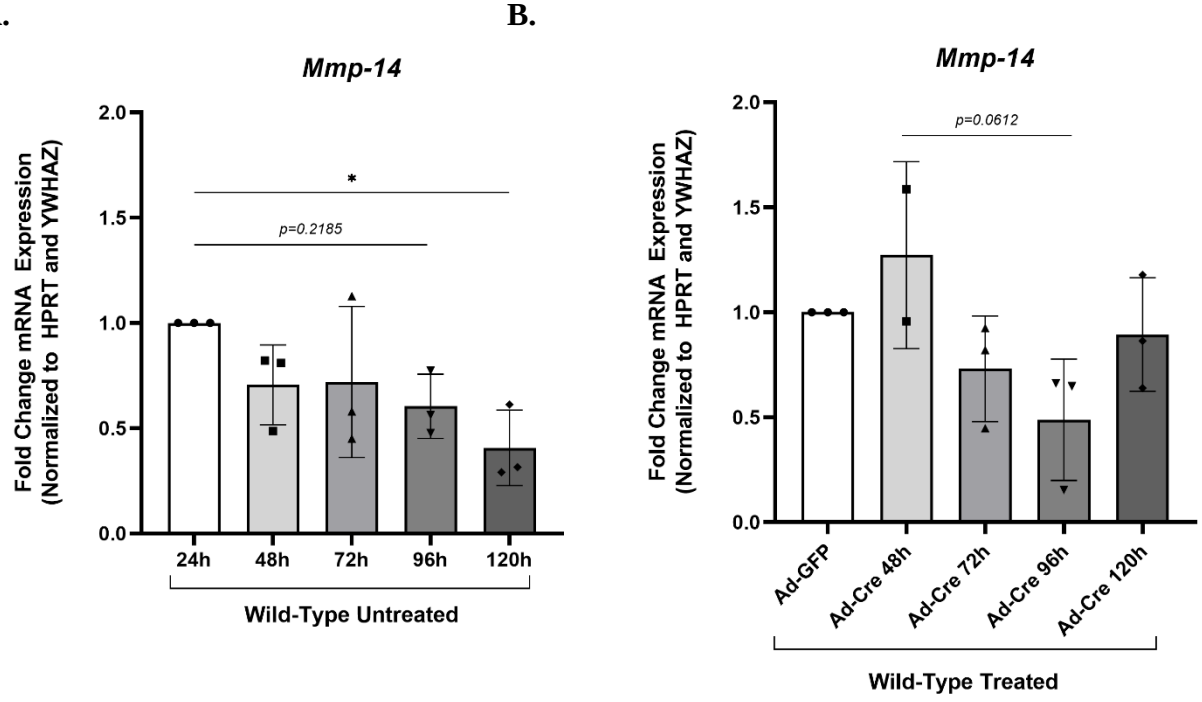

Supplemental Figure 3. ***Reduction of Mmp-14 mRNA expression in untreated wild-type primary cardiac myofibroblasts***.

mRNA was extracted from murine primary cardiac myofibroblasts cultured in plastic and analyzed in qPCR. **A.** Represents wild-type cells cultured in plastic and not submitted to any treatment but harvested every 24h after starving conditional media. **B.** Represents wild-type cells cultured in plastic and infected with Ad-GFP or Ad-Cre. These cells were harvested at 48h, 72h, 96h and 120h after infection in starving conditional media. We observed a significant reduction of *Mmp-14* mRNA expression vs control after 120h culture in untreated samples. On the other hand, we saw no significant reduction of *Mmp-14* gene expression in Ad-Cre treated samples vs controls. Total biological replicates n=3, except for Wild-Type Ad-Cre 48h with n=2. Each biological replicate was evaluated by 3 technical replicates. Ns: P ≥ 0.05; *: P < 0.05. Ad-GFP = Adenoviral-GFP (control virus); Ad-Cre = Adenoviral-Cre; *Mmp-14* = Matrix-metalloproteinase-14; HPRT = hypoxanthine phosphoribosyltransferase 1; YWHAZ = tyrosine 3-

monooxygenase/tryptophan 5-monooxygenase activation proteins zeta, both housekeeping genes used for normalization.

A. **B.**

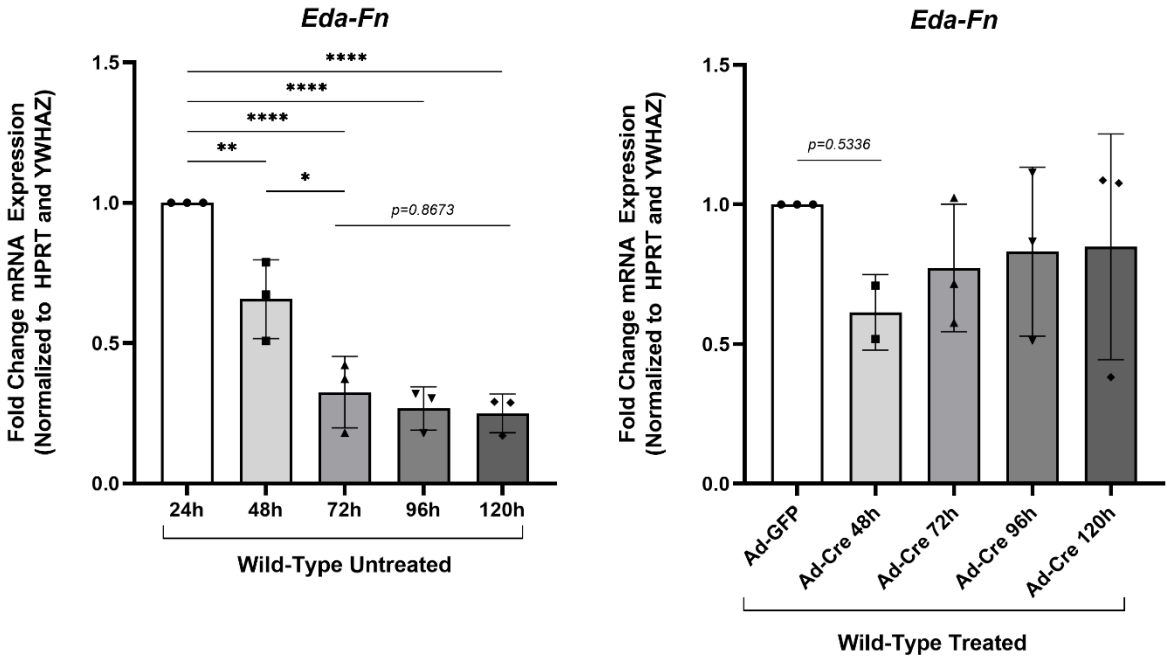

Supplemental Figure 4 ***Control vs Ad-Cre treatment of Eda- Fn mRNA expression in wild-type primary cardiac myofibroblasts.***

mRNA was extracted from murine primary cardiac myofibroblasts cultured in plastic and analyzed in qPCR. **A.** Represents wild-type cells cultured on plastic and not submitted to any treatment but harvested every 24h after starving conditional media. **B.** Represents wild-type cells cultured on plastic and infected with Ad-GFP or Ad-Cre. These cells were harvested at 48h, 72h, 96h and 120h after infection in starving conditional media. We observed a significant reduction of *Eda-Fn* mRNA expression in untreated myofibroblasts over time but observed no significant changes vs control in Ad-Cre samples. Total biological replicates n=3, except for Wild-Type Ad-Cre 48h with n=2. Each biological replicate was evaluated by 3 technical replicates. Ns: $P \geq 0.05$; **: $P < 0.01$; ****: $P < 0.0001$. Ad-GFP = Adenoviral-GFP (control virus); Ad-Cre = Adenoviral-Cre; *Eda-Fn* = Extra Domain A Fibronectin; HPRT = hypoxanthine phosphoribosyltransferase 1; YWHAZ = tyrosine 3-monooxygenase/tryptophan 5-monooxygenase activation proteins zeta, both housekeeping genes used for normalization.

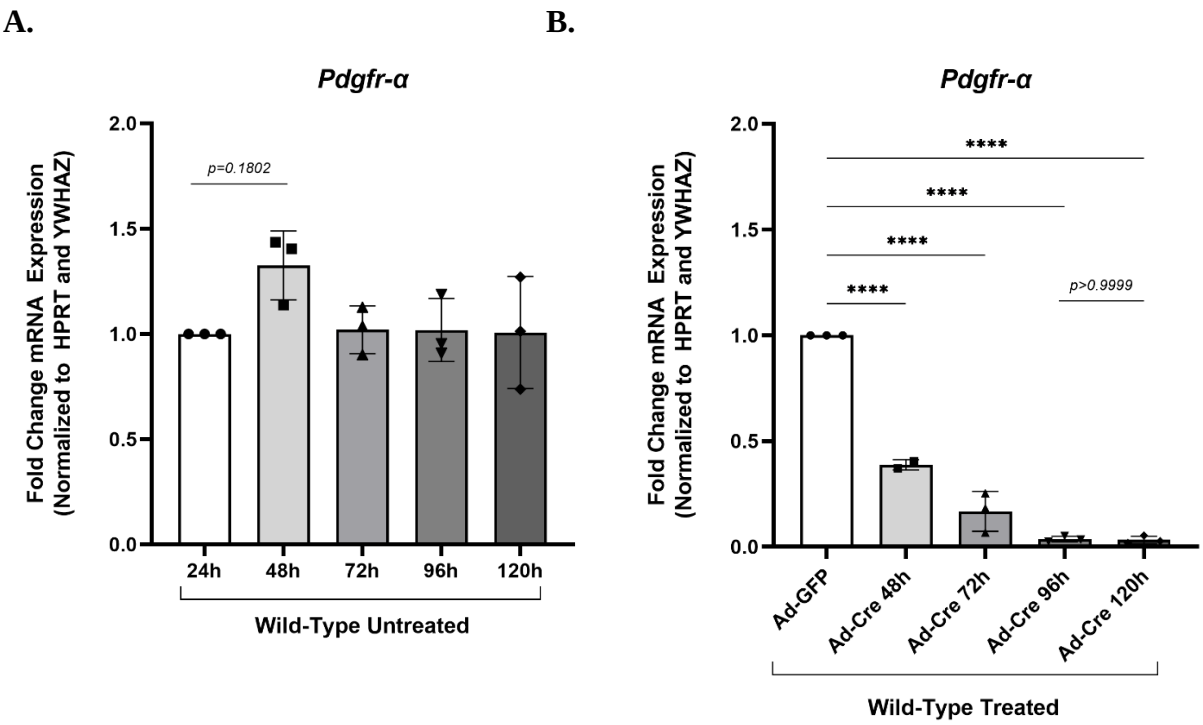

Supplemental Figure 5 ***Time-dependent reduction of Ad-Cre treatment on Pdgfr-α mRNA expression in wild-type primary cardiac myofibroblasts.***

mRNA was extracted from murine primary cardiac myofibroblasts cultured in plastic and analyzed in qPCR. **A.** Represents wild-type cells cultured in plastic and not submitted to any treatment but harvested every 24h after starving conditional media. **B.** Represents wild-type cells cultured in plastic and infected with Ad-GFP or Ad-Cre. These cells were harvested at 48h, 72h, 96h and 120h after infection in starving conditional media. We did not see any statistical differences in untreated samples vs control and experimental groups with time in *Pdgfr-α* mRNA expression. On the other hand, Ad-Cre infection significantly reduced *Pdgfr*-α mRNA expression vs control over time. Total biological replicates n=3, except for Wild-Type Ad-Cre 48h with n=2. Each biological replicate was evaluated by 3 technical replicates. Ns: $P \geq 0.05$; ****: $P < 0.0001$. Ad-GFP = Adenoviral-GFP (control virus); Ad-Cre = Adenoviral-Cre; *Pdgfr-α* = Platelet-derived growth factor receptor alpha; HPRT = hypoxanthine phosphoribosyltransferase 1; YWHAZ = tyrosine 3-monooxygenase/tryptophan 5-monooxygenase activation proteins zeta, both housekeeping genes used for normalization.

A. **B.**

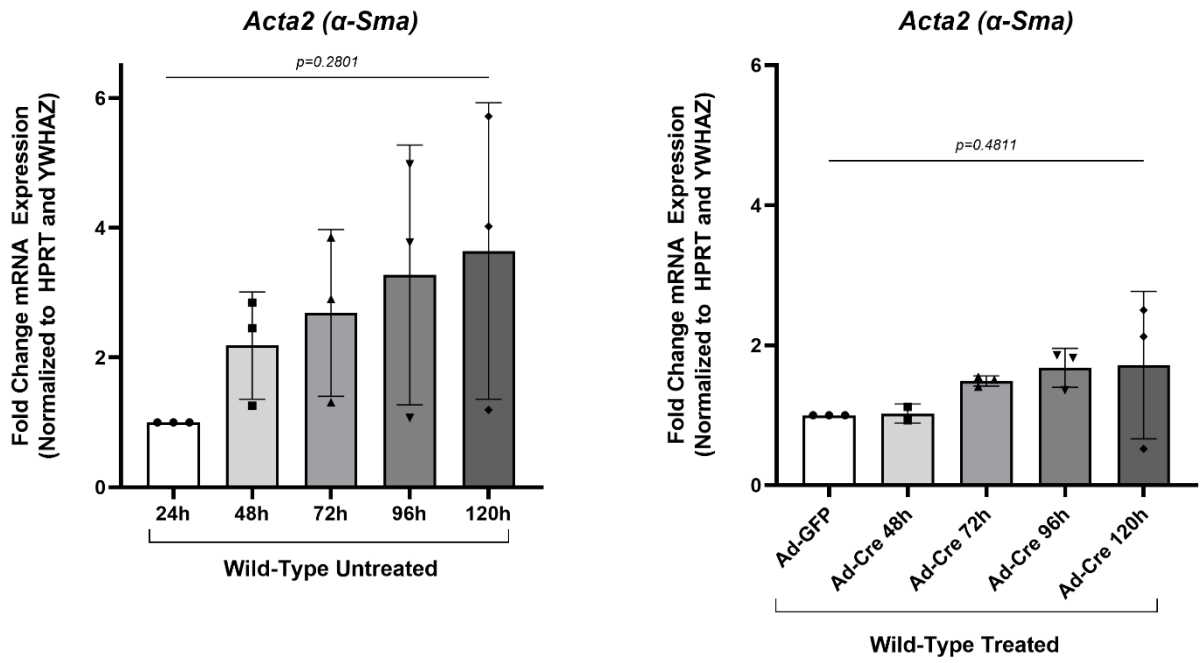

Supplemental Figure 6 ***Acta2 (α-Sma) mRNA expression is elevated over time in cardiac myofibroblast control serum-starved culture conditions. Treatment of mouse myofibroblasts with Ad-Cre was not associated wit any change in α-Sma over time.***

mRNA was extracted from murine P0 primary cardiac myofibroblasts analyzed by qPCR. **A.** Control serum-starved myofibroblast cultures harvested every 24h. **B.** Non-transgenic wild-type murine P0 cardiac myofibroblasts infected with Ad-GFP (control) or Ad-Cre. Ad-GFP samples were harvested at 72h and Ad-Cre were harvested at 48h, 72h, 96h and 120h. As the variance among samples was very high n the untreated groups, no significant change of *Acta2* mRNA expression was noted vs controls. Cre treatment was not associated with any change vs control group value. Total biological replicates n=3, except for Wild-Type Ad-Cre 48h with n=2. Each biological replicate was evaluated by 3 technical replicates. Ns: $P \geq 0.05$. Ad-GFP = Adenoviral-GFP (control virus); Ad-Cre = Adenoviral-Cre; *Acta2* = Actin alpha-2 (or *α-Sma*); HPRT = hypoxanthine phosphoribosyltransferase 1; YWHAZ = tyrosine 3-monooxygenase/tryptophan 5-monooxygenase activation proteins zeta, both housekeeping genes used for normalization.

A.

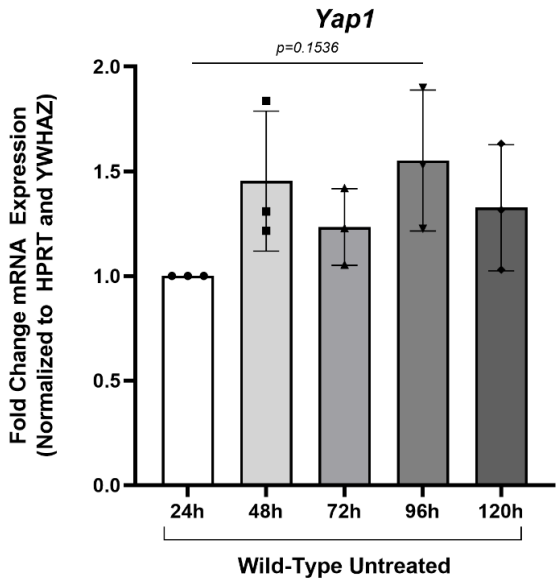

B.

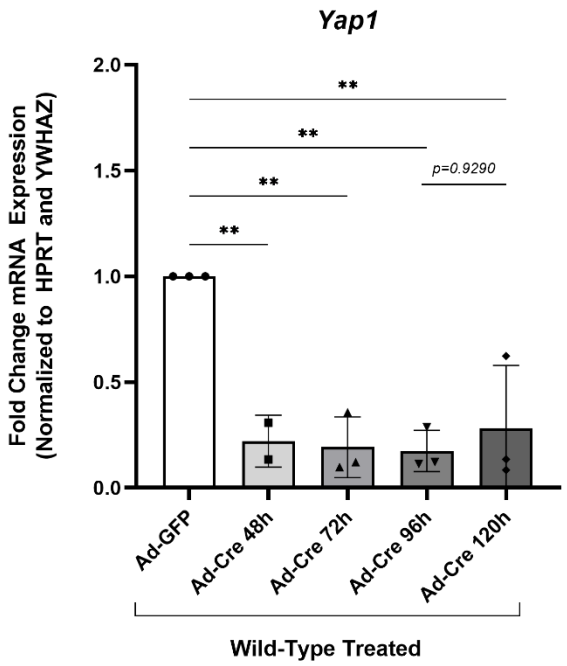

Supplemental Figure 7 ***Untreated primary myofibroblast expression of Yap1 versus Ad-Cre treatment effects in Yap1 mRNA expression.***

mRNA was extracted from murine primary cardiac myofibroblasts cultured in plastic and analyzed in qPCR. Panel **A.** Represents wild-type cells cultured on plastic culture plates and not subjected to any treatment. Myofibroblasts were harvested every 24h after starving conditional media. Panel **B.** This panel shows data from myofibroblasts cultured and infected with Ad-GFP or Ad-Cre. Ad-GFP was harvested at 72h, and Ad-Cre were harvested at 48h, 72h, 96h and 120h after infection in starving conditional media. In the untreated myofibroblast group, we saw no significant changes in *Yap1* gene expression with time, however a significant reduction of *Yap1* RNA expression is observed in Ad-Cre samples over time was seen vs control Ad-GFP infected myofibroblasts. Total biological replicates n=3, except for Wild-Type Ad-Cre 48h with n=2. Each biological replicate was evaluated by 3 technical replicates. Ns: $P \geq 0.05$; **: $P < 0.01$. Ad-GFP = Adenoviral-GFP (control virus); Ad-Cre = Adenoviral-Cre; *Yap1*= Yes-associated protein 1; HPRT = hypoxanthine phosphoribosyltransferase 1; YWHAZ = tyrosine 3-monooxygenase/tryptophan 5-monooxygenase activation proteins zeta, both housekeeping genes used for normalization.

A. **B.**

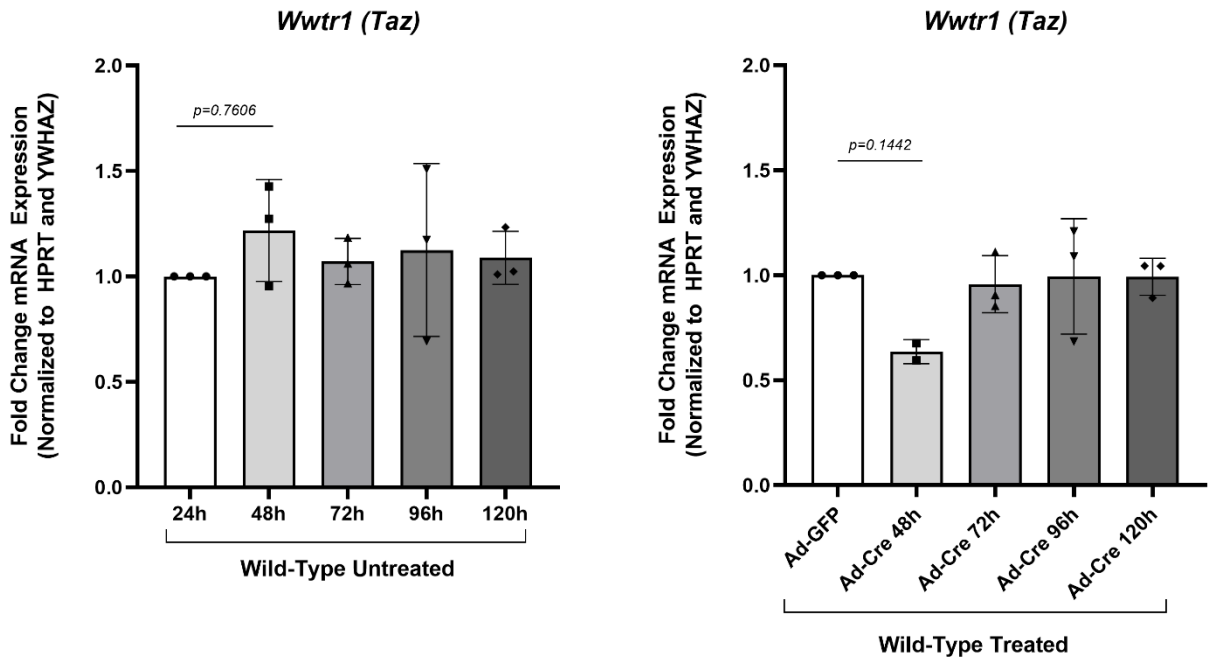

Supplemental Figure 8 ***Wwtr1 (Taz) mRNA expression is not affected in untreated or Ad-Cre treated primary cardiac myofibroblasts.***

mRNA was extracted from cultured murine P0 primary cardiac myofibroblasts and analyzed by qPCR. **A.** Untreated wild-type (non-transgenic) myofibroblasts cells cultured on plastic with serum-free media were harvested every 24h. **B.** Wild-type cells cultured on plastic and infected with Ad-GFP (control) or Ad-Cre. Control samples were harvested at 72h, while experimental group was harvested at 48h, 72h, 96h and 120h after infection. We observed no significant changes in *Wwtr1(Taz)* mRNA expression conditional groups. Total biological replicates n=3, except for Wild-Type Ad-Cre 48h with n=2. Each biological replicate was evaluated by 3 technical replicates. Ns: $P \geq 0.05$. Ad-GFP = Adenoviral-GFP (control virus); Ad-Cre = Adenoviral-Cre; *Wwtr1* = WW Domain Containing Transcription Regulator 1; HPRT = hypoxanthine phosphoribosyltransferase 1; YWHAZ = tyrosine 3-monooxygenase/tryptophan 5-monooxygenase activation proteins zeta, both housekeeping genes used for normalization.

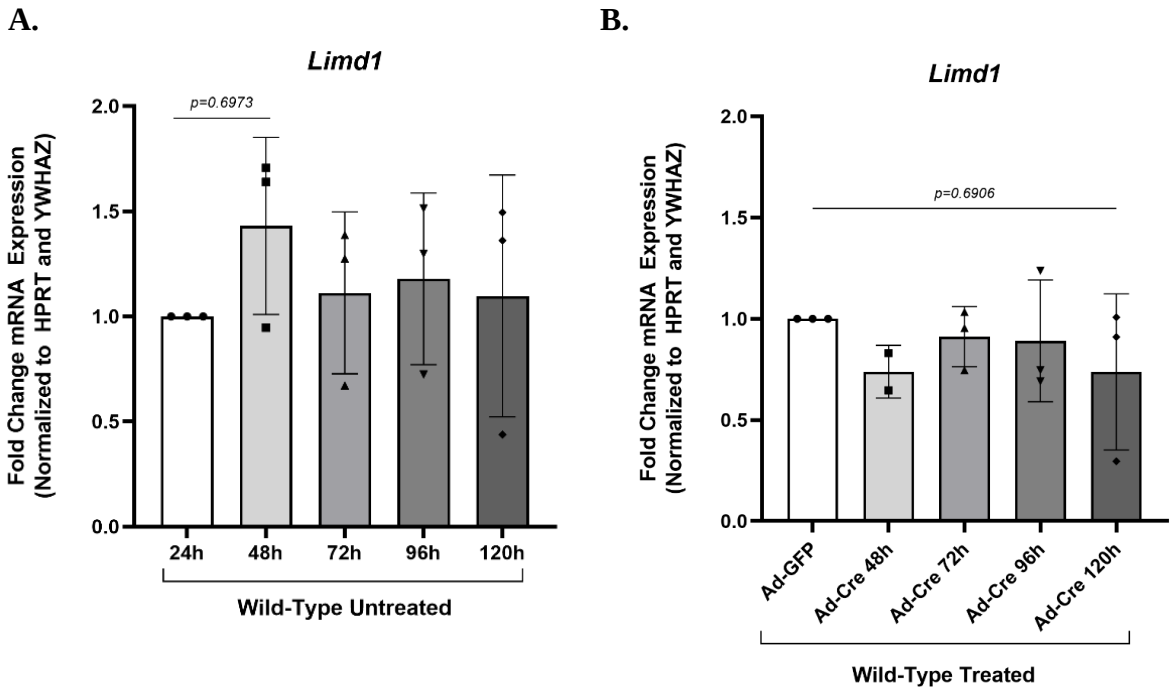

Supplemental Figure 9 ***Untreated or Ad-Cre wild-type primary cardiac fibroblasts do not interfere with Limd1 mRNA expression.***

mRNA was extracted from murine primary cardiac myofibroblasts cultured on polystyrene (plastic) and analyzed by qPCR. Panel **A.** Wild-type untreated cells cultured on plastic and harvested every 24h until 120h after cultured in serum-starved media. **B.** Represents wild-type cells cultured in plastic and infected with Ad-GFP or Ad-Cre. These cells were harvested at 48h, 72h, 96h and 120h after infection in starving conditional media. All the comparisons reached non-significant values for *Limd1* gene expression in either sets of samples. Total biological replicates n=3, except for Wild-Type Ad-Cre 48h with n=2. Each biological replicate was evaluated by 3 technical replicates. Ns: $P \geq 0.05$. Ad-GFP = Adenoviral-GFP (control virus); Ad-Cre = Adenoviral-Cre; *Limd1* = LIM Domain Containing 1; HPRT = hypoxanthine phosphoribosyltransferase 1; YWHAZ = tyrosine 3-monooxygenase/tryptophan 5-monooxygenase activation proteins zeta, both housekeeping genes used for normalization.

A. **B.**

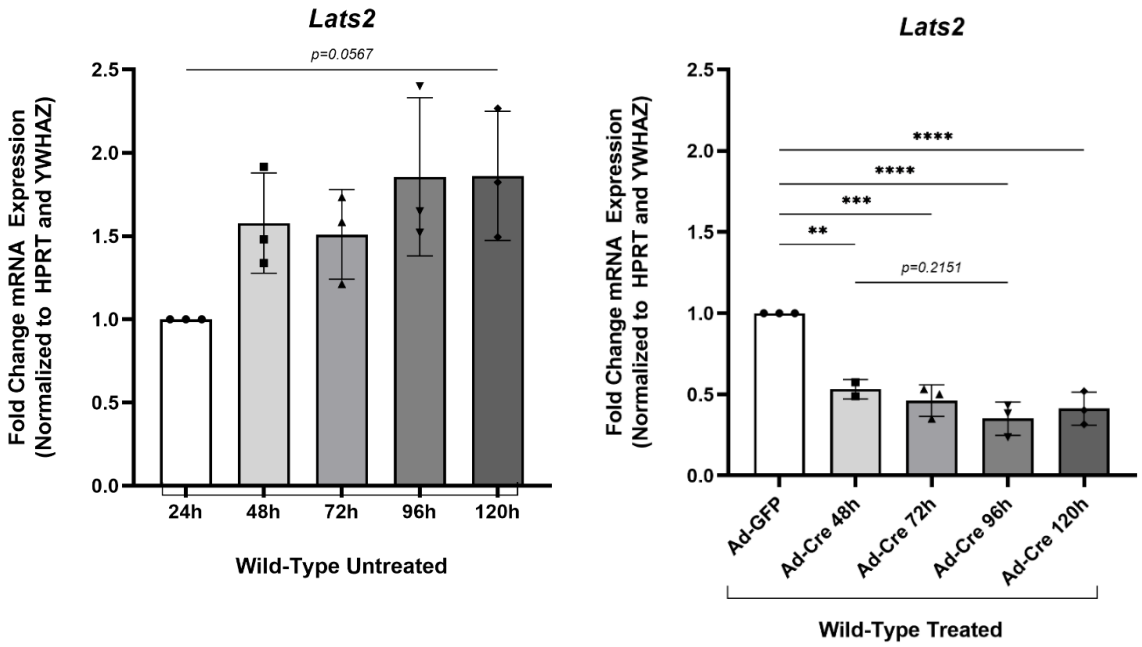

Supplemental Figure 10. ***Reduced Lats2 gene expression in Ad-Cre treated wild-type primary cardiac myofibroblasts.***

mRNA was extracted from murine primary cardiac myofibroblasts cultured on polystyrene and analyzed by qPCR. A. Untreated wild-type myofibroblasts cultured and harvested every 24h after cultured in serum-free medium. B. Cultured wild-type cardiac fibroblasts infected with Ad-GFP (control) or Ad-Cre (experimental group). Control group cells were harvested at three days and Ad-Cre were harvested at 48h, 72h, 96h and 120h after infection. We observed a gradual non-significant elevation of *Lats2* mRNA expression in untreated samples. On the other hand, *Lats2* gene expression was found to be significantly reduced in Ad-Cre samples compared to control. Total biological replicates n=3, except for Wild-Type Ad-Cre 48h with n=2. Each biological replicate was evaluated by 3 technical replicates. Ns: $P \geq 0.05$; **: $P < 0.01$; ***: $P < 0.001$; ****: $P < 0.0001$. Ad-GFP = Adenoviral-GFP (control virus); Ad-Cre = Adenoviral-Cre; *Lats2* = Large Tumor Suppressor Kinase 2; HPRT = hypoxanthine phosphoribosyltransferase 1; YWHAZ = tyrosine 3-monooxygenase/tryptophan 5-monooxygenase activation proteins zeta, both housekeeping genes used for normalization.

References

1. Roy. Failure of the Heart from Overstrain. *The British Medical Journal*. 1888:1321-1326.
2. Writing Committee M, Yancy CW, Jessup M, Bozkurt B, Butler J, Casey DE, Jr., Drazner MH, Fonarow GC, Geraci SA, Horwich T, Januzzi JL, Johnson MR, Kasper EK, Levy WC, Masoudi FA, McBride PE, McMurray JJ, Mitchell JE, Peterson PN, Riegel B, Sam F, Stevenson LW, Tang WH, Tsai EJ, Wilkoff BL and American College of Cardiology Foundation/American Heart Association Task Force on Practice G. 2013 ACCF/AHA guideline for the management of heart failure: a report of the American College of Cardiology Foundation/American Heart Association Task Force on practice guidelines. *Circulation*. 2013;128:e240-327.
3. Chaudhry SP and Stewart GC. Advanced Heart Failure: Prevalence, Natural History, and Prognosis. *Heart Fail Clin*. 2016;12:323-33.
4. Ezekowitz JA, O'Meara E, McDonald MA, Abrams H, Chan M, Ducharme A, Giannetti N, Grzeslo A, Hamilton PG, Heckman GA, Howlett JG, Koshman SL, Lepage S, McKelvie RS, Moe GW, Rajda M, Swiggum E, Virani SA, Zieroth S, Al-Hesayen A, Cohen-Solal A, D'Astous M, De S, Estrella-Holder E, Fremes S, Green L, Haddad H, Harkness K, Hernandez AF, Kouz S, LeBlanc MH, Masoudi FA, Ross HJ, Roussin A and Sussex B. 2017 Comprehensive Update of the Canadian Cardiovascular Society Guidelines for the Management of Heart Failure. *Can J Cardiol*. 2017;33:1342-1433.
5. Wu A. Heart Failure. *Ann Intern Med*. 2018;168:ITC81-ITC96.
6. Inamdar AA and Inamdar AC. Heart Failure: Diagnosis, Management and Utilization. *J Clin Med*. 2016;5.
7. Zhou P and Pu WT. Recounting Cardiac Cellular Composition. *Circ Res*. 2016;118:368-70.
8. Tallquist MD. Cardiac Fibroblast Diversity. *Annu Rev Physiol*. 2020;82:63-78.
9. Frangogiannis NG. Cardiac fibrosis: Cell biological mechanisms, molecular pathways and therapeutic opportunities. *Mol Aspects Med*. 2019;65:70-99.
10. Frangogiannis NG. The extracellular matrix in myocardial injury, repair, and remodeling. *J Clin Invest*. 2017;127:1600-1612.
11. Kuwabara JT and Tallquist MD. Tracking Adventitial Fibroblast Contribution to Disease: A Review of Current Methods to Identify Resident Fibroblasts. *Arterioscler Thromb Vasc Biol*. 2017;37:1598-1607.
12. Tomasek JJ, Gabbiani G, Hinz B, Chaponnier C and Brown RA. Myofibroblasts and mechano-regulation of connective tissue remodelling. *Nat Rev Mol Cell Biol*. 2002;3:349-63.
13. Hinz B. The myofibroblast: paradigm for a mechanically active cell. *J Biomech*. 2010;43:146-55.
14. Humeres C and Frangogiannis NG. Fibroblasts in the Infarcted, Remodeling, and Failing Heart. *JACC Basic Transl Sci*. 2019;4:449-467.
15. Ranjan P, Kumari R and Verma SK. Cardiac Fibroblasts and Cardiac Fibrosis: Precise Role of Exosomes. *Front Cell Dev Biol*. 2019;7:318.
16. Nagaraju CK, Robinson EL, Abdesselem M, Trenson S, Dries E, Gilbert G, Janssens S, Van Cleemput J, Rega F, Meyns B, Roderick HL, Driesen RB and Sipido KR. Myofibroblast Phenotype and Reversibility of Fibrosis in Patients With End-Stage Heart Failure. *J Am Coll Cardiol*. 2019;73:2267-2282.
17. Travers JG, Kamal FA, Robbins J, Yutzey KE and Blaxall BC. Cardiac Fibrosis: The Fibroblast Awakens. *Circ Res*. 2016;118:1021-40.
18. de Boer RA, De Keulenaer G, Bauersachs J, Brutsaert D, Cleland JG, Diez J, Du XJ, Ford P, Heinzel FR, Lipson KE, McDonagh T, Lopez-Andres N, Lunde IG, Lyon AR, Pollesello P, Prasad SK, Tocchetti CG, Mayr M, Sluijter JPG, Thum T, Tschope C, Zannad F, Zimmermann WH, Ruschitzka F, Filippatos G, Lindsey ML, Maack C and Heymans S. Towards better definition, quantification and treatment of fibrosis in heart failure. A scientific roadmap by the Committee of Translational Research of the Heart Failure Association (HFA) of the European Society of Cardiology. *Eur J Heart Fail*. 2019;21:272-285.

19. Prabhu SD and Frangogiannis NG. The Biological Basis for Cardiac Repair After Myocardial Infarction: From Inflammation to Fibrosis. *Circ Res*. 2016;119:91-112.
20. Borlaug BA and Redfield MM. Diastolic and systolic heart failure are distinct phenotypes within the heart failure spectrum. *Circulation*. 2011;123:2006-13; discussion 2014.
21. Foundation HaS. 2016 Report on the Health of Canadians. 2016:12.
22. Ponikowski P, Voors AA, Anker SD, Bueno H, Cleland JGF, Coats AJS, Falk V, Gonzalez-Juanatey JR, Harjola VP, Jankowska EA, Jessup M, Linde C, Nihoyannopoulos P, Parissis JT, Pieske B, Riley JP, Rosano GMC, Ruilope LM, Ruschitzka F, Rutten FH, van der Meer P and Group ESCSD. 2016 ESC Guidelines for the diagnosis and treatment of acute and chronic heart failure: The Task Force for the diagnosis and treatment of acute and chronic heart failure of the European Society of Cardiology (ESC)Developed with the special contribution of the Heart Failure Association (HFA) of the ESC. *Eur Heart J*. 2016;37:2129-2200.
23. Virani SS, Alonso A, Aparicio HJ, Benjamin EJ, Bittencourt MS, Callaway CW, Carson AP, Chamberlain AM, Cheng S, Delling FN, Elkind MSV, Evenson KR, Ferguson JF, Gupta DK, Khan SS, Kissela BM, Knutson KL, Lee CD, Lewis TT, Liu J, Loop MS, Lutsey PL, Ma J, Mackey J, Martin SS, Matchar DB, Mussolino ME, Navaneethan SD, Perak AM, Roth GA, Samad Z, Satou GM, Schroeder EB, Shah SH, Shay CM, Stokes A, VanWagner LB, Wang NY, Tsao CW, American Heart Association Council on E, Prevention Statistics C and Stroke Statistics S. Heart Disease and Stroke Statistics-2021 Update: A Report From the American Heart Association. *Circulation*. 2021;143:e254-e743.
24. Virani SS, Alonso A, Benjamin EJ, Bittencourt MS, Callaway CW, Carson AP, Chamberlain AM, Chang AR, Cheng S, Delling FN, Djousse L, Elkind MSV, Ferguson JF, Fornage M, Khan SS, Kissela BM, Knutson KL, Kwan TW, Lackland DT, Lewis TT, Lichtman JH, Longenecker CT, Loop MS, Lutsey PL, Martin SS, Matsushita K, Moran AE, Mussolino ME, Perak AM, Rosamond WD, Roth GA, Sampson UKA, Satou GM, Schroeder EB, Shah SH, Shay CM, Spartano NL, Stokes A, Tirschwell DL, VanWagner LB, Tsao CW, American Heart Association Council on E, Prevention Statistics C and Stroke Statistics S. Heart Disease and Stroke Statistics-2020 Update: A Report From the American Heart Association. *Circulation*. 2020;141:e139-e596.
25. Groenewegen A, Rutten FH, Mosterd A and Hoes AW. Epidemiology of heart failure. *Eur J Heart Fail*. 2020;22:1342-1356.
26. Thum T, Gross C, Fiedler J, Fischer T, Kissler S, Bussen M, Galuppo P, Just S, Rottbauer W, Frantz S, Castoldi M, Soutschek J, Koteliansky V, Rosenwald A, Basson MA, Licht JD, Pena JT, Rouhanifard SH, Muckenthaler MU, Tuschl T, Martin GR, Bauersachs J and Engelhardt S. MicroRNA-21 contributes to myocardial disease by stimulating MAP kinase signalling in fibroblasts. *Nature*. 2008;456:980-4.
27. Chen W, Bian W, Zhou Y and Zhang J. Cardiac Fibroblasts and Myocardial Regeneration. *Front Bioeng Biotechnol*. 2021;9:599928.
28. Cojan-Minzat BO, Zlibut A and Agoston-Coldea L. Non-ischemic dilated cardiomyopathy and cardiac fibrosis. *Heart Fail Rev*. 2021;26:1081-1101.
29. Bacmeister L, Schwarzl M, Warnke S, Stoffers B, Blankenberg S, Westermann D and Lindner D. Inflammation and fibrosis in murine models of heart failure. *Basic Res Cardiol*. 2019;114:19.
30. Johann Bauersachs JB, Peter Sandner. Heart Failure. 2017;243:581.
31. Sorrentino MJ. The Evolution from Hypertension to Heart Failure. *Heart Fail Clin*. 2019;15:447-453.
32. Kannan A and Janardhanan R. Hypertension as a risk factor for heart failure. *Curr Hypertens Rep*. 2014;16:447.
33. Messerli FH, Rimoldi SF and Bangalore S. The Transition From Hypertension to Heart Failure: Contemporary Update. *JACC Heart Fail*. 2017;5:543-551.
34. Nwabuo CC and Vasan RS. Pathophysiology of Hypertensive Heart Disease: Beyond Left Ventricular Hypertrophy. *Curr Hypertens Rep*. 2020;22:11.
35. Porter KE and Turner NA. Cardiac fibroblasts: at the heart of myocardial remodeling. *Pharmacol Ther*. 2009;123:255-78.

36. Gabriel-Costa D. The pathophysiology of myocardial infarction-induced heart failure. *Pathophysiology*. 2018;25:277-284.
37. Hinz B, McCulloch CA and Coelho NM. Mechanical regulation of myofibroblast phenoconversion and collagen contraction. *Exp Cell Res*. 2019;379:119-128.
38. Hartupee J and Mann DL. Neurohormonal activation in heart failure with reduced ejection fraction. *Nat Rev Cardiol*. 2017;14:30-38.
39. Kemp CD and Conte JV. The pathophysiology of heart failure. *Cardiovasc Pathol*. 2012;21:365-71.
40. Anderson JL and Morrow DA. Acute Myocardial Infarction. *N Engl J Med*. 2017;376:2053-2064.
41. Bahit MC, Kochar A and Granger CB. Post-Myocardial Infarction Heart Failure. *JACC Heart Fail*. 2018;6:179-186.
42. Frangogiannis NG. Pathophysiology of Myocardial Infarction. *Compr Physiol*. 2015;5:1841-75.
43. Frank A, Bonney M, Bonney S, Weitzel L, Koeppen M and Eckle T. Myocardial ischemia reperfusion injury: from basic science to clinical bedside. *Semin Cardiothorac Vasc Anesth*. 2012;16:123-32.
44. Pakshir P and Hinz B. The big five in fibrosis: Macrophages, myofibroblasts, matrix, mechanics, and miscommunication. *Matrix Biol*. 2018;68-69:81-93.
45. Darby IA and Hewitson TD. Fibroblast Differentiation in Wound Healing and Fibrosis. 2007;257:143-179.
46. Talman V and Ruskoaho H. Cardiac fibrosis in myocardial infarction-from repair and remodeling to regeneration. *Cell Tissue Res*. 2016;365:563-81.
47. V H, Titus AS, Cowling RT and Kailasam S. Collagen receptor cross-talk determines alpha-smooth muscle actin-dependent collagen gene expression in angiotensin II-stimulated cardiac fibroblasts. *J Biol Chem*. 2019;294:19723-19739.
48. Rienks M, Papageorgiou AP, Frangogiannis NG and Heymans S. Myocardial extracellular matrix: an ever-changing and diverse entity. *Circ Res*. 2014;114:872-88.
49. Hinz B. The role of myofibroblasts in wound healing. *Curr Res Transl Med*. 2016;64:171-177.
50. Li L, Zhao Q and Kong W. Extracellular matrix remodeling and cardiac fibrosis. *Matrix Biol*. 2018;68-69:490-506.
51. Blokland KEC, Pouwels SD, Schuliga M, Knight DA and Burgess JK. Regulation of cellular senescence by extracellular matrix during chronic fibrotic diseases. *Clin Sci (Lond)*. 2020;134:2681-2706.
52. Moore-Morris T, Guimaraes-Camboa N, Yutzey KE, Puceat M and Evans SM. Cardiac fibroblasts: from development to heart failure. *J Mol Med (Berl)*. 2015;93:823-30.
53. Ma ZG, Yuan YP, Wu HM, Zhang X and Tang QZ. Cardiac fibrosis: new insights into the pathogenesis. *Int J Biol Sci*. 2018;14:1645-1657.
54. Cunnington RH, Nazari M and Dixon IM. c-Ski, Smurf2, and Arkadia as regulators of TGF-beta signaling: new targets for managing myofibroblast function and cardiac fibrosis. *Can J Physiol Pharmacol*. 2009;87:764-72.
55. Czubryt MP and Hale TM. Cardiac fibrosis: Pathobiology and therapeutic targets. *Cell Signal*. 2021;85:110066.
56. Tallquist MD. Redefining the identity of cardiac fibroblasts. *Nat Rev Cardiol*. 2017;14:484-491.
57. Plikus MV, Wang X, Sinha S, Forte E, Thompson SM, Herzog EL, Driskell RR, Rosenthal N, Biernaskie J and Horsley V. Fibroblasts: Origins, definitions, and functions in health and disease. *Cell*. 2021;184:3852-3872.
58. Lajiness JD and Conway SJ. Origin, development, and differentiation of cardiac fibroblasts. *J Mol Cell Cardiol*. 2014;70:2-8.
59. Souders CA, Bowers SL and Baudino TA. Cardiac fibroblast: the renaissance cell. *Circ Res*. 2009;105:1164-76.
60. Baum J and Duffy HS. Fibroblasts and myofibroblasts: what are we talking about? *J Cardiovasc Pharmacol*. 2011;57:376-9.

61. Moore-Morris T, Cattaneo P, Puceat M and Evans SM. Origins of cardiac fibroblasts. *J Mol Cell Cardiol*. 2016;91:1-5.
62. Lynch MD and Watt FM. Fibroblast heterogeneity: implications for human disease. *J Clin Invest*. 2018;128:26-35.
63. Doppler SA, Carvalho C, Lahm H, Deutsch MA, Dressen M, Puluca N, Lange R and Krane M. Cardiac fibroblasts: more than mechanical support. *J Thorac Dis*. 2017;9:S36-S51.
64. Shinde AV and Frangogiannis NG. Fibroblasts in myocardial infarction: a role in inflammation and repair. *J Mol Cell Cardiol*. 2014;70:74-82.
65. Santiago JJ, Dangerfield AL, Rattan SG, Bathe KL, Cunnington RH, Raizman JE, Bedosky KM, Freed DH, Kardami E and Dixon IM. Cardiac fibroblast to myofibroblast differentiation in vivo and in vitro: expression of focal adhesion components in neonatal and adult rat ventricular myofibroblasts. *Dev Dyn*. 2010;239:1573-84.
66. Ribatti D and Tamma R. Giulio Gabbiani and the discovery of myofibroblasts. *Inflamm Res*. 2019;68:241-245.
67. G. Majno GG, B. J. Hirschel, G. B. Ryan and P. R. Statkov. Contraction of Granulation Tissue in vitro: Similarity to Smooth Muscle. *Science*. 1971;173:3.
68. Wang L, Yue Y, Yang X, Fan T, Mei B, Hou J, Liang M, Chen G and Wu Z. Platelet Derived Growth Factor Alpha (PDGFRalpha) Induces the Activation of Cardiac Fibroblasts by Activating c-Kit. *Med Sci Monit*. 2017;23:3808-3816.
69. Zhao S, Wu H, Xia W, Chen X, Zhu S, Zhang S, Shao Y, Ma W, Yang D and Zhang J. Periostin expression is upregulated and associated with myocardial fibrosis in human failing hearts. *J Cardiol*. 2014;63:373-8.
70. Landry NM, Cohen S and Dixon IMC. Periostin in cardiovascular disease and development: a tale of two distinct roles. *Basic Res Cardiol*. 2018;113:1.
71. Fu X, Khalil H, Kanisicak O, Boyer JG, Vagnozzi RJ, Maliken BD, Sargent MA, Prasad V, Valiente-Alandi I, Blaxall BC and Molkentin JD. Specialized fibroblast differentiated states underlie scar formation in the infarcted mouse heart. *J Clin Invest*. 2018;128:2127-2143.
72. Humeres C, Shinde AV, Hanna A, Alex L, Hernandez SC, Li R, Chen B, Conway SJ and Frangogiannis NG. Smad7 effects on TGF-beta and ErbB2 restrain myofibroblast activation and protect from postinfarction heart failure. *J Clin Invest*. 2022;132.
73. Bretherton R, Bugg D, Olszewski E and Davis J. Regulators of cardiac fibroblast cell state. *Matrix Biol*. 2020;91-92:117-135.
74. Burke RM, Burgos Villar KN and Small EM. Fibroblast contributions to ischemic cardiac remodeling. *Cell Signal*. 2021;77:109824.
75. Hinz B and Lagares D. Evasion of apoptosis by myofibroblasts: a hallmark of fibrotic diseases. *Nat Rev Rheumatol*. 2020;16:11-31.
76. Kurose H. Cardiac Fibrosis and Fibroblasts. *Cells*. 2021;10.
77. Frangogiannis NG. The role of transforming growth factor (TGF)-β in the infarcted myocardium. *Journal of Thoracic Disease*. 2017;9:S52-S63.
78. Frangogiannis NG. Transforming growth factor-beta in myocardial disease. *Nat Rev Cardiol*. 2022.
79. Hanna A and Frangogiannis NG. The Role of the TGF-beta Superfamily in Myocardial Infarction. *Front Cardiovasc Med*. 2019;6:140.
80. Hanna A, Humeres C and Frangogiannis NG. The role of Smad signaling cascades in cardiac fibrosis. *Cell Signal*. 2021;77:109826.
81. Huang S, Chen B, Humeres C, Alex L, Hanna A and Frangogiannis NG. The role of Smad2 and Smad3 in regulating homeostatic functions of fibroblasts in vitro and in adult mice. *Biochim Biophys Acta Mol Cell Res*. 2020;1867:118703.
82. Lighthouse JK and Small EM. Transcriptional control of cardiac fibroblast plasticity. *J Mol Cell Cardiol*. 2016;91:52-60.

83. Xue K, Zhang J, Li C, Li J, Wang C, Zhang Q, Chen X, Yu X, Sun L and Yu X. The role and mechanism of transforming growth factor beta 3 in human myocardial infarction-induced myocardial fibrosis. *J Cell Mol Med*. 2019;23:4229-4243.
84. Parichatikanond W, Luangmonkong T, Mangmool S and Kurose H. Therapeutic Targets for the Treatment of Cardiac Fibrosis and Cancer: Focusing on TGF-beta Signaling. *Front Cardiovasc Med*. 2020;7:34.
85. Landry NM and Dixon IMC. Fibroblast mechanosensing, SKI and Hippo signaling and the cardiac fibroblast phenotype: Looking beyond TGF-beta. *Cell Signal*. 2020;76:109802.
86. Landry NM, Rattan SG and Dixon IMC. An Improved Method of Maintaining Primary Murine Cardiac Fibroblasts in Two-Dimensional Cell Culture. *Sci Rep*. 2019;9:12889.
87. Garvin AM, Khokhar BS, Czubryt MP and Hale TM. RAS inhibition in resident fibroblast biology. *Cell Signal*. 2021;80:109903.
88. Hughes D.J. BCF, Geddes L.A., and Bourland J.D. Measurements of Young's Modulus of Elasticity of the Canine Aorta with Ultrasound. *Utrasonic Imaging*. 1979;1:356-367.
89. Roberts RJ, and Rowe, R.C. The Young's Modulus of Pharmaceutical Materials. *International Journal of Pharmaceutics*. 1987;37:15-18.
90. Cunnington RH, Wang B, Ghavami S, Bathe KL, Rattan SG and Dixon IM. Antifibrotic properties of c-Ski and its regulation of cardiac myofibroblast phenotype and contractility. *Am J Physiol Cell Physiol*. 2011;300:C176-86.
91. Wang J, Guo L, Shen D, Xu X, Wang J, Han S and He W. The Role of c-SKI in Regulation of TGFbeta-Induced Human Cardiac Fibroblast Proliferation and ECM Protein Expression. *J Cell Biochem*. 2017;118:1911-1920.
92. Yuan Q. CS, Dong Q., WangZ., Xu Y., Han Q., Ma J., Wei S., Pang J., and Yang F. ZR, Liu B., Dai S., XueL., Wang J., Xue M., Xu T., Zheng W., Xu F., Chen Y., and Guo P. ALDH2 Activation Inhibited Cardiac Fibroblast-to Myofibroblast Transformation Via the TGF-B1/Smad Signaling Pathway. *J of Cardiovasc Pharmacol*. 2019;73:248-256.
93. Hinz B. Formation and function of the myofibroblast during tissue repair. *J Invest Dermatol*. 2007;127:526-37.
94. Wang J, Zohar R and McCulloch CA. Multiple roles of alpha-smooth muscle actin in mechanotransduction. *Exp Cell Res*. 2006;312:205-14.
95. Hinz B. CG, Tomasek J.J., Gabbiani G.,and Chaponnier C. Alpha-Smooth Muscle Actin Expression Upregulates Fibroblast Contractile Activity. *Molecular Biology of the Cell*. 2001;12:2730-2741.
96. Shinde AV, Humeres C and Frangogiannis NG. The role of alpha-smooth muscle actin in fibroblast-mediated matrix contraction and remodeling. *Biochim Biophys Acta Mol Basis Dis*. 2017;1863:298-309.
97. Zhao XH, Laschinger C, Arora P, Szaszi K, Kapus A and McCulloch CA. Force activates smooth muscle alpha-actin promoter activity through the Rho signaling pathway. *J Cell Sci*. 2007;120:1801-9.
98. Pakshir P, Noskovicova N, Lodyga M, Son DO, Schuster R, Goodwin A, Karvonen H and Hinz B. The myofibroblast at a glance. *J Cell Sci*. 2020;133.
99. Hinz B, Phan SH, Thannickal VJ, Prunotto M, Desmouliere A, Varga J, De Wever O, Mareel M and Gabbiani G. Recent developments in myofibroblast biology: paradigms for connective tissue remodeling. *Am J Pathol*. 2012;180:1340-55.
100. Castella LF, Buscemi L, Godbout C, Meister JJ and Hinz B. A new lock-step mechanism of matrix remodelling based on subcellular contractile events. *J Cell Sci*. 2010;123:1751-60.
101. Wipff PJ and Hinz B. Myofibroblasts work best under stress. *J Bodyw Mov Ther*. 2009;13:121-7.
102. Hu B, Wu Z, Liu T, Ullenbruch MR, Jin H and Phan SH. Gut-enriched Kruppel-like factor interaction with Smad3 inhibits myofibroblast differentiation. *Am J Respir Cell Mol Biol*. 2007;36:78-84.
103. Burgess HA, Daugherty LE, Thatcher TH, Lakatos HF, Ray DM, Redonnet M, Phipps RP and Sime PJ. PPARgamma agonists inhibit TGF-beta induced pulmonary myofibroblast differentiation and

collagen production: implications for therapy of lung fibrosis. *Am J Physiol Lung Cell Mol Physiol*. 2005;288:L1146-53.
104. Zannad F, Rossignol P and Iraqi W. Extracellular matrix fibrotic markers in heart failure. *Heart Fail Rev*. 2010;15:319-29.
105. Bowers SL, Banerjee I and Baudino TA. The extracellular matrix: at the center of it all. *J Mol Cell Cardiol*. 2010;48:474-82.
106. Meagher PB, Lee XA, Lee J, Visram A, Friedberg MK and Connelly KA. Cardiac Fibrosis: Key Role of Integrins in Cardiac Homeostasis and Remodeling. *Cells*. 2021;10.
107. Takawale A, Sakamuri SS and Kassiri Z. Extracellular matrix communication and turnover in cardiac physiology and pathology. *Compr Physiol*. 2015;5:687-719.
108. Ruoslahti E. VA, Kuusela P., and Linder E. Fibroblast Surface Antigen: A New Serum Protein. *Biochimica et Biophysica Acta*. 1973;322:352-358.
109. Ruoslahti E. aVA. Novel human serum protein from fibroblast plasma membrane. *Nature*. 1974;248:789-790.
110. Graham J.M. aRO. Isolation and Characterization of a Cell-Surface Fraction from Hamster-Embryo Fibroblasts. *Biochemical Society Transactions*. 1975;3:761-763.
111. Schwarzbauer JE and DeSimone DW. Fibronectins, their fibrillogenesis, and in vivo functions. *Cold Spring Harb Perspect Biol*. 2011;3.
112. Lockhart M, Wirrig E, Phelps A and Wessels A. Extracellular matrix and heart development. *Birth Defects Res A Clin Mol Teratol*. 2011;91:535-50.
113. Serini G. B-PM, Ropraz P.,Geinoz A.,Borsi L., Zardi L, and Gabbiani G. The Fibronectin Domain ED-A is Crucial for Myofibroblastic Phenotype Induction by Transforming Growth Factor-B1. *Journal of Cell Biology*. 1998;142:873-881.
114. Kohan M, Muro AF, Bader R and Berkman N. The extra domain A of fibronectin is essential for allergen-induced airway fibrosis and hyperresponsiveness in mice. *J Allergy Clin Immunol*. 2011;127:439-446 e1-5.
115. Frangogiannis NG. The Extracellular Matrix in Ischemic and Nonischemic Heart Failure. *Circ Res*. 2019;125:117-146.
116. Lemanska-Perek A and Adamik B. Fibronectin and its soluble EDA-FN isoform as biomarkers for inflammation and sepsis. *Adv Clin Exp Med*. 2019;28:1561-1567.
117. Valiente-Alandi I, Schafer AE and Blaxall BC. Extracellular matrix-mediated cellular communication in the heart. *J Mol Cell Cardiol*. 2016;91:228-37.
118. Boudko SP and Bachinger HP. Structural insight for chain selection and stagger control in collagen. *Sci Rep*. 2016;6:37831.
119. Fields GB. Synthesis and biological applications of collagen-model triple-helical peptides. *Org Biomol Chem*. 2010;8:1237-58.
120. Gelse K, Poschl E and Aigner T. Collagens--structure, function, and biosynthesis. *Adv Drug Deliv Rev*. 2003;55:1531-46.
121. Brodsky B. aPAV. Molecular Structure of Collagen Triple Helix. *Advances in Protein Chemistry*. 2005;70:301-339.
122. Frangogiannis NG and Kovacic JC. Extracellular Matrix in Ischemic Heart Disease, Part 4/4: JACC Focus Seminar. *J Am Coll Cardiol*. 2020;75:2219-2235.
123. Santos A, Jang Y, Son I, Kim J and Park Y. Recapitulating Cardiac Structure and Function In Vitro from Simple to Complex Engineering. *Micromachines (Basel)*. 2021;12.
124. Van Doren SR. Matrix metalloproteinase interactions with collagen and elastin. *Matrix Biol*. 2015;44-46:224-31.
125. Hinderer S and Schenke-Layland K. Cardiac fibrosis - A short review of causes and therapeutic strategies. *Adv Drug Deliv Rev*. 2019;146:77-82.
126. Tanai E and Frantz S. Pathophysiology of Heart Failure. *Compr Physiol*. 2015;6:187-214.
127. Kisling A, Lust RM and Katwa LC. What is the role of peptide fragments of collagen I and IV in health and disease? *Life Sci*. 2019;228:30-34.

128. Walraven M and Hinz B. Therapeutic approaches to control tissue repair and fibrosis: Extracellular matrix as a game changer. *Matrix Biol*. 2018;71-72:205-224.
129. M.P. C. Common Threads in Cardiac Fibrosis, Infarct Scar Formation, and Wound Healing. *Fibrogenesis & Tissue Repais*. 2012;5:1-11.
130. Amar S, Smith L and Fields GB. Matrix metalloproteinase collagenolysis in health and disease. *Biochim Biophys Acta Mol Cell Res*. 2017;1864:1940-1951.
131. Thakur V and Bedogni B. The membrane tethered matrix metalloproteinase MT1-MMP at the forefront of melanoma cell invasion and metastasis. *Pharmacol Res*. 2016;111:17-22.
132. Stawowy P, Margeta C, Kallisch H, Seidah NG, Chretien M, Fleck E and Graf K. Regulation of matrix metalloproteinase MT1-MMP/MMP-2 in cardiac fibroblasts by TGF-beta1 involves furin-convertase. *Cardiovasc Res*. 2004;63:87-97.
133. Sounni NE, Dehne K, van Kempen L, Egeblad M, Affara NI, Cuevas I, Wiesen J, Junankar S, Korets L, Lee J, Shen J, Morrison CJ, Overall CM, Krane SM, Werb Z, Boudreau N and Coussens LM. Stromal regulation of vessel stability by MMP14 and TGFbeta. *Dis Model Mech*. 2010;3:317-32.
134. Snyman C and Niesler CU. MMP-14 in skeletal muscle repair. *J Muscle Res Cell Motil*. 2015;36:215-25.
135. Gallagher G.L. JCJ, and Hunyor S.N. Myocardial Extracellular Matrix Remodeling in Ischemic Heart Failure. *Frontiers in Bioscience*. 2007;12:1410-1419.
136. Schram K, Wong MM, Palanivel R, No EK, Dixon IM and Sweeney G. Increased expression and cell surface localization of MT1-MMP plays a role in stimulation of MMP-2 activity by leptin in neonatal rat cardiac myofibroblasts. *J Mol Cell Cardiol*. 2008;44:874-81.
137. Contreras O, Cordova-Casanova A and Brandan E. PDGF-PDGFR network differentially regulates the fate, migration, proliferation, and cell cycle progression of myogenic cells. *Cell Signal*. 2021;84:110036.
138. Papadopoulos N and Lennartsson J. The PDGF/PDGFR pathway as a drug target. *Mol Aspects Med*. 2018;62:75-88.
139. Andrae J, Gallini R and Betsholtz C. Role of platelet-derived growth factors in physiology and medicine. *Genes Dev*. 2008;22:1276-312.
140. Ivey MJ, Kuwabara JT, Riggsbee KL and Tallquist MD. Platelet-derived growth factor receptor-alpha is essential for cardiac fibroblast survival. *Am J Physiol Heart Circ Physiol*. 2019;317:H330-H344.
141. Saito Y, Chikenji T, Ozasa Y, Fujimiya M, Yamashita T, Gingery A and Iba K. PDGFR Signaling Mediates Hyperproliferation and Fibrotic Responses of Subsynovial Connective Tissue Cells in Idiopathic Carpal Tunnel Syndrome. *Sci Rep*. 2017;7:16192.
142. Ivey MJ and Tallquist MD. Defining the Cardiac Fibroblast. *Circ J*. 2016;80:2269-2276.
143. Klinkhammer BM, Floege J and Boor P. PDGF in organ fibrosis. *Mol Aspects Med*. 2018;62:44-62.
144. Liu C, Zhao W, Meng W, Zhao T, Chen Y, Ahokas RA, Liu H and Sun Y. Platelet-derived growth factor blockade on cardiac remodeling following infarction. *Mol Cell Biochem*. 2014;397:295-304.
145. Fu X, Liu Q, Li C, Li Y and Wang L. Cardiac Fibrosis and Cardiac Fibroblast Lineage-Tracing: Recent Advances. *Front Physiol*. 2020;11:416.
146. Furtado MB, Nim HT, Boyd SE and Rosenthal NA. View from the heart: cardiac fibroblasts in development, scarring and regeneration. *Development*. 2016;143:387-97.
147. Zymek P, Bujak M, Chatila K, Cieslak A, Thakker G, Entman ML and Frangogiannis NG. The role of platelet-derived growth factor signaling in healing myocardial infarcts. *J Am Coll Cardiol*. 2006;48:2315-23.
148. Hunziker M, O'Donnell AM and Puri P. Platelet-derived growth factor receptor alpha-positive cells: a new cell type in the human ureteropelvic junction. *Pediatr Res*. 2017;82:1080-1087.
149. de Oliveira Camargo R, Abual'anaz B, Rattan SG, Filomeno KL and Dixon IMC. Novel factors that activate and deactivate cardiac fibroblasts: A new perspective for treatment of cardiac fibrosis. *Wound Repair Regen*. 2021;29:667-677.

150. Zhao W, Zhao T, Huang V, Chen Y, Ahokas RA and Sun Y. Platelet-derived growth factor involvement in myocardial remodeling following infarction. *J Mol Cell Cardiol*. 2011;51:830-8.
151. J. M. TGF-β Signal Transduction. *Annu Rev Biochem*. 1998;67:753-791.
152. Lodyga M and Hinz B. TGF-beta1 - A truly transforming growth factor in fibrosis and immunity. *Semin Cell Dev Biol*. 2019.
153. Miyazono K. MS, Ito T., Kurisaki A., Asashima M., and Tanokura M. Hydrophobic Patches on Smad2 and Smad3 Determine selective Binding to cofactors. *Sci Singal*. 2018;11:1-13.
154. Lyu X, Hu M, Peng J, Zhang X and Sanders YY. HDAC inhibitors as antifibrotic drugs in cardiac and pulmonary fibrosis. *Ther Adv Chronic Dis*. 2019;10:2040622319862697.
155. Cho N, Razipour SE and McCain ML. Featured Article: TGF-beta1 dominates extracellular matrix rigidity for inducing differentiation of human cardiac fibroblasts to myofibroblasts. *Exp Biol Med (Maywood)*. 2018;243:601-612.
156. Zhang Y, Zhu Z, Wang T, Dong Y, Fan Y and Sun D. TGF-beta1-containing exosomes from cardiac microvascular endothelial cells mediate cardiac fibroblast activation under high glucose conditions. *Biochem Cell Biol*. 2021;99:693-699.
157. Kong P, Shinde AV, Su Y, Russo I, Chen B, Saxena A, Conway SJ, Graff JM and Frangogiannis NG. Opposing Actions of Fibroblast and Cardiomyocyte Smad3 Signaling in the Infarcted Myocardium. *Circulation*. 2018;137:707-724.
158. Klingberg F, Chau G, Walraven M, Boo S, Koehler A, Chow ML, Olsen AL, Im M, Lodyga M, Wells RG, White ES and Hinz B. The fibronectin ED-A domain enhances recruitment of latent TGF-beta-binding protein-1 to the fibroblast matrix. *J Cell Sci*. 2018;131.
159. Sweeney M, Corden B and Cook SA. Targeting cardiac fibrosis in heart failure with preserved ejection fraction: mirage or miracle? *EMBO Mol Med*. 2020;12:e10865.
160. Kuki K, Yamaguchi N, Iwasawa S, Takakura Y, Aoyama K, Yuki R, Nakayama Y, Kuga T, Hashimoto Y, Tomonaga T and Yamaguchi N. Enhancement of TGF-beta-induced Smad3 activity by c-Abl-mediated tyrosine phosphorylation of its coactivator SKI-interacting protein (SKIP). *Biochem Biophys Res Commun*. 2017;490:1045-1051.
161. Saadat S, Noureddini M, Mahjoubin-Tehran M, Nazemi S, Shojaie L, Aschner M, Maleki B, Abbasi-Kolli M, Rajabi Moghadam H, Alani B and Mirzaei H. Pivotal Role of TGF-beta/Smad Signaling in Cardiac Fibrosis: Non-coding RNAs as Effectual Players. *Front Cardiovasc Med*. 2020;7:588347.
162. Tecalco-Cruz AC, Rios-Lopez DG, Vazquez-Victorio G, Rosales-Alvarez RE and Macias-Silva M. Transcriptional cofactors Ski and SnoN are major regulators of the TGF-beta/Smad signaling pathway in health and disease. *Signal Transduct Target Ther*. 2018;3:15.
163. Tecalco-Cruz AC, Sosa-Garrocho M, Vazquez-Victorio G, Ortiz-Garcia L, Dominguez-Huttinger E and Macias-Silva M. Transforming growth factor-beta/SMAD Target gene SKIL is negatively regulated by the transcriptional cofactor complex SNON-SMAD4. *J Biol Chem*. 2012;287:26764-76.
164. Piersma B, Bank RA and Boersema M. Signaling in Fibrosis: TGF-beta, WNT, and YAP/TAZ Converge. *Front Med (Lausanne)*. 2015;2:59.
165. Rosenbloom J, Macarak E, Piera-Velazquez S and Jimenez SA. Human Fibrotic Diseases: Current Challenges in Fibrosis Research. *Methods Mol Biol*. 2017;1627:1-23.
166. Yousefi F, Shabaninejad Z, Vakili S, Derakhshan M, Movahedpour A, Dabiri H, Ghasemi Y, Mahjoubin-Tehran M, Nikoozadeh A, Savardashtaki A, Mirzaei H and Hamblin MR. TGF-beta and WNT signaling pathways in cardiac fibrosis: non-coding RNAs come into focus. *Cell Commun Signal*. 2020;18:87.
167. Angelini A, Trial J, Ortiz-Urbina J and Cieslik KA. Mechanosensing dysregulation in the fibroblast: A hallmark of the aging heart. *Ageing Res Rev*. 2020;63:101150.
168. Landry NM, Rattan SG, Filomeno KL, Meier TW, Meier SC, Foran SJ, Meier CF, Koleini N, Fandrich RR, Kardami E, Duhamel TA and Dixon IMC. SKI activates the Hippo pathway via LIMD1 to inhibit cardiac fibroblast activation. *Basic Res Cardiol*. 2021;116:25.

169. Zeglinski MR, Landry NM and Dixon IMC. Non-Canonical Regulation of TGF-β1 Signaling: A Role for Ski/Sno and YAP/TAZ *Cardiac Fibrosis and Heart Failure: Cause or Effect?*: Springer International Publishing Switzerland; 2015(13): 147-165.
170. Sharifi-Sanjani M, Berman M, Goncharov D, Alhamaydeh M, Avolio TG, Baust J, Chang B, Kobir A, Ross M, St Croix C, Nouraie SM, McTiernan CF, Moravec CS, Goncharova E and Al Ghouleh I. Yes-Associated Protein (Yap) Is Up-Regulated in Heart Failure and Promotes Cardiac Fibroblast Proliferation. *Int J Mol Sci*. 2021;22.
171. Reichardt IM, Robeson KZ, Regnier M and Davis J. Controlling cardiac fibrosis through fibroblast state space modulation. *Cell Signal*. 2021;79:109888.
172. Ferrari S and Pesce M. Cell-Based Mechanosensation, Epigenetics, and Non-Coding RNAs in Progression of Cardiac Fibrosis. *Int J Mol Sci*. 2019;21.
173. Passaro F, Tocchetti CG, Spinetti G, Paudice F, Ambrosone L, Costagliola C, Cacciatore F, Abete P and Testa G. Targeting fibrosis in the failing heart with nanoparticles. *Adv Drug Deliv Rev*. 2021;174:461-481.
174. Seo BR, Chen X, Ling L, Song YH, Shimpi AA, Choi S, Gonzalez J, Sapudom J, Wang K, Andresen Eguiluz RC, Gourdon D, Shenoy VB and Fischbach C. Collagen microarchitecture mechanically controls myofibroblast differentiation. *Proc Natl Acad Sci U S A*. 2020;117:11387-11398.
175. Xie M, Wu X, Zhang J, Zhang J and Li X. Ski regulates Smads and TAZ signaling to suppress lung cancer progression. *Mol Carcinog*. 2017;56:2178-2189.
176. Liu S, Tang L, Zhao X, Nguyen B, Heallen TR, Li M, Wang J, Wang J and Martin JF. Yap Promotes Noncanonical Wnt Signals From Cardiomyocytes for Heart Regeneration. *Circ Res*. 2021;129:782-797.
177. Zent J and Guo LW. Signaling Mechanisms of Myofibroblastic Activation: Outside-in and Inside-Out. *Cell Physiol Biochem*. 2018;49:848-868.
178. Nagase T, Nomura N., and Ishii S. Complex Formation Between Proteins Encoded by the Ski Gene Family *The Journal of Biological Chemistry*. 1993;268:13710-13716.
179. Kim H. YK, Matsuwaki T., and Nishihara M. Induction of Ski Protein Expression Upon Leteinization in Rat Granulosa Cells Without a Change in its mRNA Expression. *J Reprod Dev*. 2012;58:254-259.
180. Nicol R and Stavnezer E. Transcriptional repression by v-Ski and c-Ski mediated by a specific DNA binding site. *J Biol Chem*. 1998;273:3588-97.
181. Deheuninck J and Luo K. Ski and SnoN, potent negative regulators of TGF-beta signaling. *Cell Res*. 2009;19:47-57.
182. Boone B, Haspeslagh M and Brochez L. Clinical significance of the expression of c-Ski and SnoN, possible mediators in TGF-beta resistance, in primary cutaneous melanoma. *J Dermatol Sci*. 2009;53:26-33.
183. Caligaris C, Vazquez-Victorio G, Sosa-Garrocho M, Rios-Lopez DG, Marin-Hernandez A and Macias-Silva M. Actin-cytoskeleton polymerization differentially controls the stability of Ski and SnoN co-repressors in normal but not in transformed hepatocytes. *Biochim Biophys Acta*. 2015;1850:1832-41.
184. Luo K. Ski and SnoN: negative regulators of TGF-beta signaling. *Curr Opin Genet Dev*. 2004;14:65-70.
185. Yamanouchi K. Soeta C. HRNK, and Tojo H. Endometrial Expression of Cellular Protooncogene c-Ski and its Regulation by E2. *FEBS*. 1999;449:273-279.
186. Kim H. YK, Matsuwaki T., and Nishihara M. Expression of Ski in the Granulosa Cells of Atretic Follicles in the Rat Ovary. *J Reprod Dev*. 2006;52:715-721.
187. Boonmars T, Wu Z, Boonjaruspinyo S, Puapairoj A, Kaewsamut B, Nagano I, Pinlaor S, Yongvanit P, Wonkchalee O, Juasook A, Sudsarn P and Srisawangwong T. Involvement of c-Ski oncoprotein in carcinogenesis of cholangiocacinoma induced by Opisthorchis viverrini and N-nitrosodimethylamine. *Pathol Oncol Res*. 2011;17:219-27.

188. Chen D. XW, Bales E., Colmenares C., Conacci-Sorrell M., Ishii S., Stavnezer E., Campisi J., Fisher D.E., Ben-Ze'ev A., and Medrano E.E. SKI Activates Wnt/B-Catenin Signaling in Human Melanoma. *Cancer Research*. 2003;63:6626-6634.
189. Chen Y, Pirisi L and Creek KE. Ski protein levels increase during in vitro progression of HPV16-immortalized human keratinocytes and in cervical cancer. *Virology*. 2013;444:100-8.
190. Ferrand N, Atfi A and Prunier C. The oncoprotein c-ski functions as a direct antagonist of the transforming growth factor-{beta} type I receptor. *Cancer Res*. 2010;70:8457-66.
191. Fukasawa H, Yamamoto T, Togawa A, Ohashi N, Fujigaki Y, Oda T, Uchida C, Kitagawa K, Hattori T, Suzuki S, Kitagawa M and Hishida A. Ubiquitin-dependent degradation of SnoN and Ski is increased in renal fibrosis induced by obstructive injury. *Kidney Int*. 2006;69:1733-40.
192. Taguchi L, Miyakuni K, Morishita Y, Morikawa T, Fukayama M, Miyazono K and Ehata S. c-Ski accelerates renal cancer progression by attenuating transforming growth factor beta signaling. *Cancer Sci*. 2019;110:2063-2074.
193. Wang L, Hou Y, Sun Y, Zhao L, Tang X, Hu P, Yang J, Zeng Z, Yang G, Cui X and Liu M. c-Ski activates cancer-associated fibroblasts to regulate breast cancer cell invasion. *Mol Oncol*. 2013;7:1116-28.
194. Yang J, Zhang X, Li Y and Liu Y. Downregulation of Smad transcriptional corepressors SnoN and Ski in the fibrotic kidney: an amplification mechanism for TGF-beta1 signaling. *J Am Soc Nephrol*. 2003;14:3167-77.
195. Bisserier M, Milara J, Abdeldjebbar Y, Gubara S, Jones C, Bueno-Beti C, Chepurko E, Kohlbrenner E, Katz MG, Tarzami S, Cortijo J, Leopold J, Hajjar RJ, Sassi Y and Hadri L. AAV1.SERCA2a Gene Therapy Reverses Pulmonary Fibrosis by Blocking the STAT3/FOXM1 Pathway and Promoting the SNON/SKI Axis. *Mol Ther*. 2020;28:394-410.
196. Macias-Silva M, Li W, Leu JI, Crissey MA and Taub R. Up-regulated transcriptional repressors SnoN and Ski bind Smad proteins to antagonize transforming growth factor-beta signals during liver regeneration. *J Biol Chem*. 2002;277:28483-90.
197. Akiyoshi S, Inoue H, Hanai J, Kusanagi K, Nemoto N, Miyazono K and Kawabata M. c-Ski acts as a transcriptional co-repressor in transforming growth factor-beta signaling through interaction with smads. *J Biol Chem*. 1999;274:35269-77.
198. Heyman HC and Stavnezer E. A carboxyl-terminal region of the ski oncoprotein mediates homodimerization as well as heterodimerization with the related protein SnoN. *Journal of Biological Chemistry*. 1994;269:26996-27003.
199. <Structural mechanism of Smad4 recognition by the nuclear oncoprotein SKi - insights on SKi mediated repression of TGFb signaling.pdf>.
200. Bonnon C and Atanasoski S. c-Ski in health and disease. *Cell Tissue Res*. 2012;347:51-64.
201. Vazquez-Victorio G, Caligaris C, Del Valle-Espinosa E, Sosa-Garrocho M, Gonzalez-Arenas NR, Reyes-Cruz G, Briones-Orta MA and Macias-Silva M. Novel regulation of Ski protein stability and endosomal sorting by actin cytoskeleton dynamics in hepatocytes. *J Biol Chem*. 2015;290:4487-99.
202. Landry N, Kavosh MS, Filomeno KL, Rattan SG, Czubryt MP and Dixon IMC. Ski drives an acute increase in MMP-9 gene expression and release in primary cardiac myofibroblasts. *Physiol Rep*. 2018;6:e13897.
203. Cunnington RH, Northcott JM, Ghavami S, Filomeno KL, Jahan F, Kavosh MS, Davies JJ, Wigle JT and Dixon IM. The Ski-Zeb2-Meox2 pathway provides a novel mechanism for regulation of the cardiac myofibroblast phenotype. *J Cell Sci*. 2014;127:40-9.
204. Zeglinski MR, Davies JJ, Ghavami S, Rattan SG, Halayko AJ and Dixon IM. Chronic expression of Ski induces apoptosis and represses autophagy in cardiac myofibroblasts. *Biochim Biophys Acta*. 2016;1863:1261-8.
205. Liu X, Li P, Chen XY and Zhou YG. c-Ski promotes skin fibroblast proliferation but decreases type I collagen: implications for wound healing and scar formation. *Clin Exp Dermatol*. 2010;35:417-24.

206. Zhang C, Zhang Y, Zhu H, Hu J and Xie Z. MiR-34a/miR-93 target c-Ski to modulate the proliferaton of rat cardiac fibroblasts and extracellular matrix deposition in vivo and in vitro. *Cell Signal*. 2018;46:145-153.
207. He W, Chen Z, Li H, Wu W, He P, Zhong D, Jiang Y, Cheng W, Xu Z and Li J. Decreased phosphorylation facilitates the degradation of the endogenous protective molecule c-Ski in vascular smooth muscle cells. *Cell Signal*. 2021;87:110116.
208. Li J, Zhao L, Yang T, Zeng YJ and Yang K. c-Ski inhibits autophagy of vascular smooth muscle cells induced by oxLDL and PDGF. *PLoS One*. 2014;9:e98902.
209. Teichler S, Illmer T, Roemhild J, Ovcharenko D, Stiewe T and Neubauer A. MicroRNA29a regulates the expression of the nuclear oncogene Ski. *Blood*. 2011;118:1899-902.
210. Wang J, He W, Xu X, Guo L, Zhang Y, Han S and Shen D. The mechanism of TGF-beta/miR-155/c-Ski regulates endothelial-mesenchymal transition in human coronary artery endothelial cells. *Biosci Rep*. 2017;37.
211. Carmignac V, Thevenon J, Ades L, Callewaert B, Julia S, Thauvin-Robinet C, Gueneau L, Courcet JB, Lopez E, Holman K, Renard M, Plauchu H, Plessis G, De Backer J, Child A, Arno G, Duplomb L, Callier P, Aral B, Vabres P, Gigot N, Arbustini E, Grasso M, Robinson PN, Goizet C, Baumann C, Di Rocco M, Sanchez Del Pozo J, Huet F, Jondeau G, Collod-Beroud G, Beroud C, Amiel J, Cormier-Daire V, Riviere JB, Boileau C, De Paepe A and Faivre L. In-frame mutations in exon 1 of SKI cause dominant Shprintzen-Goldberg syndrome. *Am J Hum Genet*. 2012;91:950-7.
212. Schepers D, Doyle AJ, Oswald G, Sparks E, Myers L, Willems PJ, Mansour S, Simpson MA, Frysira H, Maat-Kievit A, Van Minkelen R, Hoogeboom JM, Mortier GR, Titheradge H, Brueton L, Starr L, Stark Z, Ockeloen C, Lourenco CM, Blair E, Hobson E, Hurst J, Maystadt I, Destree A, Girisha KM, Miller M, Dietz HC, Loeys B and Van Laer L. The SMAD-binding domain of SKI: a hotspot for de novo mutations causing Shprintzen-Goldberg syndrome. *Eur J Hum Genet*. 2015;23:224-8.
213. Gori I, George R, Purkiss AG, Strohbuecker S, Randall RA, Ogrodowicz R, Carmignac V, Faivre L, Joshi D, Kjaer S and Hill CS. Mutations in SKI in Shprintzen-Goldberg syndrome lead to attenuated TGF-beta responses through SKI stabilization. *Elife*. 2021;10.
214. Zhu X, Zhang Y, Wang J, Yang JF, Yang YF and Tan ZP. 576 kb deletion in 1p36.33-p36.32 containing SKI is associated with limb malformation, congenital heart disease and epilepsy. *Gene*. 2013;528:352-5.
215. Zhao X, Fang Y, Wang X, Yang Z, Li D, Tian M and Kang P. Knockdown of Ski decreases osteosarcoma cell proliferation and migration by suppressing the PI3K/Akt signaling pathway. *Int J Oncol*. 2020;56:206-218.
216. Wu ZL, Chen YJ, Zhang GZ, Xie QQ, Wang KP, Yang X, Liu TC, Wang ZQ, Zhao GH and Zhang HH. SKI knockdown suppresses apoptosis and extracellular matrix degradation of nucleus pulposus cells via inhibition of the Wnt/beta-catenin pathway and ameliorates disc degeneration. *Apoptosis*. 2022;27:133-148.
217. Ling J, Cai Z, Jin W, Zhuang X, Kan L, Wang F and Ye X. Silencing of c-Ski augments TGF-b1-induced epithelial-mesenchymal transition in cardiomyocyte H9C2 cells. *Cardiol J*. 2019;26:66-76.
218. Andrusaite A and Milling S. Should we be more cre-tical? A cautionary tale of recombination. *Immunology*. 2020;159:131-132.
219. Song AJ and Palmiter RD. Detecting and Avoiding Problems When Using the Cre-lox System. *Trends Genet*. 2018;34:333-340.
220. Doetschman T and Azhar M. Cardiac-specific inducible and conditional gene targeting in mice. *Circ Res*. 2012;110:1498-512.
221. Swonger JM, Liu JS, Ivey MJ and Tallquist MD. Genetic tools for identifying and manipulating fibroblasts in the mouse. *Differentiation*. 2016;92:66-83.
222. Capulli M, Costantini R, Sonntag S, Maurizi A, Paganini C, Monti L, Forlino A, Shmerling D, Teti A and Rossi A. Testing the Cre-mediated genetic switch for the generation of conditional knock-in mice. *PLoS One*. 2019;14:e0213660.
223. E. S. Conditional Gene Inactivation Using Cre Recombinase. *Calcif Tissue Int*. 2002;71:100-102.

224. Marecki JC, Parajuli N, Crow JP and MacMillan-Crow LA. The use of the Cre/loxP system to study oxidative stress in tissue-specific manganese superoxide dismutase knockout models. *Antioxid Redox Signal*. 2014;20:1655-70.
225. Hadjantonakis AK, Pirity M and Nagy A. Cre recombinase mediated alterations of the mouse genome using embryonic stem cells. *Methods Mol Biol*. 2008;461:111-32.
226. Smedley D, Salimova E and Rosenthal N. Cre recombinase resources for conditional mouse mutagenesis. *Methods*. 2011;53:411-6.
227. Lam PT, Padula SL, Hoang TV, Poth JE, Liu L, Liang C, LeFever AS, Wallace LM, Ashery-Padan R, Riggs PK, Shields JE, Shaham O, Rowan S, Brown NL, Glaser T and Robinson ML. Considerations for the use of Cre recombinase for conditional gene deletion in the mouse lens. *Hum Genomics*. 2019;13:10.
228. Kim H, Kim M, Im SK and Fang S. Mouse Cre-LoxP system: general principles to determine tissue-specific roles of target genes. *Lab Anim Res*. 2018;34:147-159.
229. Kwan KM. Conditional alleles in mice: practical considerations for tissue-specific knockouts. *Genesis*. 2002;32:49-62.
230. Skarnes WC, Rosen B, West AP, Koutsourakis M, Bushell W, Iyer V, Mujica AO, Thomas M, Harrow J, Cox T, Jackson D, Severin J, Biggs P, Fu J, Nefedov M, de Jong PJ, Stewart AF and Bradley A. A conditional knockout resource for the genome-wide study of mouse gene function. *Nature*. 2011;474:337-42.
231. Kam MK, Lee KY, Tam PK and Lui VC. Generation of NSE-MerCreMer transgenic mice with tamoxifen inducible Cre activity in neurons. *PLoS One*. 2012;7:e35799.
232. Turlo KA, Gallaher SD, Vora R, Laski FA and Iruela-Arispe ML. When Cre-mediated recombination in mice does not result in protein loss. *Genetics*. 2010;186:959-67.
233. Kaur H, Takefuji M, Ngai CY, Carvalho J, Bayer J, Wietelmann A, Poetsch A, Hoelper S, Conway SJ, Mollmann H, Looso M, Troidl C, Offermanns S and Wettschureck N. Targeted Ablation of Periostin-Expressing Activated Fibroblasts Prevents Adverse Cardiac Remodeling in Mice. *Circ Res*. 2016;118:1906-17.
234. Friedel RH, Wurst W, Wefers B and Kuhn R. Generating conditional knockout mice. *Methods Mol Biol*. 2011;693:205-31.
235. E.L. S. Inducible Transgenic Mouse Models. In: a. D. J. M. Hofker M.H., ed. *Transgenic Mouse Methods and Protocols.* 2 ed. UK: Springer Science+Business Media; 2011(693): 103-115.
236. Baba Y. NM, Yamada Y., Saito I., and Kanegae Y. Practical Range of Effective Dose for Cre Recombinase Expressing Recombinant Adenovirus Without Cell Toxicitiy in Mammalian Cells. *Microbiol Immunol*. 2005;49:559-570.
237. Silver D.P. aLDM. Self-Excising Retroviral Vectors Encoding the Cre Recombinase Overcome Cre-Mediated Cellular Toxicity. *Molecular Cell*. 2001;8:233-243.
238. Pfeifer A. BEP, Kotstra N., Gage F.H., and Verma I.M. Delivery of the Cre Recombinase by Self-Deleting Lentiviral Vector: Efficient Gene Targeting in vivo. *PNAS*. 2001;98:11450-11455.
239. van Dijk KW, Kypreos KE, Fallaux FJ and Hageman J. Adenovirus-mediated gene transfer. *Methods Mol Biol*. 2011;693:321-43.
240. Janbandhu VC, Moik D and Fassler R. Cre recombinase induces DNA damage and tetraploidy in the absence of loxP sites. *Cell Cycle*. 2014;13:462-70.
241. Pugach EK, Richmond PA, Azofeifa JG, Dowell RD and Leinwand LA. Prolonged Cre expression driven by the alpha-myosin heavy chain promoter can be cardiotoxic. *J Mol Cell Cardiol*. 2015;86:54-61.
242. Loonstra A. VM, Beverloo H.B., Al Allak B., van Drunen E., Kanaar R., and Berns A. Growth Inhibition and DNA Damage Induced by Cre Recombinase in Mammalian Cells. *PNAS*. 2001;98:9209-9214.
243. Balkawade RS, Chen C, Crowley MR, Crossman DK, Clapp WL, Verlander JW and Marshall CB. Podocyte-specific expression of Cre recombinase promotes glomerular basement membrane thickening. *Am J Physiol Renal Physiol*. 2019;316:F1026-F1040.

244. Bersell K, Choudhury S, Mollova M, Polizzotti BD, Ganapathy B, Walsh S, Wadugu B, Arab S and Kuhn B. Moderate and high amounts of tamoxifen in alphaMHC-MerCreMer mice induce a DNA damage response, leading to heart failure and death. *Dis Model Mech*. 2013;6:1459-69.
245. Li Y, Choi PS, Casey SC and Felsher DW. Activation of Cre recombinase alone can induce complete tumor regression. *PLoS One*. 2014;9:e107589.
246. Khatibzadeh S, Farzadfar F, Oliver J, Ezzati M and Moran A. Worldwide risk factors for heart failure: a systematic review and pooled analysis. *Int J Cardiol*. 2013;168:1186-94.
247. Thygesen K, Alpert JS, Jaffe AS, Chaitman BR, Bax JJ, Morrow DA, White HD and Executive Group on behalf of the Joint European Society of Cardiology /American College of Cardiology /American Heart Association /World Heart Federation Task Force for the Universal Definition of Myocardial I. Fourth Universal Definition of Myocardial Infarction (2018). *Circulation*. 2018;138:e618-e651.
248. Bakris G, Ali W and Parati G. ACC/AHA Versus ESC/ESH on Hypertension Guidelines: JACC Guideline Comparison. *J Am Coll Cardiol*. 2019;73:3018-3026.
249. Benjamin EJ, Muntner P, Alonso A, Bittencourt MS, Callaway CW, Carson AP, Chamberlain AM, Chang AR, Cheng S, Das SR, Delling FN, Djousse L, Elkind MSV, Ferguson JF, Fornage M, Jordan LC, Khan SS, Kissela BM, Knutson KL, Kwan TW, Lackland DT, Lewis TT, Lichtman JH, Longenecker CT, Loop MS, Lutsey PL, Martin SS, Matsushita K, Moran AE, Mussolino ME, O'Flaherty M, Pandey A, Perak AM, Rosamond WD, Roth GA, Sampson UKA, Satou GM, Schroeder EB, Shah SH, Spartano NL, Stokes A, Tirschwell DL, Tsao CW, Turakhia MP, VanWagner LB, Wilkins JT, Wong SS, Virani SS, American Heart Association Council on E, Prevention Statistics C and Stroke Statistics S. Heart Disease and Stroke Statistics-2019 Update: A Report From the American Heart Association. *Circulation*. 2019;139:e56-e528.
250. Lund LH and Savarese G. Global Public Health Burden of Heart Failure. *Cardiac Failure Review*. 2017;03:7.
251. Ziaeian B and Fonarow GC. Epidemiology and aetiology of heart failure. *Nat Rev Cardiol*. 2016;13:368-78.
252. Roger VL. Epidemiology of heart failure. *Circ Res*. 2013;113:646-59.
253. Dharmarajan K and Rich MW. Epidemiology, Pathophysiology, and Prognosis of Heart Failure in Older Adults. *Heart Fail Clin*. 2017;13:417-426.
254. Bozkurt B. Heart Failure in Women. *Methodist Debakey Cardiovascular Journal*. 2017;13.
255. Murphy SP, Ibrahim NE and Januzzi JL, Jr. Heart Failure With Reduced Ejection Fraction: A Review. *JAMA*. 2020;324:488-504.
256. Gaffey AE, Cavanagh CE, Rosman L, Wang K, Deng Y, Sims M, O'Brien EC, Chamberlain AM, Mentz RJ, Glover LM and Burg MM. Depressive Symptoms and Incident Heart Failure in the Jackson Heart Study: Differential Risk Among Black Men and Women. *J Am Heart Assoc*. 2022;11:e022514.
257. Cene CW, Leng XI, Faraz K, Allison M, Breathett K, Bird C, Coday M, Corbie-Smith G, Foraker R, Ijioma NN, Rosal MC, Sealy-Jefferson S, Shippee TP and Kroenke CH. Social Isolation and Incident Heart Failure Hospitalization in Older Women: Women's Health Initiative Study Findings. *J Am Heart Assoc*. 2022;11:e022907.
258. Foundation HS. 2016 Report on the Health of Canadians. 2016.
259. Bansal M. Cardiovascular disease and COVID-19. *Diabetes Metab Syndr*. 2020;14:247-250.
260. Mehra MR and Ruschitzka F. COVID-19 Illness and Heart Failure: A Missing Link? *JACC Heart Fail*. 2020;8:512-514.
261. Schmid A, Petrovic M, Akella K, Pareddy A and Velavan SS. Getting to the Heart of the Matter: Myocardial Injury, Coagulopathy, and Other Potential Cardiovascular Implications of COVID-19. *Int J Vasc Med*. 2021;2021:6693895.
262. Liu J, Deswal A and Khalid U. COVID-19 myocarditis and long-term heart failure sequelae. *Curr Opin Cardiol*. 2021;36:234-240.
263. Fernandes Pedro J and Reis-Pina P. Palliative Care in Patients with Advanced Heart Failure: A Systematic Review. *Acta Med Port*. 2022;35:111-118.

264. Zeglinski MR, Roche P, Hnatowich M, Jassal DS, Wigle JT, Czubryt MP and Dixon IM. TGFbeta1 regulates Scleraxis expression in primary cardiac myofibroblasts by a Smad-independent mechanism. *Am J Physiol Heart Circ Physiol*. 2016;310:H239-49.
265. N.M. L. SKI Activates Hippo Signalling to Modulate Cardiac Fibroblast Function and Activation. *Physiology and Pathophysiology*. 2020;Doctor of Philosophy:217.
266. Livak KJ and Schmittgen TD. Analysis of relative gene expression data using real-time quantitative PCR and the 2(-Delta Delta C(T)) Method. *Methods*. 2001;25:402-8.
267. Rezai Amin S, Gruszczynski C, Guiard BP, Callebert J, Launay JM, Louis F, Betancur C, Vialou V and Gautron S. Viral vector-mediated Cre recombinase expression in substantia nigra induces lesions of the nigrostriatal pathway associated with perturbations of dopamine-related behaviors and hallmarks of programmed cell death. *J Neurochem*. 2019;150:330-340.
268. Kelley LA, Mezulis S, Yates CM, Wass MN and Sternberg MJ. The Phyre2 web portal for protein modeling, prediction and analysis. *Nat Protoc*. 2015;10:845-58.
269. Reynolds CR, Islam SA and Sternberg MJE. EzMol: A Web Server Wizard for the Rapid Visualization and Image Production of Protein and Nucleic Acid Structures. *J Mol Biol*. 2018;430:2244-2248.
270. Tallquist MD. Cardiac fibroblasts: from origin to injury. *Curr Opin Physiol*. 2018;1:75-79.
271. Tarbit E, Singh I, Peart JN and Rose'Meyer RB. Biomarkers for the identification of cardiac fibroblast and myofibroblast cells. *Heart Fail Rev*. 2019;24:1-15.
272. Chistiakov DA, Orekhov AN and Bobryshev YV. The role of cardiac fibroblasts in post-myocardial heart tissue repair. *Exp Mol Pathol*. 2016;101:231-240.
273. Hinz B, Dugina V, Ballestrem C, Wehrle-Haller B and Chaponnier C. Alpha-smooth muscle actin is crucial for focal adhesion maturation in myofibroblasts. *Mol Biol Cell*. 2003;14:2508-19.
274. Chaikuad A and Bullock AN. Structural Basis of Intracellular TGF-beta Signaling: Receptors and Smads. *Cold Spring Harb Perspect Biol*. 2016;8.
275. Khalil H, Kanisicak O, Prasad V, Correll RN, Fu X, Schips T, Vagnozzi RJ, Liu R, Huynh T, Lee SJ, Karch J and Molkentin JD. Fibroblast-specific TGF-beta-Smad2/3 signaling underlies cardiac fibrosis. *J Clin Invest*. 2017;127:3770-3783.
276. Hinz B. The extracellular matrix and transforming growth factor-beta1: Tale of a strained relationship. *Matrix Biol*. 2015;47:54-65.
277. Humeres C, Venugopal H and Frangogiannis NG. Smad-dependent pathways in the infarcted and failing heart. *Curr Opin Pharmacol*. 2022;64:102207.
278. He J, Tegen SB, Krawitz AR, Martin GS and Luo K. The transforming activity of Ski and SnoN is dependent on their ability to repress the activity of Smad proteins. *J Biol Chem*. 2003;278:30540-7.
279. Le Scolan E, Zhu Q, Wang L, Bandyopadhyay A, Javelaud D, Mauviel A, Sun L and Luo K. Transforming growth factor-beta suppresses the ability of Ski to inhibit tumor metastasis by inducing its degradation. *Cancer Res*. 2008;68:3277-85.
280. Harrow J, Frankish A, Gonzalez JM, Tapanari E, Diekhans M, Kokocinski F, Aken BL, Barrell D, Zadissa A, Searle S, Barnes I, Bignell A, Boychenko V, Hunt T, Kay M, Mukherjee G, Rajan J, Despacio-Reyes G, Saunders G, Steward C, Harte R, Lin M, Howald C, Tanzer A, Derrien T, Chrast J, Walters N, Balasubramanian S, Pei B, Tress M, Rodriguez JM, Ezkurdia I, van Baren J, Brent M, Haussler D, Kellis M, Valencia A, Reymond A, Gerstein M, Guigo R and Hubbard TJ. GENCODE: the reference human genome annotation for The ENCODE Project. *Genome Res*. 2012;22:1760-74.
281. Ule J and Blencowe BJ. Alternative Splicing Regulatory Networks: Functions, Mechanisms, and Evolution. *Mol Cell*. 2019;76:329-345.
282. Frahsek M, Schulte K, Chia-Gil A, Djudjaj S, Schueler H, Leuchtle K, Smeets B, Dijkman H, Floege J and Moeller MJ. Cre recombinase toxicity in podocytes: a novel genetic model for FSGS in adolescent mice. *Am J Physiol Renal Physiol*. 2019;317:F1375-F1382.
283. Takebayashi H, Usui N, Ono K and Ikenaka K. Tamoxifen modulates apoptosis in multiple modes of action in CreER mice. *Genesis*. 2008;46:775-81.

284. Jiang Z, Zhou X, Li R, Michal JJ, Zhang S, Dodson MV, Zhang Z and Harland RM. Whole transcriptome analysis with sequencing: methods, challenges and potential solutions. *Cell Mol Life Sci*. 2015;72:3425-39.
285. Rao DD, Vorhies JS, Senzer N and Nemunaitis J. siRNA vs. shRNA: similarities and differences. *Adv Drug Deliv Rev*. 2009;61:746-59.
286. Acharya R. The recent progresses in shRNA-nanoparticle conjugate as a therapeutic approach. *Mater Sci Eng C Mater Biol Appl*. 2019;104:109928.
287. Pushparaj P.N. AJJ, Manikandan J., and Kumar S.D. siRNA, miRNA and shRNA: in vivo Applications. *J Dent Res*. 2008;87:992-1003.
288. Gavrilov K. aSWM. Therapeutic siRNA: Principles, Challenges, and Strategies. *Yale Journal of Biology and Medicine*. 2012;85:187-200.
289. Doudna JA and Charpentier E. Genome editing. The new frontier of genome engineering with CRISPR-Cas9. *Science*. 2014;346:1258096.
290. Younesi FS, Son DO, Firmino J and Hinz B. Myofibroblast Markers and Microscopy Detection Methods in Cell Culture and Histology. *Methods Mol Biol*. 2021;2299:17-47.
291. McDonald M, Virani S, Chan M, Ducharme A, Ezekowitz JA, Giannetti N, Heckman GA, Howlett JG, Koshman SL, Lepage S, Mielniczuk L, Moe GW, O'Meara E, Swiggum E, Toma M, Zieroth S, Anderson K, Bray SA, Clarke B, Cohen-Solal A, D'Astous M, Davis M, De S, Grant ADM, Grzeslo A, Heshka J, Keen S, Kouz S, Lee D, Masoudi FA, McKelvie R, Parent MC, Poon S, Rajda M, Sharma A, Siatecki K, Storm K, Sussex B, Van Spall H and Yip AMC. CCS/CHFS Heart Failure Guidelines Update: Defining a New Pharmacologic Standard of Care for Heart Failure With Reduced Ejection Fraction. *Can J Cardiol*. 2021;37:531-546.
292. Major Flynn J.E. aCMFD. The Presence and Pathogenesis of Endocardial and Subendocardial Degeneraion, Mural Thrombi, and Thromboses of the Thebesian Veins n Cardiac Failure from Causes Oher than Myocardial Infarction. *American Heart Journal*. 1945:757-768.
293. Lopez-de la Mora DA, Sanchez-Roque C, Montoya-Buelna M, Sanchez-Enriquez S, Lucano-Landeros S, Macias-Barragan J and Armendariz-Borunda J. Role and New Insights of Pirfenidone in Fibrotic Diseases. *Int J Med Sci*. 2015;12:840-7.
294. Szeto SG, Narimatsu M, Lu M, He X, Sidiqi AM, Tolosa MF, Chan L, De Freitas K, Bialik JF, Majumder S, Boo S, Hinz B, Dan Q, Advani A, John R, Wrana JL, Kapus A and Yuen DA. YAP/TAZ Are Mechanoregulators of TGF-beta-Smad Signaling and Renal Fibrogenesis. *J Am Soc Nephrol*. 2016;27:3117-3128.
295. Yamagami K, Oka T, Wang Q, Ishizu T, Lee JK, Miwa K, Akazawa H, Naito AT, Sakata Y and Komuro I. Pirfenidone exhibits cardioprotective effects by regulating myocardial fibrosis and vascular permeability in pressure-overloaded hearts. *Am J Physiol Heart Circ Physiol*. 2015;309:H512-22.
296. Lewis GA, Schelbert EB, Naish JH, Bedson E, Dodd S, Eccleson H, Clayton D, Jimenez BD, McDonagh T, Williams SG, Cooper A, Cunnington C, Ahmed FZ, Viswesvaraiah R, Russell S, Neubauer S, Williamson PR and Miller CA. Pirfenidone in Heart Failure with Preserved Ejection Fraction-Rationale and Design of the PIROUETTE Trial. *Cardiovasc Drugs Ther*. 2019;33:461-470.
297. Graziani F, Lillo R and Crea F. Rationale for the Use of Pirfenidone in Heart Failure With Preserved Ejection Fraction. *Front Cardiovasc Med*. 2021;8:678530.
298. Lewis GA, Dodd S, Clayton D, Bedson E, Eccleson H, Schelbert EB, Naish JH, Jimenez BD, Williams SG, Cunnington C, Ahmed FZ, Cooper A, Rajavarma V, Russell S, McDonagh T, Williamson PR and Miller CA. Pirfenidone in heart failure with preserved ejection fraction: a randomized phase 2 trial. *Nat Med*. 2021;27:1477-1482.
299. Aimo A, Cerbai E, Bartolucci G, Adamo L, Barison A, Lo Surdo G, Biagini S, Passino C and Emdin M. Pirfenidone is a cardioprotective drug: Mechanisms of action and preclinical evidence. *Pharmacol Res*. 2020;155:104694.
300. AlQudah M, Hale TM and Czubryt MP. Targeting the renin-angiotensin-aldosterone system in fibrosis. *Matrix Biol*. 2020;91-92:92-108.